

Solution to Quantitative Seismology

Qing Ji

Contents

1 Chapter 1: Introduction	2
2 Chapter 2: Basic Theorems in Dynamic Elasticity	2
3 Chapter 3: Representation of Seismic Sources	7
4 Chapter 4: Elastic Waves from a Point Dislocation Source	11
5 Chapter 5: Plane Waves in Homogeneous Media and their Reflection and Transmission at a Plane Boundary	22
6 Chapter 6: Reflection and Refraction of Spherical Waves; Lamb's Problem	32
7 Chapter 7: Surface Waves in a Vertically Heterogeneous Media	43
8 Chapter 8: Free Oscillations of the Earth	44
9 Chapter 9: Body Waves in Media with Depth-Dependent Properties	50
10 Chapter 10: The Seismic Source: Kinematics	50
11 Chapter 11: The Seismic Source: Dynamics	50
12 Chapter 12: Principles of Seismometry	51

1 Chapter 1: Introduction

The **Introduction** part in *Quantitative Seismology* provides various useful reference books and websites. Hope you'll also find them beneficial.

2 Chapter 2: Basic Theorems in Dynamic Elasticity

2.1 Question 1

The equation of motion is

$$\rho \ddot{u}_i = f_i + \tau_{ij,j} \quad (2.1)$$

Considering the constitutive law and the expression of strain tensor

$$\tau_{ij} = c_{ijkl} \varepsilon_{kl}, \quad \varepsilon_{ij} = \frac{1}{2} (u_{i,j} + u_{j,i}),$$

and taking into account the symmetry of the elastic tensor, we could get

$$\rho \ddot{u}_i = f_i + (c_{ijkl} u_{k,l})_j. \quad (2.2)$$

For an isotropic and homogeneous medium, the elastic tensor could be expressed as

$$c_{ijkl} = \lambda \delta_{ij} \delta_{kl} + \mu (\delta_{ik} \delta_{jl} + \delta_{il} \delta_{jk}). \quad (2.3)$$

So the corresponding displacement equation becomes

$$\begin{aligned} \rho \ddot{u}_i &= f_i + \lambda u_{j,ji} + \mu (u_{i,jj} + u_{j,ji}) \\ &= (\lambda + \mu) u_{j,ji} + \mu u_{i,jj} \end{aligned} \quad (2.4)$$

Using the following identities

$$u_{j,ji} = [\nabla(\nabla \cdot \mathbf{u})]_i, \quad u_{i,jj} = (\nabla^2 \mathbf{u})_i, \quad \nabla \times (\nabla \times \mathbf{u}) = \nabla(\nabla \cdot \mathbf{u}) - \nabla^2 \mathbf{u},$$

we could find the vector displacement equation

$$\begin{aligned} \rho \ddot{\mathbf{u}} &= \mathbf{f} + (\lambda + \mu) \nabla(\nabla \cdot \mathbf{u}) + \mu \nabla^2 \mathbf{u} \\ &= \mathbf{f} + (\lambda + 2\mu) \nabla(\nabla \cdot \mathbf{u}) - \mu \nabla \times (\nabla \times \mathbf{u}) \end{aligned} \quad (2.5)$$

2.2 Question 2

From definition, we could derive the well-known identity

$$\begin{aligned} \varepsilon_{ijk} \varepsilon_{ilm} &= \begin{vmatrix} \delta_{ii} & \delta_{ji} & \delta_{ki} \\ \delta_{il} & \delta_{jl} & \delta_{kl} \\ \delta_{im} & \delta_{jm} & \delta_{km} \end{vmatrix} = \delta_{ii}(\delta_{jl} \delta_{km} - \delta_{jm} \delta_{kl}) - \delta_{ji}(\delta_{il} \delta_{km} - \delta_{im} \delta_{kl}) + \delta_{ki}(\delta_{il} \delta_{jm} - \delta_{im} \delta_{jl}) \\ &= 3 \cdot (\delta_{jl} \delta_{km} - \delta_{jm} \delta_{kl}) - (\delta_{jl} \delta_{km} - \delta_{jm} \delta_{kl}) + (\delta_{kl} \delta_{jm} - \delta_{km} \delta_{jl}) \\ &= \delta_{jl} \delta_{km} - \delta_{jm} \delta_{kl}, \end{aligned} \quad (2.6)$$

and similarly

$$\varepsilon_{ijk} \varepsilon_{jlm} = -\varepsilon_{jik} \varepsilon_{jlm} = \delta_{im} \delta_{kl} - \delta_{il} \delta_{km}. \quad (2.7)$$

2.3 Question 3

All we need to do is express e_{kk} (dilatation) with τ_{ii} (isotropic pressure). Using the constitutive law for an isotropic elastic solid and setting $i = j$, we could get

$$\tau_{ii} = \lambda e_{kk} \delta_{ii} + 2\mu e_{ii} = (3\lambda + 2\mu)e_{kk},$$

which is equal to

$$e_{kk} = \frac{1}{3\lambda + 2\mu} \tau_{kk}. \quad (2.8)$$

Substituting Eq.(2.8) into the stress-strain relation, we could obtain the strain-stress relation

$$2\mu e_{ij} = -\frac{\lambda}{3\lambda + 2\mu} \tau_{kk} \delta_{ij} + \tau_{ij}. \quad (2.9)$$

2.4 Question 4

Reference: A piece of lecture note from Prof. Paul A. Lagace

<https://ocw.mit.edu/courses/aeronautics-and-astronautics/16-20-structural-mechanics-fall-2002/lecture-notes/unit9.pdf>

If the material is unrestrained and its temperature is raised, we would expect that the material will undergo thermal expansion. However, in this question the strain is fixed, which implies that there must be additional **thermal stress** in the body. Given that the **thermal strain** is expressed by the coefficient tensor of thermal expansion

$$\varepsilon_{kl}^T = \alpha_{kl} \Delta T, \quad (2.10)$$

the corresponding thermal stress should be

$$\sigma_{ij}^T = c_{ijkl} \cdot (-\varepsilon_{kl}^T) = -c_{ijkl} \alpha_{kl} \Delta T. \quad (2.11)$$

The negative sign represents that the mechanical strain should counteract the thermal strain. Taking into account this thermal effect, the modified stress-strain relation should be in the following form

$$\sigma_{ij} = c_{ijkl} (\varepsilon_{kl} - \alpha_{kl} \Delta T). \quad (2.12)$$

2.5 Question 5

Given $\mathbf{u}(\mathbf{x}, t)$, we could obtain the strain and stress

$$\boldsymbol{\varepsilon}(\mathbf{x}, t) = \frac{1}{2} [\nabla \mathbf{u}(\mathbf{x}, t) + (\nabla \mathbf{u}(\mathbf{x}, t))^T], \quad (2.13)$$

$$\boldsymbol{\sigma}(\mathbf{x}, t) = \mathbf{c}(\mathbf{x}, t) : \boldsymbol{\varepsilon}(\mathbf{x}, t). \quad (2.14)$$

The traction could be derived from the stress

$$\mathbf{T}(\mathbf{x}, t) = \hat{\mathbf{n}}(\mathbf{x}, t) \cdot \boldsymbol{\sigma}(\mathbf{x}, t), \quad (2.15)$$

and the body force could be expressed based on the equation of motion

$$\mathbf{f}(\mathbf{x}, t) = \rho(\mathbf{x}, t) \ddot{\mathbf{u}}(\mathbf{x}, t) - \nabla \cdot \boldsymbol{\sigma}(\mathbf{x}, t) \quad (2.16)$$

2.6 Question 6

Relations (2.21)-(2.25) in the book do not involve the dependency of stress on strain or strain rate, so they should not change.

2.7 Question 7

The traction is obtained by Eq.(2.15). In an isotropic medium,

$$\sigma_{ij} = \lambda \varepsilon_{kk} \delta_{ij} + 2\mu \varepsilon_{ij} \quad (2.17)$$

$$\boldsymbol{\sigma} = \lambda(\nabla \cdot \mathbf{u})\mathbf{I} + \mu[\nabla \mathbf{u} + (\nabla \mathbf{u})^T]. \quad (2.18)$$

So the traction could be expressed as

$$\begin{aligned} \mathbf{T}(\mathbf{u}, \hat{\mathbf{n}}) &= \hat{\mathbf{n}} \cdot \boldsymbol{\sigma} \\ &= \lambda(\nabla \cdot \mathbf{u})\hat{\mathbf{n}} + \mu[\hat{\mathbf{n}} \cdot (\nabla \mathbf{u}) + (\nabla \mathbf{u}) \cdot \hat{\mathbf{n}}]. \end{aligned}$$

Using the following expression

$$\begin{aligned} [\hat{\mathbf{n}} \times (\nabla \times \mathbf{u})]_i &= \varepsilon_{ijk} n_j (\varepsilon_{klm} \partial_l u_m) \\ &= (\delta_{il} \delta_{jm} - \delta_{im} \delta_{jl}) n_j \partial_l u_m \\ &= n_j \partial_l u_j - n_j \partial_j u_i \\ &= [(\nabla \mathbf{u}) \cdot \hat{\mathbf{n}} - \hat{\mathbf{n}} \cdot (\nabla \mathbf{u})]_i \end{aligned}$$

and its corresponding vector formula

$$\hat{\mathbf{n}} \times (\nabla \times \mathbf{u}) = (\nabla \mathbf{u}) \cdot \hat{\mathbf{n}} - \hat{\mathbf{n}} \cdot (\nabla \mathbf{u}) = (\nabla \mathbf{u}) \cdot \hat{\mathbf{n}} - (\hat{\mathbf{n}} \cdot \nabla) \mathbf{u}, \quad (2.19)$$

we could derive the traction

$$\begin{aligned} \mathbf{T}(\mathbf{u}, \hat{\mathbf{n}}) &= \lambda(\nabla \cdot \mathbf{u})\hat{\mathbf{n}} + \mu[\hat{\mathbf{n}} \cdot (\nabla \mathbf{u}) + (\nabla \mathbf{u}) \cdot \hat{\mathbf{n}}] \\ &= \lambda(\nabla \cdot \mathbf{u})\hat{\mathbf{n}} + \mu[2(\hat{\mathbf{n}} \cdot \nabla) \mathbf{u} + \hat{\mathbf{n}} \times (\nabla \times \mathbf{u})] \\ &= \lambda(\nabla \cdot \mathbf{u})\hat{\mathbf{n}} + \mu \left[2 \frac{\partial \mathbf{u}}{\partial n} + \hat{\mathbf{n}} \times (\nabla \times \mathbf{u}) \right]. \end{aligned} \quad (2.20)$$

2.8 Question 8

a) Fig. 2.1 is the same with Fig. 2.4 in the book. According to its force equilibrium state, we could find

$$\mathbf{T}(\mathbf{x} + \delta \mathbf{x}, \hat{\mathbf{n}}) + \mathbf{T}(\mathbf{x}, -\hat{\mathbf{n}}) \rightarrow 0 \quad \text{as} \quad \delta \mathbf{x} \rightarrow 0.$$

Using eq. (2.7) in the book, we could show that traction is a continuous function of position

$$\mathbf{T}(\mathbf{x} + \delta \mathbf{x}, \hat{\mathbf{n}}) - \mathbf{T}(\mathbf{x}, \hat{\mathbf{n}}) \rightarrow 0 \quad \text{as} \quad \delta \mathbf{x} \rightarrow 0. \quad (2.21)$$

Here, $\delta \mathbf{x}$ is taken parallel to the direction $\hat{\mathbf{n}}$.

b) For the area which the book lies on, the traction is non-zero. However, for the part outside of the above area, the traction is zero. Assume that the z-direction is perpendicular to the flat surface of the table, the traction is not a continuous function in the x- or y-direction.

c) In problem a), $\delta \mathbf{x}$ is taken parallel to the direction $\hat{\mathbf{n}}$. The continuity of traction in this sense (i.e. in the z-direction) still holds true for the table if we analyze the traction inside it, but this does not contradict with the fact that the traction is not continuous in the x- or y-directions.

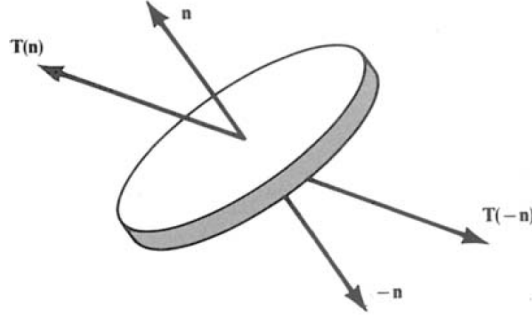


Fig. 2.1 A small disc within a stressed medium (Figure 2.4)

d) First choose $\delta\mathbf{x}$ to be parallel to the z -direction, the continuity of the traction gives

$$\mathbf{T}(\mathbf{x}) = \begin{bmatrix} \tau_{xz}(\mathbf{x}) \\ \tau_{yz}(\mathbf{x}) \\ \tau_{zz}(\mathbf{x}) \end{bmatrix} \text{ is continuous of } z.$$

We could also choose $\delta\mathbf{x}$ to be parallel to the x - or y -directions and obtain that

$$\tau_{ij}(\mathbf{x}) \text{ is continuous in the } i\text{- and } j\text{-directions.}$$

Using the above conclusion, we could know that τ_{zz} need not be continuous in the x - or y -directions, and that τ_{xx} , τ_{yy} and τ_{xy} need not be continuous in the z -direction.

2.9 Question 9

First, we express the stress tensor with isotropic and deviatoric strain, as well as the Lamé parameters:

$$\begin{aligned} \tau_{ij} &= \lambda e_{kk} \delta_{ij} + 2\mu e_{ij} \\ &= \lambda e_{kk} \delta_{ij} + 2\mu \left(\frac{1}{3} e_{kk} \delta_{ij} + e'_{ij} \right) \\ &= \left(\lambda + \frac{2}{3}\mu \right) e_{kk} \delta_{ij} + 2\mu e'_{ij}. \end{aligned}$$

Therefore the strain energy density is given by

$$\begin{aligned} \mathcal{U} &= \frac{1}{2} \tau_{ij} e_{ij} = \frac{1}{2} \left[\left(\lambda + \frac{2}{3}\mu \right) e_{kk} \delta_{ij} + 2\mu e'_{ij} \right] \left(\frac{1}{3} e_{kk} \delta_{ij} + e'_{ij} \right) \\ &= \frac{1}{2} \left[\left(\lambda + \frac{2}{3}\mu \right) e_{ii} e_{kk} + 2\mu e'_{ij} e'_{ij} \right], \end{aligned} \quad (2.22)$$

where we use properties $\delta_{ij} \delta_{ij} = 3$ and $\text{tr}(\mathbf{e}') = e'_{ii} = 0$.

Let's see why $\theta = e_{ii}$ is called **dilatation**. Consider a cuboid and the lengths of its three sides are a, b and c separately. The percentage change of its volume after an infinitesimal deformation is

$$\begin{aligned} \frac{\Delta V}{V} &= \frac{V + \Delta V}{V} - 1 = \frac{a(1 + e_{xx}) \cdot b(1 + e_{yy}) \cdot c(1 + e_{zz})}{abc} - 1 \\ &= (1 + e_{xx})(1 + e_{yy})(1 + e_{zz}) - 1 \doteq e_{ii} = \text{tr}(\mathbf{e}). \end{aligned} \quad (2.23)$$

The isotropic and deviatoric strains and stresses, as well as the corresponding moduli, are summarized in Table 2.1,

which is modified from Table 6.1 in Dahlen & Tromp (1998). Table 2.1 shows why κ , the **bulk modulus** or **incompressibility**, and μ , the **shear modulus**, are widely used in seismology, since they have clearer physical meanings than Lamé parameters. In addition, from Eq. (2.22) we know that these two moduli should be positive so that the strain energy density is positive.

Variable	Isotropic	Deviatoric
Strain ε	$\theta = \text{tr}(\mathbf{e})$	$\mathbf{e}' = \mathbf{e} - \frac{1}{3}\text{tr}(\mathbf{e})\mathbf{I}$
Stress σ	$-p = \frac{1}{3}\text{tr}(\boldsymbol{\tau})$	$\boldsymbol{\tau}' = \boldsymbol{\tau} - \frac{1}{3}\text{tr}(\boldsymbol{\tau})\mathbf{I}$
Modulus M	κ	2μ

Table 2.1 Constitutive laws for isotropic and deviatoric components. Modified from Dahlen & Tromp (1998).

Reference: Chapter 6 in Dahlen, F. A., and J. Tromp, *Theoretical Global Seismology*, Princeton, New Jersey: Princeton University Press, 1998.

2.10 Question 10

We consider the representation theorem in the following form

$$\mathbf{u}(\mathbf{x}, t) = \iiint_V \int_0^t \mathbf{G}(\mathbf{x}, t - \tau; \mathbf{x}', \tau) \cdot \mathbf{f}(\mathbf{x}', \tau) d\tau d^3 \mathbf{x}'. \quad (2.24)$$

In this problem, the force could be expressed as

$$\mathbf{f}(\mathbf{x}', \tau) = \nu \delta(\mathbf{x}' - \xi) \delta(\tau). \quad (2.25)$$

Therefore, we could obtain the displacement vector

$$\mathbf{u}(\mathbf{x}, t) = \mathbf{G}(\mathbf{x}, t; \xi, 0) \cdot \nu, \quad (2.26)$$

and its component in the \mathbf{n} -direction

$$u_n(\mathbf{x}, t) = \mathbf{n} \cdot \mathbf{u}(\mathbf{x}, t) = n_i G_{ip}(\mathbf{x}, t; \xi, 0) \nu_p. \quad (2.27)$$

Using the reciprocity of the Green tensor, we could get

$$\begin{aligned} u_n(\mathbf{x}, t) &= n_i G_{ip}(\mathbf{x}, t; \xi, 0) \nu_p \\ &= u_\nu(\xi, t) = \nu_p G_{pi}(\xi, t; \mathbf{x}, 0) n_i. \end{aligned}$$

3 Chapter 3: Representation of Seismic Sources

3.1 Question 1

- a) **Generalize eq. (3.26) in the book to a vector equation.** Using the following relation

$$\mathbf{M} = M_0 \left(\hat{\mathbf{n}}\hat{\mathbf{d}} + \hat{\mathbf{d}}\hat{\mathbf{n}} \right), \quad M_{ij} = M_0(n_i d_j + n_j d_i) \quad (3.1)$$

and the assumption that S is planar and constant (i.e. $\hat{\mathbf{n}}$ does not change) and that the displacement discontinuity for each event is a shear (i.e. $\hat{\mathbf{n}} \cdot \hat{\mathbf{d}} = 0$), we could obtain

$$\mathbf{M} \cdot \hat{\mathbf{n}} = M_0 \hat{\mathbf{d}}. \quad (3.2)$$

The right part of Eq. (3.2) allows us to obtain the slips in each direction. Therefore, the generalized vector version of eq. (3.26) in the book should be

$$\Delta \mathbf{U} = \frac{\left(\sum_{i=1}^N \mathbf{M}^i \right) \cdot \hat{\mathbf{n}}}{\mu S} \quad (3.3)$$

- b) **Generalize eq. (3.34) in the book to a tensor equation.** For an isotropic medium with volume V , the relationship between moment tensors and strains is

$$M_{ij} = c_{ijkl} \Delta e_{kl} V. \quad (3.4)$$

Recall the result in Section 2.3, we could find the total strain, i.e. the generalized tensor version of eq. (3.34) in the book

$$\Delta E_{ij} = \frac{1}{2\mu V} \cdot \sum_{n=1}^N \left(-\frac{\lambda}{3\lambda + 2\mu} M_{kk}^n \delta_{ij} + M_{ij}^n \right). \quad (3.5)$$

3.2 Question 2

For eq. (3.2) in the book, we can rewrite it using the reciprocity of Green's function:

$$\begin{aligned} u_n(\mathbf{x}, t) &= \int_{-\infty}^{\infty} d\tau \iint_{\Sigma} [u_i(\xi, \tau)] c_{ijpq} v_j \frac{\partial}{\partial \xi_q} G_{np}(\mathbf{x}, t - \tau; \xi, 0) d\Sigma \\ &= \int_{-\infty}^{\infty} d\tau \iint_{\Sigma} [u_i(\xi, 0)] c_{ijpq} v_j \frac{\partial}{\partial \xi_q} G_{pn}(\xi, t - \tau; \mathbf{x}, 0) d\Sigma. \end{aligned} \quad (3.6)$$

Therefore, the following part in the integrand

$$c_{ijpq} v_j \frac{\partial}{\partial \xi_q} G_{pn}(\xi, t - \tau; \mathbf{x}, 0)$$

can be interpreted as a traction on the internal surface Σ . According to the continuity of traction, we can still derive eq. (3.2) from eq. (3.1) in the book, but now $\partial G_{np}/\partial \xi_q$ may not be continuous across the surface.

3.3 Question 3

If $\bar{u}(t)$ is averaged over the area $A(t)$ that has ruptured at time t , then we need to use $A(t)$ to calculate $M_0(t) = \mu \bar{u}(t) A(t)$. Similarly, if $\bar{u}(t)$ is averaged over the area $A(\infty)$, the ultimate ruptured area, then we need to use $A(\infty)$ to calculate $M_0(t) = \mu \bar{u}(t) A(\infty)$. Hence, consistency of the definition of ‘average’ throughout computation matters.

3.4 Question 4

This problem is equivalent to finding the eigenvalues of matrix \mathbf{M} . Since we have

$$|\lambda \mathbf{I} - \mathbf{M}| = \lambda(\lambda^2 - M_0^2), \quad (3.7)$$

the eigenvalues are M_0 , 0 and $-M_0$. Consequently, under the principal coordinates a double-couple can be equivalently described by $\mathbf{M} = \text{diag}(M_0, 0, -M_0)$.

3.5 Question 5

A symmetric second-order moment tensor \mathbf{M} can be diagonalized. Therefore, in the principal coordinates, we have

$$\begin{aligned}\mathbf{M} &= \begin{bmatrix} \lambda_1 & 0 & 0 \\ 0 & \lambda_2 & 0 \\ 0 & 0 & \lambda_3 \end{bmatrix} = \frac{\text{tr}(\mathbf{M})}{3} \cdot \mathbf{I} + \begin{bmatrix} \lambda'_1 & 0 & 0 \\ 0 & \lambda'_2 & 0 \\ 0 & 0 & \lambda'_3 \end{bmatrix} \\ &= \frac{\text{tr}(\mathbf{M})}{3} \cdot \mathbf{I} + \begin{bmatrix} \lambda'_1 & 0 & 0 \\ 0 & -\lambda'_1 & 0 \\ 0 & 0 & 0 \end{bmatrix} + \begin{bmatrix} 0 & 0 & 0 \\ 0 & -\lambda'_3 & 0 \\ 0 & 0 & \lambda'_3 \end{bmatrix},\end{aligned}\quad (3.8)$$

which implies that \mathbf{M} can be thought of as an isotropic point source plus two double couples. This decomposition of a point source is not unique.

We can also write \mathbf{M} in the form

$$\begin{aligned}\mathbf{M} &= \frac{\text{tr}(\mathbf{M})}{3} \cdot \mathbf{I} + \begin{bmatrix} \lambda'_1 & 0 & 0 \\ 0 & \lambda'_2 & 0 \\ 0 & 0 & \lambda'_3 \end{bmatrix} \\ &= \frac{\text{tr}(\mathbf{M})}{3} \cdot \mathbf{I} + \left(\lambda'_1 + \frac{\lambda'_3}{2} \right) \begin{bmatrix} 1 & 0 & 0 \\ 0 & -1 & 0 \\ 0 & 0 & 0 \end{bmatrix} + \lambda'_3 \begin{bmatrix} -\frac{1}{2} & 0 & 0 \\ 0 & -\frac{1}{2} & 0 \\ 0 & 0 & 1 \end{bmatrix},\end{aligned}\quad (3.9)$$

which implies the decomposition of \mathbf{M} into the best double couple and the associated CLVD component.

3.6 Question 6

Integration by parts in three dimensions can be derived based on the product rule for divergence, which is

$$\nabla \cdot (u \mathbf{V}) = u \nabla \cdot \mathbf{V} + \nabla u \cdot \mathbf{V}. \quad (3.10)$$

This leads to

$$\iint_S u \mathbf{V} \cdot \hat{\mathbf{n}} dS = \iiint_V u \nabla \cdot \mathbf{V} dV + \iiint_V \nabla u \cdot \mathbf{V} dV. \quad (3.11)$$

I will use Eq. (3.11) to derive the equivalent body force.

For the following body force

$$\mathbf{f}(\mathbf{x}, t) = -\mathbf{M}(t) \cdot \nabla \delta(\mathbf{x} - \boldsymbol{\xi}), \quad (3.12)$$

the representation theorem gives

$$\begin{aligned}u_n(\mathbf{x}, t) &= \int_{-\infty}^{+\infty} d\tau \iiint_V f_p(\boldsymbol{\eta}, \tau) G_{np}(\mathbf{x}, t - \tau; \boldsymbol{\eta}, 0) dV(\boldsymbol{\eta}) \\ &= - \int_{-\infty}^{+\infty} d\tau \iiint_V M_{pq}(\tau) G_{np}(\mathbf{x}, t - \tau; \boldsymbol{\eta}, 0) \frac{\partial \delta(\boldsymbol{\eta} - \boldsymbol{\xi})}{\partial \eta_q} dV(\boldsymbol{\eta}) \\ &= \int_{-\infty}^{+\infty} d\tau \iiint_V M_{pq}(\tau) \left[\frac{\partial}{\partial \eta_q} G_{np}(\mathbf{x}, t - \tau; \boldsymbol{\eta}, 0) \right] \delta(\boldsymbol{\eta} - \boldsymbol{\xi}) dV(\boldsymbol{\eta}) \\ &= M_{pq}(t) * \frac{\partial}{\partial \xi_q} G_{np}(\mathbf{x}, t; \boldsymbol{\xi}, 0).\end{aligned}\quad (3.13)$$

From the second row to the third row, I use Eq. (3.11) with the scalar function u now being the δ function. Therefore, Eq. (3.12) is the equivalent body force to a point source at $\boldsymbol{\xi}$ with moment tensor \mathbf{M} .

3.7 Question 7

a) In the spherical coordinate, the curl of a vector \mathbf{A} is calculated as

$$\nabla \times \mathbf{A} = \frac{1}{r^2 \sin \theta} \begin{vmatrix} \mathbf{e}_r & r\mathbf{e}_\theta & r \sin \theta \mathbf{e}_\varphi \\ \partial_r & \partial_\theta & \partial_\varphi \\ A_r & rA_\theta & r \sin \theta A_\varphi \end{vmatrix}. \quad (3.14)$$

Therefore, when the displacement is only in the radial direction, we have $\nabla \times \mathbf{u} = 0$. For the final static displacement, the inertial term and the external force term are also zero. Based on the vector wave equation in Eq. (2.5), the final static displacement satisfies $\nabla(\nabla \cdot \mathbf{u}) = 0$.

b) Since we have

$$\nabla(\nabla \cdot \mathbf{u}) = \frac{d}{dr} \left[\frac{1}{r^2} \frac{d}{dr} (r^2 u_r) \right] = 0, \quad (3.15)$$

its general solution is

$$u_r = Ar + \frac{B}{r^2}. \quad (3.16)$$

For the external solution when $r \geq a$, the constraint $u_r \rightarrow 0$ for $r \rightarrow \infty$ guarantees that the radial displacement is proportional to $1/r^2$.

c) The stress-strain relation for τ_{rr} , based on eq. (2.50) in the book, can be written as

$$\tau_{rr} = \lambda(e_{rr} + e_{\theta\theta} + e_{\varphi\varphi}) + 2\mu e_{rr}. \quad (3.17)$$

From eq. (2.45) in the book, with $h^1 = 1, h^2 = r$ and $h^3 = r \sin \theta$ for the spherical coordinate, we have

$$\begin{aligned} e_{rr} &= \frac{u_r}{r}, \\ e_{\theta\theta} &= \frac{1}{r} \frac{\partial u_\theta}{\partial \theta} + \frac{u_r}{r}, \\ e_{\varphi\varphi} &= \frac{1}{r \sin \theta} \frac{\partial u_\varphi}{\partial \varphi} + \frac{u_r}{r} + \frac{\cot \theta}{r} u_\theta. \end{aligned} \quad (3.18)$$

Therefore, when we only have radial displacement u_r , Eq. (3.17) leads to

$$\tau_{rr} = (\lambda + 2\mu) \frac{\partial u_r}{\partial r} + \frac{2\lambda}{r} u_r. \quad (3.19)$$

d) The external solution has the form $u_r = B/r^2$. We also know that the walls of the cavity at $r = a$ experience $\tau_{rr} = -\delta p$. With this condition, we have

$$-\delta p = (\lambda + 2\mu) \cdot \frac{-2B}{a^3} + 2\lambda \cdot \frac{B}{a^3} = -4\mu \cdot \frac{B}{a^3}, \quad (3.20)$$

which gives $B = \delta p \cdot a^3 / 4\mu$. Therefore, the final outward static displacement at $r = a$ is

$$\delta a = u_r(a) = \frac{\delta p \cdot a}{4\mu}, \quad (3.21)$$

which is equivalent to

$$\delta p = 4\mu \frac{\delta a}{a}. \quad (3.22)$$

3.8 Question 8

a) Following the procedure in Question 7, the internal solution has the form $u_r = Ar$. With Eq. (3.19) we have

$$\delta p = -\tau_{rr} = -(3\lambda + 2\mu)A. \quad (3.23)$$

b) The effects of confinement reduces the static displacement at $r = a$ from Δa to δa , which can be expressed as

$$u_r(a) = Aa = -(\Delta a - \delta a), \quad (3.24)$$

from which we can determine the constant A . This leads to

$$\delta p = \frac{3\lambda + 2\mu}{a}(\Delta a - \delta a). \quad (3.25)$$

Using Eq. (3.22) from Question 7, we obtain

$$\begin{aligned} 4\mu\delta a &= (3\lambda + 2\mu)(\Delta a - \delta a) \\ \Delta a &= \frac{\lambda + 2\mu}{\lambda + \frac{2}{3}\mu}\delta a. \end{aligned} \quad (3.26)$$

c) Because $\Delta V = 4\pi a^2 \Delta a$ and $\delta V = 4\pi a^2 \delta a$, the proportionality between ΔV and δV is the same as in Eq. (3.26). Therefore,

$$M_0(\infty) = \left(\lambda + \frac{2}{3}\mu\right)\Delta V = (\lambda + 2\mu)\delta V. \quad (3.27)$$

d) The external solution gives that $u_r = B/r^2$ where B is a constant determined by δp and the source region radius a_0 . Therefore, when we evaluate the outward actual static displacement for a new surface at r , the corresponding actual final (static) volume change is

$$\delta V = 4\pi r^2 u_r = 4\pi B = \pi a_0^3 \frac{\delta p}{\mu}. \quad (3.28)$$

Hence, δV is unchanged in value. In other words, it is independent of where the outward actual static displacement is measured.

4 Chapter 4: Elastic Waves from a Point Dislocation Source

4.1 Question 1

When the source time function is $S(t) = \delta(t)$, we have

$$\begin{aligned} G_{np}(\mathbf{x}, t; \mathbf{0}, 0) &= \frac{3\gamma_n\gamma_p - \delta_{np}}{4\pi\rho r^3} t [H(t - t_P) - H(t - t_S)] \\ &\quad + \frac{\gamma_n\gamma_p}{4\pi\rho\alpha^2 r} \delta(t - t_P) - \frac{\gamma_n\gamma_p - \delta_{np}}{4\pi\rho\beta^2 r} \delta(t - t_S). \end{aligned} \quad (4.1)$$

Therefore, the area under the near-field pulse can be calculated as

$$S^{NF} \propto \frac{1}{r^3} \int_{t_P}^{t_S} t dt = \frac{1}{2r} \left(\frac{1}{\beta^2} - \frac{1}{\alpha^2} \right), \quad (4.2)$$

which is proportional to $1/r$. It is obvious that for the far-field terms, the area under each pulse is proportional to $1/r$.

In the frequency domain, the P-wave term is

$$G_{np}^P(\mathbf{x}, \omega; \mathbf{0}, 0) = \frac{e^{i\omega r/\alpha}}{4\pi\rho\alpha^2 r} \left[\gamma_n\gamma_p + (3\gamma_n\gamma_p - \delta_{np}) \left(-\frac{\alpha}{i\omega r} \right) + (3\gamma_n\gamma_p - \delta_{np}) \left(-\frac{\alpha}{i\omega r} \right)^2 \right], \quad (4.3)$$

and similarly, the S-wave term is

$$G_{np}^S(\mathbf{x}, \omega; \mathbf{0}, 0) = -\frac{e^{i\omega r/\beta}}{4\pi\rho\beta^2 r} \left[(\gamma_n\gamma_p - \delta_{np}) + (3\gamma_n\gamma_p - \delta_{np}) \left(-\frac{\beta}{i\omega r} \right) + (3\gamma_n\gamma_p - \delta_{np}) \left(-\frac{\beta}{i\omega r} \right)^2 \right]. \quad (4.4)$$

As $\omega \rightarrow 0$, we have

$$e^{i\omega r/\alpha} \approx 1 + \left(\frac{i\omega r}{\alpha} \right) + \frac{1}{2} \left(\frac{i\omega r}{\alpha} \right)^2. \quad (4.5)$$

Therefore, Eqs. (4.3) and (4.4) can be written as

$$G_{np}^P(\mathbf{x}, \omega; \mathbf{0}, 0) = \frac{1}{4\pi\rho r} \left(\frac{\delta_{np} - \gamma_n\gamma_p}{2\alpha^2} - \frac{3\gamma_n\gamma_p - \delta_{np}}{\omega^2 r^2} \right) + O(\omega^0), \quad (4.6)$$

$$G_{np}^S(\mathbf{x}, \omega; \mathbf{0}, 0) = \frac{1}{4\pi\rho r} \left(\frac{\delta_{np} + \gamma_n\gamma_p}{2\beta^2} + \frac{3\gamma_n\gamma_p - \delta_{np}}{\omega^2 r^2} \right) + O(\omega^0), \quad (4.7)$$

which leads to

$$\lim_{\omega \rightarrow 0} G_{np}(\mathbf{x}, \omega; \mathbf{0}, 0) = \lim_{\omega \rightarrow 0} (G_{np}^P + G_{np}^S) = \frac{1}{8\pi\rho r} \left(\frac{\delta_{np} - \gamma_n\gamma_p}{\alpha^2} + \frac{\delta_{np} + \gamma_n\gamma_p}{\beta^2} \right). \quad (4.8)$$

Hence, the distance dependence as $\omega \rightarrow 0$ is indeed like $1/r$. Besides, Eq. (4.8) is also the static solution as $t \rightarrow \infty$ for the Heaviside source time function $S(t) = H(t)$.

Fig. 4.1 shows the three component seismograms generated by a vertical point-force with a sharp Gaussian source time function. The near-field and far-field terms are clearly separated. However, when the source time function has a longer duration, as shown in Fig. 4.2, all terms are equally important in the near field. This can be related to a seismometer that is sensitive only to periods comparable to (or much longer than) the S-P time.

4.2 Question 2

For a general point-force $S(t)$ in the p -th direction at the origin, we have

$$\begin{aligned} u_n(\mathbf{x}, t) &= \frac{3\gamma_n\gamma_p - \delta_{np}}{4\pi\rho r^3} \int_{t_P}^{t_S} \tau S(t - \tau) d\tau \\ &\quad + \frac{\gamma_n\gamma_p}{4\pi\rho\alpha^2 r} S(t - t_P) - \frac{\gamma_n\gamma_p - \delta_{np}}{4\pi\rho\beta^2 r} S(t - t_S). \end{aligned} \quad (4.9)$$

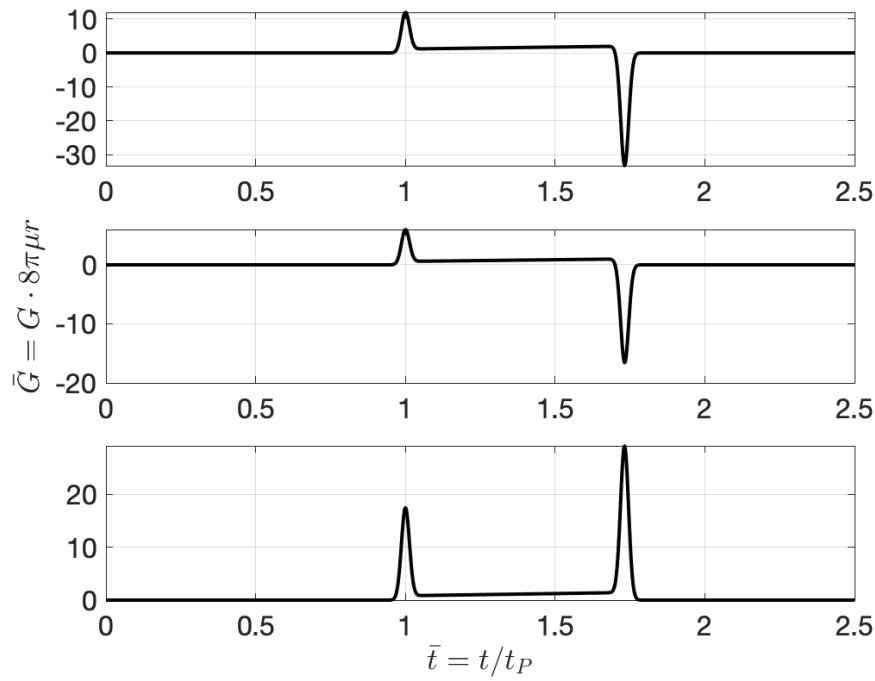


Fig. 4.1 Three component seismograms generated by a vertical point-force at receiver $\mathbf{x} = (2, 1, 3)$ km. The time axis is normalized by the P-wave travel time $t_P = r/\alpha$, and the displacement is multiplied by factor $8\pi\mu r$, which also helps visualize the dependence on $1/r$. The source time function is a Gaussian with $\sigma = 0.01$ s.

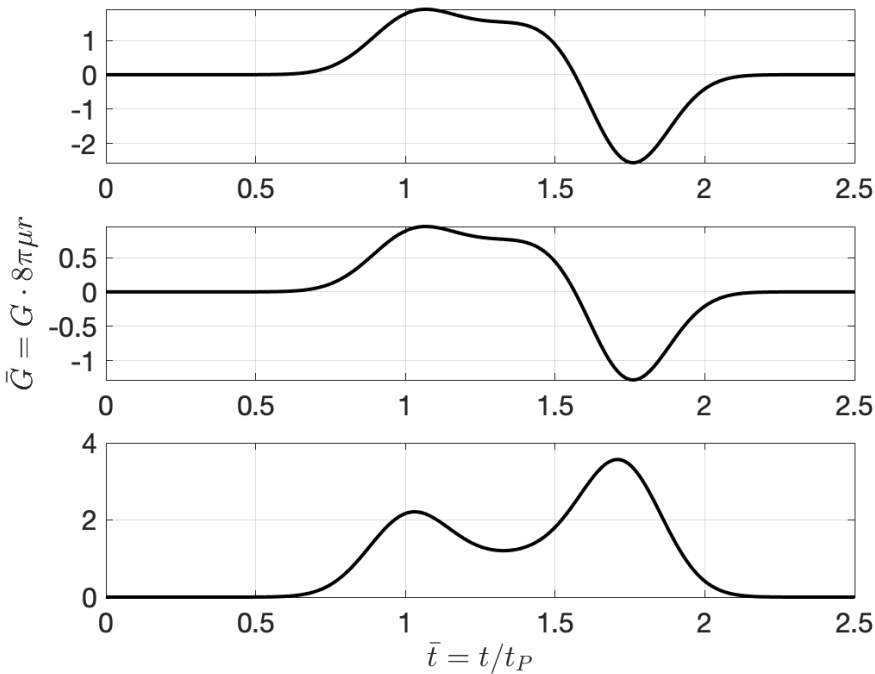


Fig. 4.2 Three component seismograms generated by a vertical point-force at receiver $\mathbf{x} = (2, 1, 3)$ km. The source time function is a Gaussian with $\sigma = 0.1$ s.

When the force is constant, we have $S(t) = H(t)$, which leads to

$$u_n(\mathbf{x}, t) = \frac{3\gamma_n\gamma_p - \delta_{np}}{8\pi\rho r^3} [(t^2 - t_P^2)H(t - t_P) - (t^2 - t_S^2)H(t - t_S)] + \frac{\gamma_n\gamma_p}{4\pi\rho\alpha^2 r} H(t - t_P) - \frac{\gamma_n\gamma_p - \delta_{np}}{4\pi\rho\beta^2 r} H(t - t_S). \quad (4.10)$$

Hence, the static solution at $t \rightarrow \infty$ is

$$u_n^{\text{static}}(\mathbf{x}) = \frac{1}{8\pi\rho r} \left(\frac{\delta_{np} - \gamma_n\gamma_p}{\alpha^2} + \frac{\delta_{np} + \gamma_n\gamma_p}{\beta^2} \right), \quad (4.11)$$

which is the same as derived in Section 4.1.

4.3 Question 3

Under the principal coordinates, the moment tensor can be described as $\mathbf{M} = \text{diag}(M_0, 0, -M_0)$. Therefore, ξ'_1 marks the tension axis (T), while ξ'_3 marks the pressure axis (P).

The tension axis (T) corresponds to maximum outward particle motion, while the pressure axis (P) corresponds to maximum inward particle motion.

4.4 Question 4

Note that $\delta\Delta$ should be measured at the same radius for two ray paths close to each other. Now consider a point \mathbf{x} on the ray path in a **spherically symmetric medium**. In the azimuth direction, the elementary area has a side length of $|\mathbf{x}| \sin \Delta \delta\phi$. For the take-off angle direction, when the rays are going down, the elementary area has a side length of $|\mathbf{x}| \cos i_x \delta\Delta$, with $i_x < 90^\circ$ and $\delta\Delta > 0$. On the contrary, when the rays are going up, the length is also $|\mathbf{x}| \cos i_x \delta\Delta$, with $i_x > 90^\circ$ and $\delta\Delta < 0$. This case is shown in Fig. 4.3. Therefore, the cross-sectional area of the ray tube at \mathbf{x} is

$$\delta A = |\mathbf{x}|^2 \cos i_x \sin \Delta \delta\Delta \delta\phi. \quad (4.12)$$

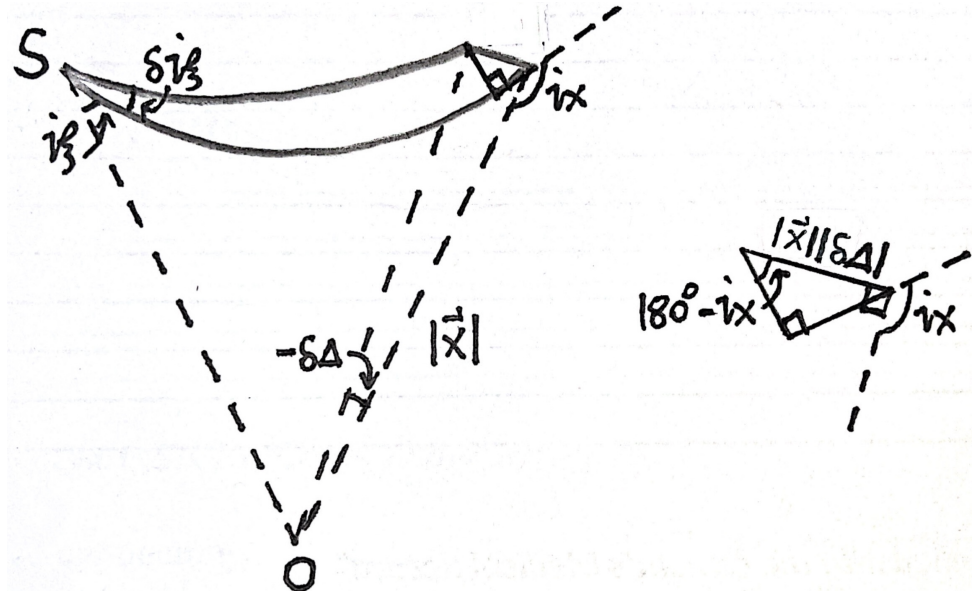


Fig. 4.3 Illustration of the side length in the take-off angle direction.

Given that the solid angle $\delta\Omega = \sin i_\xi \delta i_\xi \delta\phi$, the geometrical spreading function is

$$\mathcal{R}(\mathbf{x}, \boldsymbol{\xi}) = \sqrt{\frac{\delta A}{\delta\Omega}} = |\mathbf{x}| \sqrt{\frac{\cos i_x \sin \Delta \delta\Delta}{\sin i_\xi \delta i_\xi}}. \quad (4.13)$$

From the ray parameter, we have

$$p = \frac{|\boldsymbol{\xi}| \sin i_\xi}{c(\boldsymbol{\xi})}, \quad \delta p = \frac{|\boldsymbol{\xi}| \cos i_\xi}{c(\boldsymbol{\xi})} \delta i_\xi = p \cot i_\xi \delta i_\xi. \quad (4.14)$$

Using Eq. (4.14), we have $\delta p > 0$ (assuming $i_\xi < 90^\circ$), and thus we obtain

$$\begin{aligned} \mathcal{R}(\mathbf{x}, \boldsymbol{\xi}) c(\boldsymbol{\xi}) &= |\mathbf{x}| \frac{|\boldsymbol{\xi}| \sin i_\xi}{p} \sqrt{\frac{p \cos i_x \cos i_\xi \sin \Delta \delta\Delta}{\sin^2 i_\xi \delta p}} \\ &= |\mathbf{x}| |\boldsymbol{\xi}| \left[\frac{\cos i_x \cos i_\xi \sin \Delta}{p} \frac{\partial \Delta}{\partial p} \right]^{1/2}. \end{aligned} \quad (4.15)$$

Eq. (4.15) directly implies the reciprocity $\mathcal{R}(\mathbf{x}, \boldsymbol{\xi}) c(\boldsymbol{\xi}) = \mathcal{R}(\boldsymbol{\xi}, \mathbf{x}) c(\mathbf{x})$.

4.5 Question 5

From the following far-field P-wave Green's function

$$G_{ij}^P = \frac{\gamma_i \gamma_j}{4\pi \rho \alpha^2 r} \delta \left(t - \frac{r}{\alpha} \right), \quad (4.16)$$

we need to generalize it into the form

$$G_{ij}^{P,\text{ray}} = \frac{C(\boldsymbol{\xi}) \mathcal{F}^P}{4\pi \sqrt{\rho(\mathbf{x}) \alpha(\mathbf{x})} \mathcal{R}^P(\mathbf{x}, \boldsymbol{\xi})} \delta [t - T^P(\mathbf{x}, \boldsymbol{\xi})]. \quad (4.17)$$

Here, we already identify and generalize r/α as the ray travel time T^P , $1/r$ as the geometrical spreading factor $1/\mathcal{R}^P(\mathbf{x}, \boldsymbol{\xi})$, and $1/\rho \alpha^2$ as the factor $C(\boldsymbol{\xi})/\sqrt{\rho(\mathbf{x}) \alpha(\mathbf{x})}$, which implies that the constant $C(\boldsymbol{\xi}) = 1/\sqrt{\rho(\boldsymbol{\xi}) \alpha^3(\boldsymbol{\xi})}$. The radiation pattern $\gamma_i \gamma_j$, similarly, can be generalized by replacing the source-receiver direction unit vectors $\hat{\gamma}$ with the ray direction unit vector $\hat{l}(\boldsymbol{\xi})$ and $\hat{l}(\mathbf{x})$. Therefore, we obtain

$$G_{ij}^{P,\text{ray}} = \frac{l_i(\mathbf{x}) l_j(\boldsymbol{\xi})}{4\pi \sqrt{\rho(\mathbf{x}) \alpha(\mathbf{x}) \rho(\boldsymbol{\xi}) \alpha^3(\boldsymbol{\xi})} \mathcal{R}^P(\mathbf{x}, \boldsymbol{\xi})} \delta [t - T^P(\mathbf{x}, \boldsymbol{\xi})]. \quad (4.18)$$

Reciprocity states that

$$G_{ij}(\mathbf{x}; \boldsymbol{\xi}) = G_{ji}(\boldsymbol{\xi}; \mathbf{x}), \quad (4.19)$$

which, using Eq. (4.18), gives

$$\frac{l_i(\mathbf{x}) l_j(\boldsymbol{\xi})}{\sqrt{\rho(\mathbf{x}) \alpha(\mathbf{x}) \rho(\boldsymbol{\xi}) \alpha^3(\boldsymbol{\xi})} \mathcal{R}^P(\mathbf{x}, \boldsymbol{\xi})} = \frac{l_j(\boldsymbol{\xi}) l_i(\mathbf{x})}{\sqrt{\rho(\boldsymbol{\xi}) \alpha(\boldsymbol{\xi}) \rho(\mathbf{x}) \alpha^3(\mathbf{x})} \mathcal{R}^P(\boldsymbol{\xi}, \mathbf{x})}. \quad (4.20)$$

Now we prove that

$$\mathcal{R}^P(\mathbf{x}, \boldsymbol{\xi}) \alpha(\boldsymbol{\xi}) = \mathcal{R}^P(\boldsymbol{\xi}, \mathbf{x}) \alpha(\mathbf{x}) \quad (4.21)$$

4.6 Question 6

The far-field radiation patterns for P and S waves from a **point source of fault slip** are

$$\mathbf{A}^{FP} = \sin 2\theta \cos \phi \hat{\mathbf{r}}, \quad \mathbf{A}^{FS} = \cos 2\theta \cos \phi \hat{\theta} - \cos \theta \sin \phi \hat{\phi}. \quad (4.22)$$

The RMS values for these radiation patterns, averaged over the focal sphere, are calculated as

$$\begin{aligned} a^{FP} &= \sqrt{\frac{1}{4\pi} \int_0^{2\pi} d\phi \int_0^\pi d\theta |\mathbf{A}^{FP}(\theta, \phi)|^2 \sin \theta} = \sqrt{\frac{1}{4\pi} \int_0^{2\pi} \cos^2 \phi d\phi \cdot \int_0^\pi \sin^2 2\theta \sin \theta d\theta} \\ &= \sqrt{\frac{1}{4\pi} \cdot \pi \cdot 8 \left(\frac{2}{3} - \frac{4}{5} \cdot \frac{2}{3} \right)} = \sqrt{\frac{4}{15}}. \end{aligned} \quad (4.23)$$

$$\begin{aligned} a^{FS} &= \sqrt{\frac{1}{4\pi} \int_0^{2\pi} d\phi \int_0^\pi d\theta |\mathbf{A}^{FS}(\theta, \phi)|^2 \sin \theta} \\ &= \sqrt{\frac{1}{4\pi} \int_0^{2\pi} \cos^2 \phi d\phi \cdot \int_0^\pi \cos^2 2\theta \sin \theta d\theta + \sqrt{\frac{1}{4\pi} \int_0^{2\pi} \sin^2 \phi d\phi \cdot \int_0^\pi \cos^2 \theta \sin \theta d\theta}} \\ &= \sqrt{\frac{1}{4\pi} \cdot \pi \cdot \left(\frac{14}{15} + \frac{2}{3} \right)} = \sqrt{\frac{2}{5}}. \end{aligned} \quad (4.24)$$

The energy radiated seismically from a **double-couple point source in a homogeneous full-space**, as P waves for example, is

$$E_P = \int_0^{2\pi} \int_0^\pi r^2 \sin \theta d\theta d\phi \int_0^{+\infty} dt \rho \alpha |\mathbf{u}_P(r, \theta, \phi, t)|^2. \quad (4.25)$$

Note that only far-field P waves behave as r^{-1} decay, which is able to cancel out the factor r^2 from the spherical surface area in Eq. (4.25). Therefore, the total radiated energy we will obtain later is far-field result in the limit of $r \rightarrow \infty$. Through calculation, we have

$$E_P = 4\pi \cdot (a^{FP})^2 \cdot \frac{\int_0^\infty [\ddot{M}_0(t)]^2 dt}{16\pi^2 \rho \alpha^5} = \frac{\int_0^\infty [\ddot{M}_0(t)]^2 dt}{15\pi \rho \alpha^5}, \quad (4.26)$$

$$E_S = 4\pi \cdot (a^{FS})^2 \cdot \frac{\int_0^\infty [\ddot{M}_0(t)]^2 dt}{16\pi^2 \rho \beta^5} = \frac{\int_0^\infty [\ddot{M}_0(t)]^2 dt}{10\pi \rho \beta^5}. \quad (4.27)$$

These formulae indeed represent the source (i.e., its integrated source time function), but to convert observed E_P or E_S to the source property, we need to use the radiated energy measured at the far-field.

4.7 Question 7

The point force solution described in the Cartesian coordinates, only showing the far-field components, is

$$u_i = F_j * G_{ij} = \frac{\gamma_i \gamma_j}{4\pi \rho \alpha^2 r} F_j \left(t - \frac{r}{\alpha} \right) - \frac{\gamma_i \gamma_j - \delta_{ij}}{4\pi \rho \beta^2} F_j \left(t - \frac{r}{\beta} \right). \quad (4.28)$$

In vector form, with $\hat{\gamma} = \hat{\mathbf{r}}$, we have

$$\mathbf{u} = \frac{\hat{\mathbf{r}}(\hat{\mathbf{r}} \cdot \mathbf{F})}{4\pi \rho \alpha^2 r} + \frac{\mathbf{F} - \hat{\mathbf{r}}(\hat{\mathbf{r}} \cdot \mathbf{F})}{4\pi \rho \beta^2 r}. \quad (4.29)$$

Since in the spherical polar coordinates, there is identity $\mathbf{F} = (\hat{\mathbf{r}} \cdot \mathbf{F}) \hat{\mathbf{r}} + (\hat{\theta} \cdot \mathbf{F}) \hat{\theta} + (\hat{\phi} \cdot \mathbf{F}) \hat{\phi}$, which is simply the projection of a vector onto the basis vectors, we thus obtain

$$\mathbf{u} = \frac{\hat{\mathbf{r}}(\hat{\mathbf{r}} \cdot \mathbf{F})}{4\pi \rho \alpha^2 r} + \frac{\hat{\theta}(\hat{\theta} \cdot \mathbf{F}) + \hat{\phi}(\hat{\phi} \cdot \mathbf{F})}{4\pi \rho \beta^2 r}. \quad (4.30)$$

Each component can be written as

$$u_i = F_j * G_{ij} = \frac{1}{4\pi \rho \alpha^2} \frac{\hat{r}_i \hat{r}_j}{r} F_j \left(t - \frac{r}{\alpha} \right) + \frac{1}{4\pi \rho \beta^2} \frac{\hat{\theta}_i \hat{\theta}_j + \hat{\phi}_i \hat{\phi}_j}{r} F_j \left(t - \frac{r}{\beta} \right). \quad (4.31)$$

4.8 Question 8

Start from the ray equation

$$\frac{d\mathbf{x}}{ds} = c\nabla T. \quad (4.32)$$

We choose a scalar variable σ to define the position along the ray with

$$\frac{d\sigma}{ds} = c(\mathbf{x}(s)), \quad \sigma(s) = \int_0^s c(\mathbf{x}(s)) ds, \quad (4.33)$$

which represents the integral of wave speed along the ray path. Therefore, we have

$$\frac{d\mathbf{x}}{ds} = \frac{d\mathbf{x}}{d\sigma} \frac{d\sigma}{ds} = c\nabla T, \quad \frac{d\mathbf{x}}{d\sigma} = \nabla T. \quad (4.34)$$

When deriving the differential equation for a ray, we have the following result

$$\frac{d}{ds} \nabla T = \frac{c}{2} \nabla \left(\frac{1}{c^2} \right). \quad (4.35)$$

Similarly, we can obtain

$$\frac{d^2\mathbf{x}}{d\sigma^2} = \frac{d}{d\sigma} \nabla T = \frac{1}{2} \nabla \left(\frac{1}{c^2} \right), \quad (4.36)$$

which demonstrates that solving for a ray path is equivalent to solving for the motion of a particle moving in a force field with potential $1/(2c^2)$.

4.9 Question 9

As the wave speed $c(z)$ only depends on depth z , the ray paths are within the xz -plane. From Snell's law, we know

$$p = \frac{\sin i}{c(z)} = \text{const.} \quad (4.37)$$

The angle i is the one between the z -direction (downward) and the ray. It also depends on ray distance s (although the function dependence is not explicitly written out). The ray equation is

$$\frac{dx}{ds} = \sin i, \quad \frac{dz}{ds} = \cos i. \quad (4.38)$$

With $c(z) = az + b$, Eqs (4.37) and (4.38) lead to

$$\sin i = p(az + b), \quad \cos i \cdot \frac{di}{ds} = pa \cdot \frac{dz}{ds} = pa \cdot \cos i. \quad (4.39)$$

Therefore, we obtain the following result

$$\frac{1}{R} = \left| \frac{di}{ds} \right| = |pa| = \text{const}, \quad (4.40)$$

which indicates that the radius of curvature R is a constant, and the ray path is thus a circular arc with radius $R = |pa|^{-1}$. To find the center of the circle, we can first solve for the ray turning depth z_m , which is

$$c(z_m) = az_m + b = \frac{1}{p}, \quad z_m = \frac{1}{pa} - \frac{b}{a} = R - \frac{b}{a}. \quad (4.41)$$

Hence, the center of the circle lies at the depth $z = -b/a$.

A more general way is to directly apply the definition of the radius of curvature R . Denoting the ray path as $z = z(x)$

for the portion with well-defined $z(x)$, we have

$$R = \frac{[1 + (z')^2]^{\frac{3}{2}}}{|z''|}. \quad (4.42)$$

The derivatives can be obtained as

$$z' = \frac{dz}{dx} = \cot i, \quad z'' = \frac{d^2z}{dx^2} = -\frac{1}{\sin^2 i} \cdot \frac{di}{dx}. \quad (4.43)$$

From the Snell's law in Eq. (4.37), we have

$$\sin i = pc(z), \quad \cos i \cdot \frac{di}{dx} = pc'(z) \frac{dz}{dx}, \quad \frac{di}{dx} = \frac{pc'(z)}{\sin i}. \quad (4.44)$$

Therefore, the radius of curvature is evaluated as

$$R = \frac{(1 + \cot^2 i)^{\frac{3}{2}}}{|pc'(z)/\sin^3 i|} = \frac{1}{|pc'(z)|}. \quad (4.45)$$

With $c(z) = az + b$, we have a constant $R = |pa|^{-1}$.

For a spherically symmetric medium, Snell's law and the ray equation now become

$$p = \frac{r \sin i}{c(r)} = \text{const.} \quad \frac{r d\theta}{ds} = \sin i, \quad \frac{dr}{ds} = -\cos i, \quad (4.46)$$

where r and θ are the polar coordinates for the ray plane. Now denoting the ray path as $r = r(\theta)$ for the portion with well-defined $r(\theta)$, we have the following equation for the radius of curvature

$$R = \frac{(r^2 + r_\theta^2)^{\frac{3}{2}}}{|r^2 + 2r_\theta^2 - rr_{\theta\theta}|}. \quad (4.47)$$

The derivatives can be similarly obtained as

$$r_\theta = \frac{dr}{d\theta} = -r \cot i, \quad r_{\theta\theta} = \frac{d^2r}{d\theta^2} = -\cot i \cdot \frac{dr}{d\theta} + \frac{r}{\sin^2 i} \cdot \frac{di}{d\theta} = r \cot^2 i + \frac{r}{\sin^2 i} \cdot \frac{di}{d\theta}. \quad (4.48)$$

From the Snell's law, we have

$$\sin i = \frac{pc(r)}{r}, \quad \cos i \cdot \frac{di}{d\theta} = \frac{rpc'(r) - pc(r)}{r^2} \cdot \frac{dr}{d\theta}, \quad \frac{di}{d\theta} = -\frac{rpc'(r) - pc(r)}{r \sin i}. \quad (4.49)$$

Therefore, the radius of curvature is evaluated as

$$(r^2 + r_\theta^2)^{\frac{3}{2}} = \frac{r^3}{\sin^3 i}, \quad |r^2 + 2r_\theta^2 - rr_{\theta\theta}| = \frac{r^2}{\sin^2 i} \left| 1 - \frac{di}{d\theta} \right|, \quad (4.50)$$

$$R = \frac{r^2}{\left| r \sin i - r \sin i \cdot \frac{di}{d\theta} \right|} = \frac{r}{|pc'(r)|}. \quad (4.51)$$

With $c(r) = a - br^2$, we have a constant $R = |2pb|^{-1}$, and thus the ray paths are circular arcs. We can also solve for the ray turning radius r_m , which satisfies

$$\frac{pc(r_m)}{r_m} = 1, \quad r_m^2 + \frac{r_m}{pb} - \frac{a}{b} = 0. \quad (4.52)$$

4.10 Question 10

In this problem, the unit tangent along a ray is \mathbf{l} , and the travel time gradient is $\nabla T = \mathbf{l}/c$.

a) Since the curl of a gradient is zero, we have

$$\nabla \times \left(\frac{\mathbf{l}}{c} \right) = \nabla \times (\nabla T) = \mathbf{0}. \quad (4.53)$$

b) Using the identity $\nabla \times (\psi \mathbf{A}) = \psi (\nabla \times \mathbf{A}) + (\nabla \psi) \times \mathbf{A}$, we have

$$\nabla \times \mathbf{l} = \nabla \times (c \nabla T) = \nabla c \times \left(\frac{\mathbf{l}}{c} \right) = \left(\frac{\nabla c}{c} \right) \times \mathbf{l} = -c \mathbf{l} \times \left(\frac{\nabla c}{c^2} \right) = c \mathbf{l} \times \nabla \left(\frac{1}{c} \right). \quad (4.54)$$

c) We know the differential equation for a ray (eq. 4.44 in the book) is

$$\mathbf{l} = \frac{d\mathbf{x}}{ds}, \quad \frac{d}{ds} \left(\frac{1}{c} \frac{d\mathbf{x}}{ds} \right) = \nabla \left(\frac{1}{c} \right). \quad (4.55)$$

This leads to

$$\frac{d}{ds} \left(\frac{1}{c} \frac{d\mathbf{x}}{ds} \right) = \frac{1}{c} \frac{d\mathbf{l}}{ds} + \mathbf{l} \frac{d}{ds} \left(\frac{1}{c} \right) = \nabla \left(\frac{1}{c} \right), \quad \frac{d\mathbf{l}}{ds} = c \nabla \left(\frac{1}{c} \right) - c \mathbf{l} \frac{d}{ds} \left(\frac{1}{c} \right). \quad (4.56)$$

On the other hand, using the triple product expansion $(\mathbf{a} \times \mathbf{b}) \times \mathbf{c} = \mathbf{b}(\mathbf{c} \cdot \mathbf{a}) - \mathbf{a}(\mathbf{b} \cdot \mathbf{c})$, we have

$$(\nabla \times \mathbf{l}) \times \mathbf{l} = \left[c \mathbf{l} \times \nabla \left(\frac{1}{c} \right) \right] \times \mathbf{l} = c \nabla \left(\frac{1}{c} \right) - c \mathbf{l} \left[\mathbf{l} \cdot \nabla \left(\frac{1}{c} \right) \right]. \quad (4.57)$$

Finally, note that the derivative along the ray path d/ds can be expanded as

$$\frac{d}{ds} = \frac{d\mathbf{x}}{ds} \cdot \nabla = \mathbf{l} \cdot \nabla. \quad (4.58)$$

Therefore, we prove that

$$(\nabla \times \mathbf{l}) \times \mathbf{l} = \frac{d\mathbf{l}}{ds}. \quad (4.59)$$

d) Based on the following result

$$\nabla (\ln c) = \frac{\nabla c}{c} = -c \nabla \left(\frac{1}{c} \right), \quad (4.60)$$

Eq. (4.57) can be modified to

$$\frac{d\mathbf{l}}{ds} = c \nabla \left(\frac{1}{c} \right) - \left[c \mathbf{l} \cdot \nabla \left(\frac{1}{c} \right) \right] \mathbf{l} = [\mathbf{l} \cdot \nabla (\ln c)] \mathbf{l} - \nabla (\ln c). \quad (4.61)$$

e) Using the forward Euler scheme, we have

$$\frac{d\mathbf{x}}{ds} = \mathbf{l} \quad \rightarrow \quad \mathbf{x}_{m+1} = \mathbf{x}_m + \Delta s \mathbf{l}_m, \quad (4.62)$$

$$\frac{d\mathbf{l}}{ds} = [\mathbf{l} \cdot \nabla (\ln c)] \mathbf{l} - \nabla (\ln c) \quad \rightarrow \quad \mathbf{l}_{m+1} = \mathbf{l}_m + \Delta s [(\mathbf{l}_m \cdot \mathbf{g}_m) \mathbf{l}_m - \mathbf{g}_m], \quad (4.63)$$

where $\mathbf{g} = \nabla (\ln c)$ and the subscript m denotes variables evaluated at step m .

f) We can further simplify Eq. (4.61) as

$$\frac{d\mathbf{l}}{ds} = -\frac{\nabla c}{c} + \left(\mathbf{l} \cdot \frac{\nabla c}{c} \right) \mathbf{l}. \quad (4.64)$$

Using the orthogonal unit vectors \mathbf{l} and \mathbf{n} , the gradient of the wave speed can be described as $\nabla c = \alpha \mathbf{l} + \beta \mathbf{n}$ with $\alpha, \beta \in \mathbb{R}$. Therefore, the change of ray direction becomes

$$\frac{d\mathbf{l}}{ds} = -\frac{\alpha \mathbf{l} + \beta \mathbf{n}}{c} + \frac{\alpha \mathbf{l}}{c} = \frac{\beta \mathbf{n}}{c}. \quad (4.65)$$

If \mathbf{l} is parallel to ∇c , we have $\beta = 0$, $d\mathbf{l}/ds = \mathbf{0}$ and thus \mathbf{l} does not change direction along the ray. If \mathbf{l} is perpendicular to ∇c , we have $\alpha = 0$ and β reaches the largest magnitude at this location, which implies that the ray changes direction at the maximum rate here.

4.11 Question 11

For P -wave generated by a shear dislocation with scalar moment $M_0(t)$, the far-field and intermediate-field terms are (from eq. 4.32 in the book)

$$\mathbf{u}^P(\mathbf{x}, t) = \frac{1}{4\pi\rho\alpha^3} \mathbf{A}^{FP} \frac{1}{r} \dot{M}_0 \left(t - \frac{r}{\alpha} \right) + \frac{1}{4\pi\rho\alpha^2} \mathbf{A}^{IP} \frac{1}{r^2} M_0 \left(t - \frac{r}{\alpha} \right). \quad (4.66)$$

Only focused on the radial component, the radiation patterns \mathbf{A}^{FP} and \mathbf{A}^{IP} become (from eq. 4.33 in the book)

$$\mathbf{A}^{FP} \cdot \hat{\mathbf{r}} = \sin 2\theta \cos \phi, \quad \mathbf{A}^{IP} \cdot \hat{\mathbf{r}} = 4 \sin 2\theta \cos \phi. \quad (4.67)$$

Now with $T^P = r/\alpha$ as the travel time, the P -wave displacement pulse shape is proportional to

$$u_r^P(\mathbf{x}, t) \propto \dot{M}_0 \left(t - T^P \right) + \frac{4\alpha}{r} M_0 \left(t - T^P \right) = \dot{M}_0 \left(t - T^P \right) + \frac{4}{T^P} M_0 \left(t - T^P \right). \quad (4.68)$$

4.12 Question 12

The rays whose travel times are stationary but not minima correspond to surface-reflected phases. As an example shown in Fig. 4.4, consider the true ray path $A-P_0-B$ with the surface reflection point P_0 . Without losing generality, we assume that the radius of the sphere is $R = 1$ and A is the North pole with coordinate $(\theta, \phi) = (0, 0)$. Under this coordinate system, we can set $P_0 = (\theta, 0)$ and $B = (2\theta, 0)$. The distance of the true ray path can be calculated as

$$L_0 = \overline{AP_0} + \overline{P_0B} = 4 \sin \left(\frac{\theta}{2} \right). \quad (4.69)$$

Now consider another $P = (\theta_P, 0)$ which is not the true surface reflection point. The path length can be calculated as

$$L(P) = \overline{AP} + \overline{PB} = 2 \left[\sin \left(\frac{\theta_P}{2} \right) + \sin \left(\theta - \frac{\theta_P}{2} \right) \right] = 4 \sin \left(\frac{\theta}{2} \right) \cos \left(\frac{\theta - \theta_P}{2} \right). \quad (4.70)$$

Therefore, we always have $L(P) < L_0$ as long as $P \neq P_0$. By taking the derivative, we can also show that

$$\frac{\partial L}{\partial \theta_P} = 2 \sin \left(\frac{\theta}{2} \right) \sin \left(\frac{\theta - \theta_P}{2} \right) = 0 \quad \text{at } \theta_P = \theta. \quad (4.71)$$

This demonstrates that the true ray path corresponds to a travel time that is stationary, and moreover, is maximal along the θ -direction. On the other hand, along the ϕ -direction, the travel time should be minimal.

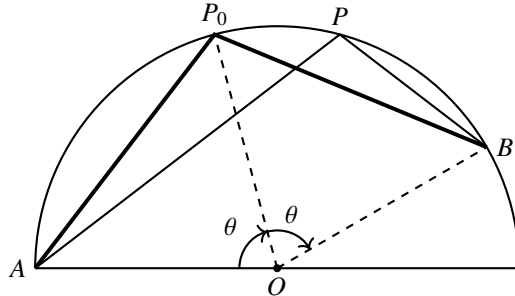


Fig. 4.4 Illustration of the surface-reflected phase in a homogeneous sphere. The true ray path is $A-P_0-B$ with P_0 being the midpoint of the arc, while P denotes the perturbed surface reflection point.

4.13 Question 13

Consider a Cartesian coordinate system with x -, y -, and z -directions in the North, East, and Down directions, respectively. The Cartesian components of moment tensor \mathbf{M} are related to the components of fault slip $\bar{\mathbf{u}}$ and fault normal $\boldsymbol{\nu}$ as

$$M_{pq} = \mu A (\bar{u}_p v_q + \bar{u}_q v_p). \quad (4.72)$$

a) If we have $M_{xz} = M_{zx} \neq 0$ as the only non-zero components, the shear faulting can have two potential setups.

1. A horizontal fault plane ($\boldsymbol{\nu} = \hat{\mathbf{e}}_z$) with slip in the North direction ($\bar{\mathbf{u}} = \bar{u} \hat{\mathbf{e}}_x$).
2. A vertical fault plane following East-West strike direction ($\boldsymbol{\nu} = \hat{\mathbf{e}}_x$) with slip in the vertical direction ($\bar{\mathbf{u}} = \bar{u} \hat{\mathbf{e}}_z$).

b) As already shown in **a)**, there are two scenarios corresponding to the same moment tensor.

c) If we have $M_{xz} = M_{zx} \neq 0$ and $M_{yz} = M_{zy} \neq 0$ as the only non-zero components, we can first consider a horizontal fault plane ($\boldsymbol{\nu} = \hat{\mathbf{e}}_z$) and then sum up the fault slips. The total fault slip can be obtained as

$$\bar{\mathbf{u}} = \frac{M_{xz}}{\mu A} \hat{\mathbf{e}}_x + \frac{M_{yz}}{\mu A} \hat{\mathbf{e}}_y, \quad \text{in the direction } \phi = \arctan \left(\frac{M_{yz}}{M_{xz}} \right). \quad (4.73)$$

Note that the direction ϕ is with respect to the x -axis, pointing toward the y -axis. Therefore, this moment tensor can have two potential setups.

1. A horizontal fault plane ($\boldsymbol{\nu} = \hat{\mathbf{e}}_z$) with slip in the ϕ direction.
2. A vertical fault plane whose strike is orthogonal to the ϕ direction, with slip in the vertical direction ($\bar{\mathbf{u}} = \bar{u} \hat{\mathbf{e}}_z$).

d) Based on the Hooke's Law for an isotropic solid elastic medium, we have

$$e_{zx} = \frac{\tau_{zx}}{2\mu}, \quad e_{zy} = \frac{\tau_{zy}}{2\mu}. \quad (4.74)$$

At the traction-free surface of the Earth, there are no shear strains e_{zx} and e_{zy} .

4.14 Question 14

For a **shear dislocation** of arbitrary orientation, its moment tensor \mathbf{M} can be decomposed into four elementary moment tensors (Box 4.4 in the book)

$$\mathbf{M} = \mathbf{M}^{(1)} \cos \delta \cos \lambda + \mathbf{M}^{(2)} \sin \delta \cos \lambda - \mathbf{M}^{(3)} \cos 2\delta \sin \lambda + \mathbf{M}^{(4)} \sin 2\delta \sin \lambda. \quad (4.75)$$

The elementary matrices $\mathbf{M}^{(2)}$ and $\mathbf{M}^{(4)}$ are given as

$$\mathbf{M}^{(2)}(\phi_s) = M_0 \begin{bmatrix} -\sin 2\phi_s & \cos 2\phi_s & 0 \\ \cos 2\phi_s & \sin 2\phi_s & 0 \\ 0 & 0 & 0 \end{bmatrix}, \quad \mathbf{M}^{(4)}(\phi_s) = M_0 \begin{bmatrix} -\sin^2 \phi_s & \frac{1}{2} \sin 2\phi_s & 0 \\ \frac{1}{2} \sin 2\phi_s & -\cos^2 \phi_s & 0 \\ 0 & 0 & 1 \end{bmatrix}. \quad (4.76)$$

For this problem, we denote

$$\tilde{\mathbf{M}}^{(2)} = \mathbf{M}^{(2)}(\phi_s), \quad \tilde{\mathbf{M}}^{(4)} = \mathbf{M}^{(4)}\left(\phi_s^{(4)}\right), \quad \text{with } \phi_s^{(4)} = \phi_s + \frac{\pi}{4}. \quad (4.77)$$

Since we have

$$\sin^2 \phi_s^{(4)} = \frac{1 + \sin 2\phi_s}{2}, \quad \cos^2 \phi_s^{(4)} = \frac{1 - \sin 2\phi_s}{2}, \quad \sin 2\phi_s^{(4)} = \cos 2\phi_s, \quad (4.78)$$

when the strike of the $\tilde{\mathbf{M}}^{(4)}$ dislocation is $\pi/4$ greater than that of the $\tilde{\mathbf{M}}^{(2)}$ dislocation, we have

$$\frac{1}{2}\tilde{\mathbf{M}}^{(2)} = \tilde{\mathbf{M}}^{(4)} + M_0 \begin{bmatrix} \frac{1}{2} & 0 & 0 \\ 0 & \frac{1}{2} & 0 \\ 0 & 0 & -1 \end{bmatrix}. \quad (4.79)$$

Note that $\tilde{\mathbf{M}}^{(2)}$ represents a vertical strike-slip fault, while $\tilde{\mathbf{M}}^{(4)}$ represents a thrust fault dipping at 45° with pure up-dip slip, but having a strike angle that is 45° greater.

We now focus on the radiation pattern of the far-field SH waves. Note that the second term on the right-hand side of Eq. (4.79) represents a CLVD source. For an arbitrary moment tensor, the far-field S wave is (eq. 4.29 in the book)

$$u_n^{FS} = -\left(\frac{\gamma_n \gamma_p - \delta_{np}}{4\pi \rho \beta^3}\right) \gamma_q \frac{1}{r} \dot{M}_{pq} \left(t - \frac{r}{\beta}\right). \quad (4.80)$$

For a CLVD source, the displacement becomes

$$u_n^{FS} \propto -\frac{1}{2} (\gamma_n \gamma_1 - \delta_{n1}) \gamma_1 - \frac{1}{2} (\gamma_n \gamma_2 - \delta_{n2}) \gamma_2 + (\gamma_n \gamma_3 - \delta_{n3}) \gamma_3, \quad (4.81)$$

where $\hat{\gamma}$ is the same as the radial direction $\hat{\mathbf{r}}$ in the spherical coordinate. The SH direction then corresponds to $\hat{\phi}$, which has $\phi_3 = 0$ and is orthogonal to $\hat{\gamma}$, stated as below

$$\hat{\phi} = (-\sin \phi, \cos \phi, 0), \quad \hat{\gamma} \cdot \hat{\phi} = \gamma_n \phi_n = \gamma_1 \phi_1 + \gamma_2 \phi_2 = 0. \quad (4.82)$$

Therefore, we can show that

$$\mathbf{u}^{FS} \cdot \hat{\phi} = u_n^{FS} \phi_n \propto -\frac{1}{2} \gamma_n \phi_n (\gamma_1^2 + \gamma_2^2 - 2\gamma_3^2) + \frac{1}{2} (\gamma_1 \phi_1 + \gamma_2 \phi_2 - 2\gamma_3 \phi_3) = 0, \quad (4.83)$$

which indicates that a CLVD source does not contribute to far-field SH waves. Hence, the two elementary moment tensors $\tilde{\mathbf{M}}^{(2)}/2$ and $\tilde{\mathbf{M}}^{(4)}$ have the same radiation pattern, and thus generate same SH waves in a spherically symmetric Earth.

However, if the sources are in an isotropic but laterally inhomogeneous Earth, the heterogeneity can couple the P-SV and SH systems together, so a CLVD source can also contribute to SH waves and the above conclusion will be changed.

5 Chapter 5: Plane Waves in Homogeneous Media and their Reflection and Transmission at a Plane Boundary

5.1 Question 1

Start from the inhomogeneous P-wave and SV-wave given in eqns (5.52) and (5.53) in the book

$$\hat{P} \left(\alpha p, 0, i\sqrt{\alpha^2 p^2 - 1} \right) \exp \left(-\omega \sqrt{p^2 - \frac{1}{\alpha^2}} z \right) \exp [i\omega(px - t)], \quad (5.1)$$

$$\hat{S} \left(i\sqrt{\beta^2 p^2 - 1}, 0, -\beta p \right) \exp \left(-\omega \sqrt{p^2 - \frac{1}{\beta^2}} z \right) \exp [i\omega(px - t)], \quad \text{with } \frac{1}{\alpha} < \frac{1}{\beta} < p. \quad (5.2)$$

For a rigid surface, we have $u_x = u_z = 0$ at $z = 0$. These two conditions give

$$\begin{cases} \alpha p \hat{P} + i\sqrt{\beta^2 p^2 - 1} \hat{S} = 0, \\ i\sqrt{\alpha^2 p^2 - 1} \hat{P} - \beta p \hat{S} = 0. \end{cases} \quad (5.3)$$

The determinant of coefficients should vanish, which leads to

$$-\alpha\beta p^2 + \sqrt{\alpha^2 p^2 - 1} \sqrt{\beta^2 p^2 - 1} = 0, \quad \alpha^2 p^2 + \beta^2 p^2 = 1. \quad (5.4)$$

However, when $\alpha^{-1} < \beta^{-1} < p$ we always have $\alpha^2 p^2 + \beta^2 p^2 > 2$. This implies that Eq. (5.4) does not have a solution, and there can be no corresponding surface wave of tractions when the surface is rigid.

5.2 Question 2

At the boundary between two homogeneous half-spaces, the interface SH-wave is given as

$$\hat{S} \exp \left(\omega \sqrt{p^2 - \frac{1}{\beta_1^2}} z \right) \exp [i\omega(px - t)], \quad (5.5)$$

$$\hat{S} \exp \left(-\omega \sqrt{p^2 - \frac{1}{\beta_2^2}} z \right) \exp [i\omega(px - t)], \quad \text{with } p > \max \left\{ \frac{1}{\beta_1}, \frac{1}{\beta_2} \right\}. \quad (5.6)$$

The continuity of displacement u_y and shear traction τ_{yz} at $z = 0$ gives

$$\begin{cases} \hat{S} - \hat{S} = 0, \\ \sqrt{p^2 - \frac{1}{\beta_1^2}} \hat{S} + \sqrt{p^2 - \frac{1}{\beta_2^2}} \hat{S} = 0. \end{cases} \quad (5.7)$$

There is no appropriate p that can make the determinant of coefficients. Hence, there is no interface SH-wave at the boundary between two homogeneous half-spaces.

5.3 Question 3

For a solid half-space $z > 0$, the P-SV scattering matrix can be obtained from eq. (5.34) in the book, by setting all amplitudes in medium 1 to zero and choosing the appropriate equations for boundary conditions. We then rearrange them into a convenient form to obtain the scattering matrix, as shown below

$$\mathbf{M} \begin{bmatrix} \hat{P} \\ \hat{S} \end{bmatrix} = \mathbf{N} \begin{bmatrix} \hat{P} \\ \hat{S} \end{bmatrix}, \quad \mathbf{M}^{-1} \mathbf{N} = \begin{bmatrix} \hat{P}\hat{P} & \hat{S}\hat{P} \\ \hat{P}\hat{S} & \hat{S}\hat{S} \end{bmatrix}. \quad (5.8)$$

a) When we set $u_z = 0$ and $\tau_{zx} = 0$ on $z = 0$, we obtain

$$\begin{cases} \cos i (\dot{P} - \dot{P}') - \sin j (\dot{S} - \dot{S}') = 0, \\ 2\beta p \cos i (\dot{P} - \dot{P}') + (1 - 2\beta^2 p^2) (\dot{S} - \dot{S}') = 0. \end{cases} \quad (5.9)$$

In this case, we have

$$\mathbf{M} = \mathbf{N} = \begin{bmatrix} \cos i & -\sin j \\ 2\beta p \cos i & 1 - 2\beta^2 p^2 \end{bmatrix}, \quad \mathbf{M}^{-1} \mathbf{N} = \begin{bmatrix} \dot{P}\dot{P}' & \dot{S}\dot{P}' \\ \dot{P}\dot{S}' & \dot{S}\dot{S}' \end{bmatrix} = \begin{bmatrix} 1 & 0 \\ 0 & 1 \end{bmatrix}. \quad (5.10)$$

b) When we set $u_x = 0$ and $\tau_{zz} = 0$ on $z = 0$, we obtain

$$\begin{cases} \sin i (\dot{P} + \dot{P}') + \cos j (\dot{S} + \dot{S}') = 0, \\ \alpha(1 - 2\beta^2 p^2) (\dot{P} + \dot{P}') - 2\beta^2 p \cos j (\dot{S} + \dot{S}') = 0. \end{cases} \quad (5.11)$$

In this case, we have

$$\mathbf{M} = -\mathbf{N} = \begin{bmatrix} \sin i & \cos j \\ \alpha(1 - 2\beta^2 p^2) & -2\beta^2 p \cos j \end{bmatrix}, \quad \mathbf{M}^{-1} \mathbf{N} = \begin{bmatrix} \dot{P}\dot{P}' & \dot{S}\dot{P}' \\ \dot{P}\dot{S}' & \dot{S}\dot{S}' \end{bmatrix} = \begin{bmatrix} -1 & 0 \\ 0 & -1 \end{bmatrix}. \quad (5.12)$$

Therefore, by adding the reflections derived from the above two sets of boundary conditions, all downward reflections are eliminated. This trick can be useful in numerical methods to eliminate unwanted reflections from grid boundaries.

5.4 Question 4

a) The inhomogeneous P-wave and S-wave are again shown below

$$\dot{P} \left(\alpha p, 0, i\sqrt{\alpha^2 p^2 - 1} \right) \exp \left(-\omega \sqrt{p^2 - \frac{1}{\alpha^2}} z \right) \exp [i\omega(px - t)], \quad (5.13)$$

$$\dot{S} \left(i\sqrt{\beta^2 p^2 - 1}, 0, -\beta p \right) \exp \left(-\omega \sqrt{p^2 - \frac{1}{\beta^2}} z \right) \exp [i\omega(px - t)], \quad \text{with } \frac{1}{\alpha} < \frac{1}{\beta} < p. \quad (5.14)$$

Taking the real part of the expression gives

$$\mathbf{u}_P \propto \left(\alpha p \cos [\omega(px - t)], 0, -\sqrt{\alpha^2 p^2 - 1} \sin [\omega(px - t)] \right), \quad (5.15)$$

$$\mathbf{u}_{SV} \propto \left(\sqrt{\beta^2 p^2 - 1} \sin [\omega(px - t)], 0, \beta p \cos [\omega(px - t)] \right). \quad (5.16)$$

The plane waves propagate in the $+x$ -direction and note that $+z$ -direction points **downward**. To determine the particle motion, we can set $x = 0$ and consider the time $t = 0$ to $t = 0^+$. In the xz -plane, we have the following analysis:

- P-wave goes from $(\alpha p, 0)$ at $t = 0$ to $(\alpha p-, 0+)$ at $t = 0^+$, corresponding to a prograde motion.
- SV-wave goes from $(0, \beta p)$ at $t = 0$ to $(0-, \beta p-)$ at $t = 0^+$, corresponding to a prograde motion.

b) & c) The free surface boundary conditions constrain the ratio between \dot{P} and \dot{S} . From eq. (5.54) in the book, we have

$$\dot{S} = i \frac{2p\beta\sqrt{\alpha^2 p^2 - 1}}{2\beta^2 p^2 - 1} \dot{P}. \quad (5.17)$$

Adding Eqs (5.13) and (5.14) together with this amplitude ratio, at the free surface $z = 0$, the real part gives

$$u_x^R \propto \left(\alpha p - \frac{2p\beta\sqrt{\alpha^2 p^2 - 1}\sqrt{\beta^2 p^2 - 1}}{2\beta^2 p^2 - 1} \right) \cos [\omega(px - t)] = A_x \cos [\omega(px - t)], \quad (5.18)$$

$$u_z^R \propto - \left(\sqrt{\alpha^2 p^2 - 1} - \frac{2\beta^2 p^2 \sqrt{\alpha^2 p^2 - 1}}{2\beta^2 p^2 - 1} \right) \sin [\omega(px - t)] = A_z \sin [\omega(px - t)]. \quad (5.19)$$

We need to determine the signs of A_x and A_z . From the Rayleigh function (eq. 5.56 in the book), we can obtain

$$\sqrt{\alpha^2 p^2 - 1} \sqrt{\beta^2 p^2 - 1} = \frac{\alpha}{4p^2 \beta^3} (2\beta^2 p^2 - 1)^2. \quad (5.20)$$

The amplitudes A_x and A_z can be simplified to

$$A_x = \frac{\alpha}{2p\beta^2} > 0, \quad A_z = \frac{\sqrt{\alpha^2 p^2 - 1}}{2\beta^2 p^2 - 1} > 0. \quad (5.21)$$

This implies that the particle motion for the free surface is retrograde elliptical.

- d) The exponential decay for the P-wave amplitude is faster. At sufficient depth, the sum of the two components will be dominated by SV-wave, which itself is prograde elliptical.

Note The above result is consistent with the displacement vector given in the book. The complex displacement field at $z = 0$ can be derived as

$$\tilde{u}_x^R = i\dot{S} \left(-\frac{\alpha}{2\beta} \cdot \frac{2\beta^2 p^2 - 1}{\sqrt{\alpha^2 p^2 - 1}} + \sqrt{\beta^2 p^2 - 1} \right) \exp [i\omega(px - t)], \quad (5.22)$$

$$\tilde{u}_z^R = \dot{S} \left(\frac{2\beta^2 p^2 - 1}{2\beta p} - \beta p \right) \exp [i\omega(px - t)] = \frac{-\dot{S}}{2\beta p} \exp [i\omega(px - t)]. \quad (5.23)$$

Again, using Eq. (5.20) to substitute $\sqrt{\alpha^2 p^2 - 1}$, we can show that

$$\tilde{u}_x^R = -\frac{i\dot{S}\sqrt{\beta^2 p^2 - 1}}{2\beta^2 p^2 - 1} \exp [i\omega(px - t)], \quad \tilde{u}_z^R = \frac{2i\beta p\sqrt{\beta^2 p^2 - 1}}{2\beta^2 p^2 - 1}. \quad (5.24)$$

Note that $p = c_R^{-1}$ for Rayleigh wave. For the expressions given in the book, we can similarly calculate

$$\frac{\tilde{u}_x^R}{\tilde{u}_z^R} = \frac{2i}{c_R} \sqrt{\frac{1}{c_R^2} - \frac{1}{\beta^2}} \cdot \left(\frac{2}{c_R^2} - \frac{1}{\beta^2} \right)^{-1} = \frac{2ip\sqrt{p^2 - \beta^{-2}}}{2p^2 - \beta^{-2}} = \frac{2i\beta p\sqrt{\beta^2 p^2 - 1}}{2\beta^2 p^2 - 1}. \quad (5.25)$$

Therefore, we can also write out the complex displacement field using the vector given in the book.

5.5 Question 5

We only need to compare the signs of the Rayleigh wave amplitudes, as given in Eqs (5.23) and (5.24), with those for the pure SV-wave which dominates at sufficient depth, as given in Eq. (5.14). It is the horizontal (and not the vertical) component of the Rayleigh wave that goes through zero as depth increases.

	$\text{Im } \{A_x\}$	$\text{Re } \{A_z\}$
Rayleigh	$-\frac{\dot{S}\sqrt{\beta^2 p^2 - 1}}{2\beta^2 p^2 - 1} < 0$	$\frac{-\dot{S}}{2\beta p} < 0$
SV-wave	$\dot{S}\sqrt{\beta^2 p^2 - 1} > 0$	$-\dot{S}\beta p < 0$

5.6 Question 6

For a P-wave incident from below, the total displacement at the free surface $z = 0$ is

$$\mathbf{u}_P = \check{P} \left(\sin i + \check{P}\check{P} \sin i + \check{P}\check{S} \cos j, 0, -\cos i + \check{P}\check{P} \cos i - \check{P}\check{S} \sin j \right) \exp [i\omega(px - t)]. \quad (5.26)$$

Similarly, for an SV-wave incident from below, we have

$$\mathbf{u}_{SV} = \check{S} \left(\cos j + \check{S}\check{P} \sin i + \check{S}\check{S} \cos j, 0, \sin j + \check{S}\check{P} \cos i - \check{S}\check{S} \sin j \right) \exp [i\omega(px - t)]. \quad (5.27)$$

Denote the following symbols

$$m = \frac{1}{\beta^2} - 2p^2, \quad s_\alpha = 2p \frac{\cos i}{\alpha}, \quad s_\beta = 2p \frac{\cos j}{\beta}. \quad (5.28)$$

The displacement reflection coefficients can be simply expressed as

$$\check{P}\check{P} = \frac{-m^2 + s_\alpha s_\beta}{m^2 + s_\alpha s_\beta}, \quad \check{P}\check{S} = \frac{2\alpha}{\beta} \frac{ms_\alpha}{m^2 + s_\alpha s_\beta}, \quad \check{S}\check{P} = \frac{2\beta}{\alpha} \frac{ms_\beta}{m^2 + s_\alpha s_\beta}, \quad \check{S}\check{S} = \frac{m^2 - s_\alpha s_\beta}{m^2 + s_\alpha s_\beta}. \quad (5.29)$$

As a result, using the definition of p , we have

$$\begin{aligned} \sin i + \check{P}\check{P} \sin i + \check{P}\check{S} \cos j &= \frac{1}{m^2 + s_\alpha s_\beta} \cdot \frac{\alpha s_\alpha s_\beta}{\beta^2 p}, \\ -\cos i + \check{P}\check{P} \cos i - \check{P}\check{S} \sin j &= \frac{-m}{m^2 + s_\alpha s_\beta} \cdot \frac{\alpha s_\alpha}{\beta^2 p}, \\ \cos j + \check{S}\check{P} \sin i + \check{S}\check{S} \cos j &= \frac{m}{m^2 + s_\alpha s_\beta} \cdot \frac{s_\beta}{\beta p}, \\ \sin j + \check{S}\check{P} \cos i - \check{S}\check{S} \sin j &= \frac{1}{m^2 + s_\alpha s_\beta} \cdot \frac{s_\alpha s_\beta}{\beta p}. \end{aligned} \quad (5.30)$$

The total displacement at the free surface becomes

$$\mathbf{u}_P = \frac{\check{P} \left[\frac{4\alpha p \cos i \cos j}{\beta^2} \frac{1}{\alpha} \frac{1}{\beta}, 0, \frac{-2\alpha \cos i}{\beta^2} \left(\frac{1}{\beta^2} - 2p^2 \right) \right] \exp [i\omega(px - t)]}{\left(\frac{1}{\beta^2} - 2p^2 \right)^2 + 4p^2 \frac{\cos i \cos j}{\alpha} \frac{1}{\beta}}, \quad (5.31)$$

$$\mathbf{u}_{SV} = \frac{\check{S} \left[\frac{2 \cos j}{\beta} \left(\frac{1}{\beta^2} - 2p^2 \right), 0, \frac{4p \cos i \cos j}{\beta} \right] \exp [i\omega(px - t)]}{\left(\frac{1}{\beta^2} - 2p^2 \right)^2 + 4p^2 \frac{\cos i \cos j}{\alpha} \frac{1}{\beta}}. \quad (5.32)$$

For an SH-wave incident from below, as $\check{S}\check{S} = 1$ at the free surface, the displacement is simply doubled.

5.7 Question 7

For the incident SV-wave, using $\cos 2j = 1 - 2\beta^2 p^2$, we have

$$R(t) = \check{S}(t) \frac{2\alpha \cos j \cos 2j}{\alpha \cos^2 2j + 4p^2 \beta^3 \cos i \cos j}, \quad Z(t) = -\check{S}(t) \frac{4p\beta^2 \cos i \cos j}{\alpha \cos^2 2j + 4p^2 \beta^3 \cos i \cos j}. \quad (5.33)$$

The minus sign in $Z(t)$ is because $Z(t)$ is measured as positive upward. Also using $\sin j = \beta p$, we can see that

$$\check{S}(t) = \frac{\cos 2j}{2 \cos j} \cdot R(t) - \sin j \cdot Z(t) = \frac{1 - 2\beta^2 p^2}{2\sqrt{1 - \beta^2 p^2}} \cdot R(t) - \beta p \cdot Z(t). \quad (5.34)$$

Similarly, for the incident P-wave we have

$$R(t) = \dot{P}(t) \frac{4\rho\alpha\beta \cos i \cos j}{\alpha \cos^2 2j + 4p^2\beta^3 \cos i \cos j}, \quad Z(t) = \dot{P}(t) \frac{2\alpha \cos i \cos 2j}{\alpha \cos^2 2j + 4p^2\beta^3 \cos i \cos j}. \quad (5.35)$$

The incident waveform can be estimated as

$$\dot{P}(t) = \frac{\cos 2j}{2 \cos i} \cdot Z(t) + \frac{\beta}{\alpha} \sin j \cdot R(t) = \frac{1 - 2\beta^2 p^2}{2\sqrt{1 - \alpha^2 p^2}} \cdot Z(t) + \frac{\beta^2 p}{\alpha} \cdot R(t). \quad (5.36)$$

When $p > 1/\alpha$, we have $\sqrt{1 - \alpha^2 p^2} \rightarrow i\sqrt{\alpha^2 p^2 - 1}$, and this leads to a Hilbert transform of $Z(t)$.

5.8 Question 8

If the two half-spaces under consideration have similar properties, correct to first order in the jumps $\Delta\rho$, $\Delta\alpha$, $\Delta\beta$, the reflection coefficient $\dot{P}\dot{P}$ can be approximated as (eq. 5.46 in the book)

$$\dot{P}\dot{P} = \frac{1}{2} \left(1 - 4\beta^2 p^2 \right) \frac{\Delta\rho}{\rho} - 4\beta^2 p^2 \frac{\Delta\beta}{\beta} + \frac{1}{2 \cos^2 i} \frac{\Delta\alpha}{\alpha}. \quad (5.37)$$

Note that $p = \alpha^{-1} \sin i$ also depends on the incident angle i . At small angle we have $\cos^{-2} i \approx 1 + \sin^2 i$, and the expression is simplified to

$$\dot{P}\dot{P} \approx \frac{1}{2} \left(\frac{\Delta\rho}{\rho} + \frac{\Delta\alpha}{\alpha} \right) + B \sin^2 i, \quad \text{with } B = \frac{1}{2} \frac{\Delta\alpha}{\alpha} - 2 \frac{\beta^2}{\alpha^2} \left(\frac{\Delta\rho}{\rho} + 2 \frac{\Delta\beta}{\beta} \right). \quad (5.38)$$

This formula is related to the amplitude variation with offset analysis (AVO).

5.9 Question 9

Consider a general plane P-wave propagating in $\hat{\mathbf{k}}$ direction (longitudinal), where \mathbf{k} is the wavenumber

$$\mathbf{u}_P = A_P \hat{\mathbf{k}} \exp [i(\mathbf{k} \cdot \mathbf{x} - \omega t)]. \quad (5.39)$$

Note that the P-wave particle motion is in the propagating direction. The compressional P-wave corresponds to $A_P > 0$, and the first motion is in $\hat{\mathbf{k}}$ direction (outward). Vice versa, the first motion of the dilatational P wave is inward.

5.10 Question 10

With the plane wave factor $\exp [i\omega(px - t)]$, we can recognize

$$\frac{\partial}{\partial t} \leftrightarrow -i\omega, \quad \frac{\partial}{\partial x} \leftrightarrow i\omega p.$$

For P-SV waves, we have the equations of motion

$$-\rho\omega^2 u_x = i\omega p \tau_{xx} + \frac{\partial \tau_{xz}}{\partial z}, \quad -\rho\omega^2 u_z = i\omega p \tau_{zx} + \frac{\partial \tau_{zz}}{\partial z}. \quad (5.40)$$

The constitutive relations become

$$\tau_{xx} = i\omega p(\lambda + 2\mu)u_x + \lambda \frac{\partial u_z}{\partial z}, \quad \tau_{zz} = i\omega p\lambda u_x + (\lambda + 2\mu) \frac{\partial u_z}{\partial z}, \quad \tau_{xz} = \mu \frac{\partial u_x}{\partial z} + i\omega p\mu u_z. \quad (5.41)$$

We have $f_1(z) \sim f_4(z)$ corresponds to u_x, u_z, τ_{zx} and τ_{zz} , respectively. From the constitutive relations (eq. 5.41), we obtain

$$\frac{df_1}{dz} = -i\omega p f_2 + \frac{f_3}{\mu}, \quad \frac{df_2}{dz} = -\frac{i\omega p \lambda}{\lambda + 2\mu} f_1 + \frac{f_4}{\lambda + 2\mu}. \quad (5.42)$$

From the equations of motion (eq. 5.40), we can obtain

$$\begin{aligned}\frac{df_3}{dz} &= -\rho\omega^2 f_1 + \omega^2 p^2(\lambda + 2\mu)f_1 - i\omega p\lambda \frac{df_2}{dz} = \left[\frac{4\omega^2 p^2 \mu(\lambda + \mu)}{\lambda + 2\mu} - \rho\omega^2 \right] f_1 - \frac{i\omega p\lambda}{\lambda + 2\mu} f_4, \\ \frac{df_4}{dz} &= -\rho\omega^2 f_2 - i\omega p f_3.\end{aligned}\quad (5.43)$$

The corresponding ODE system is written in the form of

$$\frac{d}{dz} \begin{bmatrix} \tilde{u}_x \\ \tilde{u}_z \\ \tilde{\tau}_{zx} \\ \tilde{\tau}_{zz} \end{bmatrix} = \begin{bmatrix} 0 & -i\omega p & \frac{1}{\mu} & 0 \\ \frac{-i\omega p\lambda}{\lambda + 2\mu} & 0 & 0 & \frac{1}{\lambda + 2\mu} \\ \frac{4\omega^2 p^2 \mu(\lambda + \mu)}{\lambda + 2\mu} - \rho\omega^2 & 0 & 0 & \frac{-i\omega p\lambda}{\lambda + 2\mu} \\ 0 & -\rho\omega^2 & -i\omega p & 0 \end{bmatrix} \begin{bmatrix} \tilde{u}_x \\ \tilde{u}_z \\ \tilde{\tau}_{zx} \\ \tilde{\tau}_{zz} \end{bmatrix}, \quad \frac{d\mathbf{f}(z)}{dz} = \mathbf{A}\mathbf{f}(z). \quad (5.44)$$

Consider eq. (5.63) in the book, and we can show that when \mathbf{A} is constant, it is the solution of the ODE system

$$\mathbf{f} = \mathbf{v}^\alpha \exp[\lambda^\alpha(z - z_{\text{ref}})], \quad \frac{d\mathbf{f}}{dz} = \lambda^\alpha \mathbf{v}^\alpha \exp[\lambda^\alpha(z - z_{\text{ref}})] = \mathbf{A}\mathbf{v}^\alpha \exp[\lambda^\alpha(z - z_{\text{ref}})] = \mathbf{A}\mathbf{f}, \quad (5.45)$$

where λ^α and \mathbf{v}^α are the eigenvalue and eigenvector of \mathbf{A} . However, when the properties ρ, λ, μ also vary with z , we have

$$\frac{d\mathbf{f}(z)}{dz} = \mathbf{A}(z)\mathbf{f}(z). \quad (5.46)$$

Now $\lambda^\alpha(z)$ and $\mathbf{v}^\alpha(z)$ also depends on z , and thus $\mathbf{f}'(z)$ becomes more complicated and does not equal to $\mathbf{A}(z)\mathbf{f}(z)$. In fact, Eq. (5.46) does not have a close-form solution.

Note The solution of Eq. (5.44) can be expressed in the form of a matrix exponential

$$\mathbf{f}(z) = e^{\mathbf{A}(z-z_0)} \mathbf{f}_0, \quad \text{where } e^{\mathbf{X}} = \sum_{k=0}^{+\infty} \frac{\mathbf{X}^k}{k!} = \lim_{n \rightarrow \infty} \left(\mathbf{I} + \frac{\mathbf{X}}{n} \right)^n. \quad (5.47)$$

Compare with eq. (5.64) in the book, we can identify that

$$\mathbf{f}(z) = \mathbf{F}\mathbf{w}, \quad \text{with } \mathbf{F} = \mathbf{E}e^{\mathbf{A}(z-z_0)}, \quad \mathbf{w} = \mathbf{E}^{-1}\mathbf{f}_0, \quad \mathbf{A} = \mathbf{E}\mathbf{\Lambda}\mathbf{E}^{-1}, \quad (5.48)$$

where the last expression represents the diagonalization of matrix \mathbf{A} . The columns of \mathbf{E} are the eigenvectors.

5.11 Question 11

For a P-wave potential $\phi(x, z, t)$, the displacement $\mathbf{u} = (u_x, u_y, u_z)$ and traction $\mathbf{T} = (\tau_{zx}, \tau_{zy}, \tau_{zz})$ are calculated as

$$\mathbf{u}_P = \left(\frac{\partial \phi}{\partial x}, 0, \frac{\partial \phi}{\partial z} \right), \quad \mathbf{T}_P = \left(2\mu \frac{\partial^2 \phi}{\partial x \partial z}, 0, \lambda \nabla^2 \phi + 2\mu \frac{\partial^2 \phi}{\partial z^2} \right). \quad (5.49)$$

For an SV-wave potential $\psi(x, z, t)$, the displacement and traction are calculated as

$$\mathbf{u}_{SV} = \left(-\frac{\partial \psi}{\partial z}, 0, \frac{\partial \psi}{\partial x} \right), \quad \mathbf{T}_{SV} = \left(\mu \frac{\partial^2 \psi}{\partial x^2} - \mu \frac{\partial^2 \psi}{\partial z^2}, 0, 2\mu \frac{\partial^2 \psi}{\partial x \partial z} \right). \quad (5.50)$$

For a down-going P-wave $\phi = A \exp[i\omega(pz + \xi z - t)]$, we have

$$u_x = i\omega p\phi, \quad u_z = i\omega \xi \phi, \quad \tau_{zx} = -2\mu\omega^2 p\xi \phi, \quad \tau_{zz} = -\lambda \frac{\omega^2}{\alpha^2} \phi - 2\mu\omega^2 \xi^2 \phi \quad (5.51)$$

The first eigenvector \mathbf{v}^1 is related to this down-going P-wave, which is

$$\mathbf{v}^1 = \frac{-i\alpha}{\omega} \left[i\omega p, i\omega \xi, -2\omega^2 \rho \beta^2 p \xi, -\omega^2 \rho (1 - 2\beta^2 p^2) \right]^T = \left[\alpha p, \alpha \xi, 2i\omega \rho \alpha \beta^2 p \xi, i\omega \rho \alpha (1 - 2\beta^2 p^2) \right]^T. \quad (5.52)$$

For a down-going SV-wave $\psi = B \exp [i\omega(px + \eta z - t)]$, we have

$$\mathbf{v}^2 = \frac{i\beta}{\omega} \left[-i\omega \eta, i\omega p, \omega^2 \rho (1 - 2\beta^2 p^2), -2\omega^2 \rho \beta^2 p \eta \right]^T = \left[\beta \eta, -\beta p, i\omega \rho \beta (1 - 2\beta^2 p^2), -2i\omega \rho \beta^3 p \eta \right]^T. \quad (5.53)$$

For an up-going P-wave $\phi = C \exp [i\omega(px - \xi z - t)]$, we simply substitute $\xi \rightarrow -\xi$ and obtain

$$\mathbf{v}^3 = \left[\alpha p, -\alpha \xi, -2i\omega \rho \alpha \beta^2 p \xi, i\omega \rho \alpha (1 - 2\beta^2 p^2) \right]^T. \quad (5.54)$$

For an up-going SV-wave $\psi = D \exp [i\omega(px - \eta z - t)]$, we simply substitute $\eta \rightarrow -\eta$ and obtain (by reversing the sign to ensure that the first element is positive)

$$\mathbf{v}^4 = \left[\beta \eta, \beta p, -i\omega \rho \beta (1 - 2\beta^2 p^2), -2i\omega \rho \beta^3 p \eta \right]^T. \quad (5.55)$$

These wave potentials are equivalent to the wave system $\mathbf{f} = \mathbf{F}\mathbf{w}$ with

$$\mathbf{w} = \left[\frac{i\omega A}{\alpha}, \frac{-i\omega B}{\beta}, \frac{i\omega C}{\alpha}, \frac{i\omega D}{\beta} \right]^T. \quad (5.56)$$

For example, the first coefficient for the down-going P-wave is recognized by comparing Eqs (5.51) and (5.52).

5.12 Question 12

The attenuation of amplitude can be expressed as

$$A(t) = A_0 \exp \left[-\frac{\omega t}{2Q(\omega)} \right]. \quad (5.57)$$

Note that for both $\omega > 0$ and $\omega < 0$, Eq. (5.57) should give an exponential decay of the amplitude. Hence, $Q(\omega)$ should be an odd function with $Q(-\omega) = -Q(\omega)$. The pulse shape of the attenuated wave $p(x, t)$ is given by eq. (5.72) in the book

$$p(x, t) = \frac{1}{2\pi} \int_{-\infty}^{+\infty} \exp \left[-\frac{\omega x}{2cQ(\omega)} \right] \exp \left[i\omega \left(\frac{x}{c} - t \right) \right] d\omega. \quad (5.58)$$

If there is no dispersion (constant c), at a specific distance x , the Fourier transform of $p(t - x/c)$ is

$$\hat{p}(\omega) = \mathcal{F} \left\{ p \left(t - \frac{x}{c} \right) \right\} = \exp \left[-\frac{\omega x}{2cQ(\omega)} \right], \quad \hat{p}(\omega) = \hat{p}(-\omega), \quad (5.59)$$

which is an even function of ω . Therefore, the attenuated impulse is always symmetric about $t = x/c$.

5.13 Question 13

The Kramers-Krönig relation implies that the real and imaginary parts of the complex wavenumber K should satisfy

$$K = \frac{\omega}{c(\omega)} + i\alpha(\omega), \quad \frac{\omega}{c(\omega)} = \frac{\omega}{c_\infty} + \mathcal{H} \{ \alpha(\omega) \}, \quad (5.60)$$

in order to ensure causality (i.e., there is no signal when $t < x/c_\infty$). The attenuation factor $Q(\omega)$ is then, by definition, related to $\alpha(\omega)$ and $c(\omega)$ as

$$\alpha(\omega) = \frac{\omega}{2c(\omega)Q(\omega)}. \quad (5.61)$$

a) The imaginary wavenumber is given as (for $\omega > 0$)

$$\alpha(\omega) = \frac{\alpha_0\omega}{1 + \alpha_2\omega^2}, \quad \mathcal{H}\{\alpha(\omega)\} = \frac{\alpha_0}{\pi} \frac{\omega}{1 + \alpha_2\omega^2} \ln\left(\frac{1}{\alpha_2\omega^2}\right). \quad (5.62)$$

With $\alpha_2\omega^2 \ll 1$ for the seismic band, we can obtain

$$\frac{1}{c(\omega)} = \frac{1}{c_\infty} + \frac{\alpha_0}{\pi} \frac{1}{1 + \alpha_2\omega^2} \ln\left(\frac{1}{\alpha_2\omega^2}\right) \approx \frac{1}{c_\infty} + \frac{\alpha_0}{\pi} \ln\left(\frac{1}{\alpha_2\omega^2}\right). \quad (5.63)$$

The attenuation factor $Q(\omega)$ is approximately constant over the seismic frequencies

$$Q(\omega) \approx \frac{1}{2c_\infty\alpha_0} + \frac{1}{2\pi} \ln\left(\frac{1}{\alpha_2\omega^2}\right) \approx \frac{1}{2c_\infty\alpha_0}. \quad (5.64)$$

The phase velocity ratio can thus be approximated as

$$\frac{c(\omega_1)}{c(\omega_2)} \approx \left[1 + \frac{c_\infty\alpha_0}{\pi} \ln\left(\frac{1}{\alpha_2\omega^2}\right)\right] \left[1 - \frac{c_\infty\alpha_0}{\pi} \ln\left(\frac{1}{\alpha_2\omega^2}\right)\right] \approx 1 + \frac{1}{\pi Q} \ln\left(\frac{\omega_1}{\omega_2}\right). \quad (5.65)$$

b) The imaginary wavenumber is given as (for $\omega > 0$)

$$\alpha(\omega) = \alpha_0\omega [H(\omega - \omega_l) - H(\omega - \omega_h)], \quad \mathcal{H}\{\alpha(\omega)\} = \frac{\alpha_0\omega}{\pi} \ln\left(\frac{\omega_h^2 - \omega^2}{\omega^2 - \omega_l^2}\right). \quad (5.66)$$

With $\omega_l \ll \omega \ll \omega_h$ for the seismic band, we can obtain

$$\frac{1}{c(\omega)} = \frac{1}{c_\infty} + \frac{\alpha_0}{\pi} \ln\left(\frac{\omega_h^2 - \omega^2}{\omega^2 - \omega_l^2}\right) \approx \frac{1}{c_\infty} + \frac{2\alpha_0}{\pi} \ln\left(\frac{\omega_h}{\omega}\right). \quad (5.67)$$

The attenuation factor $Q(\omega)$ is approximately constant over the seismic frequencies

$$Q(\omega) \approx \frac{1}{2c_\infty\alpha_0} + \frac{1}{\pi} \ln\left(\frac{\omega_h}{\omega}\right) \approx \frac{1}{2c_\infty\alpha_0}, \quad \text{for } \omega_l < \omega < \omega_h. \quad (5.68)$$

The phase velocity ratio can thus be approximated as

$$\frac{c(\omega_1)}{c(\omega_2)} \approx \left[1 + \frac{2c_\infty\alpha_0}{\pi} \ln\left(\frac{\omega_h}{\omega_2}\right)\right] \left[1 - \frac{2c_\infty\alpha_0}{\pi} \ln\left(\frac{\omega_h}{\omega_1}\right)\right] \approx 1 + \frac{1}{\pi Q} \ln\left(\frac{\omega_1}{\omega_2}\right), \quad (5.69)$$

5.14 Question 14

The imaginary wavenumber is given as (with s slightly less than one)

$$\alpha(\omega) = \alpha_0|\omega|^s, \quad \mathcal{H}\left\{\frac{\alpha(\omega)}{\omega}\right\} = \alpha_0\mathcal{H}\{\operatorname{sgn}\omega \cdot |\omega|^{s-1}\} = \alpha_0|\omega|^{s-1} \tan\frac{s\pi}{2}. \quad (5.70)$$

The modified relation between $c(\omega)$ and $\alpha(\omega)$, appropriate for this problem, is

$$\frac{1}{c(\omega)} = \frac{1}{c_\infty} + \mathcal{H}\left\{\frac{\alpha(\omega)}{\omega}\right\} = \frac{1}{c_\infty} + \frac{\alpha(\omega)}{|\omega|} \tan\frac{s\pi}{2}. \quad (5.71)$$

The absolute dispersion (with respect to c_∞) may be large for s slightly less than one, since the term $\tan(s\pi/2)$ dominates over c_∞^{-1} . On the other hand, $\alpha_0|\omega|^{s-1}$ is effectively a constant, which implies that the dependency of $c^{-1}(\omega)$ on ω is very weak. Hence, the relative dispersion over the seismic frequency range might be small and hard to detect.

5.15 Question 15

The phase velocity can be approximated from eq. (5.102) in the book as

$$\begin{aligned} c &= \sqrt{\frac{\text{Re}\mu}{\rho}} \sqrt{\frac{2(1+Q^{-2})}{1+\sqrt{1+\sec^2\gamma Q^{-2}}}} \approx \sqrt{\frac{\text{Re}\mu}{\rho}} \cdot \sqrt{2} \left(1 + \frac{1}{2}Q^{-2}\right) \cdot \left[1 + 1 + \frac{\sec^2\gamma}{2}Q^{-2}\right]^{-1/2} \\ &\approx \sqrt{\frac{\text{Re}\mu}{\rho}} \left(1 + \frac{1}{2}Q^{-2}\right) \left(1 - \frac{\sec^2\gamma}{8}Q^{-2}\right) \approx \sqrt{\frac{\text{Re}\mu}{\rho}} \left[1 + \left(\frac{1}{2} - \frac{\sec^2\gamma}{8}\right)Q^{-2}\right]. \end{aligned} \quad (5.72)$$

The correction of order Q^{-1} on velocity is related to the phase velocity dispersion, i.e., c as a function of ω . However, Eq. (5.72) describes the variation of c related to angle γ between \mathbf{P} and \mathbf{A} for two-dimensional plane waves.

5.16 Question 16

Based on the complex elastic moduli, the attenuation factors Q for S-wave and P-wave are defined as

$$Q_S^{-1} = -\frac{\text{Im}\{\mu\}}{\text{Re}\{\mu\}}, \quad Q_P^{-1} = -\frac{\text{Im}\{\kappa + 4\mu/3\}}{\text{Re}\{\kappa + 4\mu/3\}}. \quad (5.73)$$

The wave speeds are defined as

$$\beta = \sqrt{\frac{\text{Re}\{\mu\}}{\rho}}, \quad \alpha = \sqrt{\frac{\text{Re}\{\kappa + 4\mu/3\}}{\rho}}. \quad (5.74)$$

When the bulk modulus κ is purely real, the ratio of Q is calculated as

$$\frac{Q_P}{Q_S} = \frac{\text{Re}\{\kappa + 4\mu/3\}}{\text{Re}\{\mu\}} \cdot \frac{\text{Im}\{\mu\}}{\text{Im}\{4\mu/3\}} = \frac{3\alpha^2}{4\beta^2}. \quad (5.75)$$

More generally, we can obtain

$$\frac{Q_\kappa}{Q_P} = \left(1 - \frac{4\beta^2}{3\alpha^2}\right) \left(1 + \frac{4\text{Im}\{\mu\}}{3\text{Im}\{\kappa\}}\right), \quad \frac{Q_\kappa}{Q_S} = \left(\frac{\alpha^2}{\beta^2} - \frac{4}{3}\right) \frac{\text{Im}\{\mu\}}{\text{Im}\{\kappa\}}. \quad (5.76)$$

This leads to

$$\frac{Q_\kappa/Q_P}{1 - 4\beta^2/3\alpha^2} - 1 = \frac{4\beta^2}{3\alpha^2} \frac{Q_\kappa/Q_S}{1 - 4\beta^2/3\alpha^2}, \quad \frac{Q_\kappa}{Q_P} - 1 = \frac{4\beta^2}{3\alpha^2} \left(\frac{Q_\kappa}{Q_S} - 1\right). \quad (5.77)$$

Hence, we obtain the following result

$$\frac{1}{Q_P} - \frac{1}{Q_\kappa} = \frac{4\beta^2}{3\alpha^2} \left(\frac{1}{Q_S} - \frac{1}{Q_\kappa}\right). \quad (5.78)$$

5.17 Question 17

Consider a box function $f(t)$ that is unity for $T < t < 2T$. Its Hilbert transform is

$$\mathcal{H}\{f(t)\} = \frac{1}{\pi} \int_T^{2T} \frac{dt}{t-t} = \frac{1}{\pi} \ln \left| \frac{2T-t}{T-t} \right|. \quad (5.79)$$

When $|t-T| \ll T$, we have $|2T-t| \approx T$, and the box function $f(t)$ is effectively a Heaviside function $H(t-T)$. This eventually leads to

$$\mathcal{H}\{H(t-T)\} \approx -\frac{1}{\pi} \ln \left| \frac{t-T}{T} \right|, \quad \text{for } |t-T| \ll T. \quad (5.80)$$

5.18 Question 18

For an attenuating plane wave at frequency ω , the stress-strain relation is given by eq. (5.84) in the book

$$M_U \varepsilon(t) = \sigma(t) \left[1 + \int_0^{+\infty} \dot{\phi}(\tau) e^{i\omega\tau} d\tau \right]. \quad (5.81)$$

One example of the creep function $\phi(t)$ for rocks is described by the logarithmic law

$$\phi(t) = q \ln(1 + at) H(t), \quad \dot{\phi}(t) = \frac{aq}{1 + at} H(t). \quad (5.82)$$

in which the fundamental frequency a may be as high as the vibration frequency of a vacancy in the crystal lattice (i.e., of the order of 10 GHz), and the parameter q is related to the attenuation factor as $q \sim 2/(\pi Q)$. For seismic frequencies, we have $\omega \ll a$ and the Fourier transform of $\dot{\phi}(t)$ is evaluated as (eq. 5.87 in the book)

$$\mathcal{F}\{\dot{\phi}(t)\} = aq \int_0^{+\infty} \frac{e^{i\omega\tau}}{1 + a\tau} d\tau \sim -q \left[\gamma + \ln\left(\frac{\omega}{a}\right) - \frac{i\pi}{2} \right] e^{-i\omega/a}. \quad (5.83)$$

As a result, we obtain

$$\frac{M_U \varepsilon(t)}{\sigma(t)} = 1 - q \left[\gamma + \ln\left(\frac{\omega}{a}\right) - \frac{i\pi}{2} \right] e^{-i\omega/a}. \quad (5.84)$$

With $q \sim Q^{-1} \ll 1$ and $\omega \ll a$, the real and imaginary parts are approximated as

$$\begin{aligned} \operatorname{Re}\left\{\frac{M_U \varepsilon(t)}{\sigma(t)}\right\} &= 1 - q \left[\gamma + \ln\left(\frac{\omega}{a}\right) \right] \cos\left(\frac{\omega}{a}\right) + \frac{\pi q}{2} \sin\left(\frac{\omega}{a}\right) \approx 1, \\ \operatorname{Im}\left\{\frac{M_U \varepsilon(t)}{\sigma(t)}\right\} &= q \left[\gamma + \ln\left(\frac{\omega}{a}\right) \right] \sin\left(\frac{\omega}{a}\right) + \frac{\pi q}{2} \cos\left(\frac{\omega}{a}\right) \approx \frac{\pi q}{2}. \end{aligned} \quad (5.85)$$

Therefore, the phase difference between stress and strain is

$$\phi = \operatorname{Arg}\left\{\frac{M_U \varepsilon(t)}{\sigma(t)}\right\} = \arctan\left(\frac{\pi q}{2}\right) \approx \frac{1}{Q}, \quad (5.86)$$

which amounts to $1/(\omega Q)$ seconds. The stress leads the strain. Fig. 5.1 shows the hysteresis loop of the stress-strain curve (exaggerated for visualization). One definition of Q is based on the energy loss over one cycle, which is

$$Q^{-1} = -\frac{\Delta E}{2\pi E}. \quad (5.87)$$

Because the area is proportional to the squared amplitude, Eq. (5.87) can be evaluated as

$$-\frac{\Delta E}{2\pi E} \sim \frac{A_0^2 - A_1^2}{2\pi A_0^2} = \frac{1 - e^{-2\pi/Q}}{2\pi} \approx \frac{1}{Q}. \quad (5.88)$$

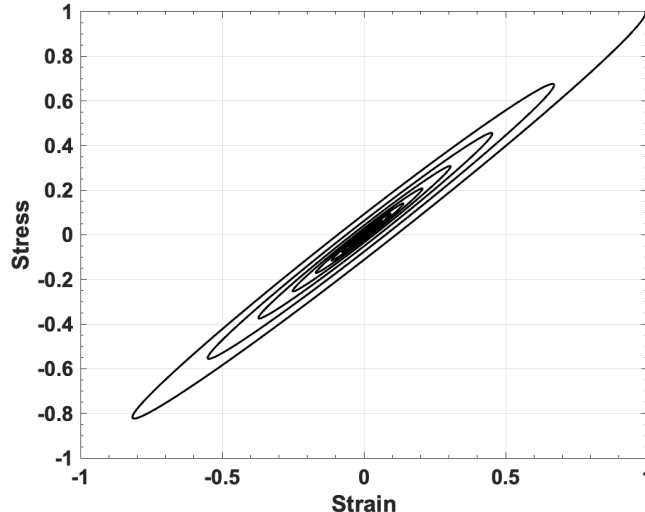


Fig. 5.1 Stress-strain hysteresis loop. The attenuation is exaggerated for visualization.

6 Chapter 6: Reflection and Refraction of Spherical Waves; Lamb's Problem

6.1 Question 1

Eq. (6.93) in the book is the solution for two half-spaces in welded contact along $z = 0$ with a point source of SH-wave acting at $z_0 < 0$ in the upper medium. When head waves can occur, the contribution from the Cagniard path starts at the branch cut $p(t_h) = \beta_2^{-1}$, with t_h being the head wave arrival time. The approximation $|pr| \gg t - t'$ is thus equivalent to

$$\min |pr| \gg \max (t - t'), \quad rp(t_h) = \frac{r}{\beta_2} \gg t - t_h. \quad (6.1)$$

When $\beta_2 < \beta_1$, the contribution from the Cagniard path starts at the departure point $p(t_0)$ corresponding to the reflection, which is given as

$$t_0 = \frac{R_0}{\beta_1}, \quad p(t_0) = \frac{r}{R_0 \beta_1}, \quad R_0 = \sqrt{r^2 + (z + z_0)^2}. \quad (6.2)$$

The approximation $|pr| \gg t - t'$ is thus equivalent to

$$\min |pr| \gg \max (t - t'), \quad rp(t_0) = \frac{r^2}{R_0 \beta_1} \gg t - t_0 = t - \frac{R_0}{\beta_1}. \quad (6.3)$$

Now we compare the convolution solution with the wavefront approximation. In the wavefront approximation, e.g., eq. (6.26) in the book, at distances near critical with $L \rightarrow 0$, the head wave amplitude $r^{-1/2} L^{-3/2}$ blows up. Meanwhile, the approximation of the wide-angle reflection wave (eq. 6.21 in the book) also fails. On the contrary, for the convolution solution (eq. 6.96 in the book), the singularity in $\psi(t)$ is integrable near the reflection time ($1/\sqrt{t^2 - R_0^2/\beta_1^2}$), and there is no issue with applying it near the critical distance.

6.2 Question 2

Eq. (6.42) in the book states the equation of motion for an SH-wave

$$\rho \ddot{v} = A \delta(x) \delta(z) \delta(t) + \mu \nabla^2 v = A \delta(x) \delta(z) \delta(t) + \left(\frac{\partial \sigma_{yx}}{\partial x} + \frac{\partial \sigma_{yz}}{\partial z} \right). \quad (6.4)$$

With the double transform (Fourier transform in x , Laplace transform in t), we have

$$\frac{\partial}{\partial z} \sigma_{yz}(k_x, z, s) = -A \delta(z) + \rho s^2 v(k_x, z, s) - i k_x \sigma_{yx}(k_x, z, s). \quad (6.5)$$

Integrating Eq. (6.5) from $z = 0^-$ to $z = 0^+$ gives the magnitude of the step A in the stress component σ_{yz} , which is related to the discontinuity in $\partial v / \partial z$.

6.3 Question 3

We start with the transmitted field given by eq. (6.14) in the book

$$P^{\text{trans}} = i \omega e^{-i \omega t} \int_0^\infty \frac{C p}{\xi_1} J_0(\omega p r) \exp(-i \omega \xi_1 z_0 + i \omega \xi_2 z) dp, \quad \text{in } z > 0, \quad (6.6)$$

in which the vertical slowness is defined as

$$\xi_1 = \sqrt{\alpha_1^{-2} - p^2}, \quad \xi_2 = \sqrt{\alpha_2^{-2} - p^2}, \quad \text{with } \text{Im } \xi_1, \text{ Im } \xi_2 \geq 0. \quad (6.7)$$

The amplitude $C(p)$ is determined from the boundary conditions as (eq. 6.15 in the book)

$$C(p) = A \frac{2 \rho_2 \xi_1}{\rho_1 \xi_2 + \rho_2 \xi_1}. \quad (6.8)$$

First, we rewrite Eq. (6.6) using the Hankel function and the fact that $C(p)$ is even in p , which leads to

$$P^{\text{trans}} = \frac{i\omega}{2} e^{-i\omega t} \int_{-\infty}^{+\infty} \frac{Cp}{\xi_1} H_0^{(1)}(\omega pr) \exp(-i\omega\xi_1 z_0 + i\omega\xi_2 z) dp, \quad \text{in } z > 0. \quad (6.9)$$

Second, when $r \gg \lambda$ we have $\omega pr \gg 1$, and the asymptotic expansion of the Hankel function is

$$H_0^{(1)}(\omega pr) = \sqrt{\frac{2}{\pi\omega pr}} e^{i(\omega pr - \pi/4)} \left[1 - \frac{i}{8\omega pr} + O\left(\frac{1}{\omega^2 p^2 r^2}\right) \right]. \quad (6.10)$$

Keep the first term in the expansion, and note that the source location $z_0 < 0$. We finally obtain

$$P^{\text{trans}} = \sqrt{\frac{\omega}{2\pi r}} e^{-i(\omega t - \pi/4)} \int_{-\infty}^{+\infty} \frac{C(p)\sqrt{p}}{\xi_1} \exp[i\omega(pr + \xi_1|z_0| + \xi_2 z)] dp. \quad (6.11)$$

The saddle-point analysis is carried out as

$$f(p) = i(pr + \xi_1|z_0| + \xi_2 z), \quad f'(p) = i\left(r - \frac{p|z_0|}{\xi_1} - \frac{pz}{\xi_2}\right), \quad f''(p) = -i\left(\frac{|z_0|}{\alpha_1^2 \xi_1^3} + \frac{z}{\alpha_2^2 \xi_2^3}\right). \quad (6.12)$$

Therefore, the saddle point $p = p_s$ satisfies

$$p_s = \frac{\sin i_1}{\alpha_1} = \frac{\sin i_2}{\alpha_2}, \quad r = \frac{p|z_0|}{\xi_1} + \frac{pz}{\xi_2} = |z_0| \tan i_1 + z \tan i_2. \quad (6.13)$$

The saddle occurs for the ray parameter p which gives the transmitted ray between the source and the receiver, as illustrated in Fig. 6.1.

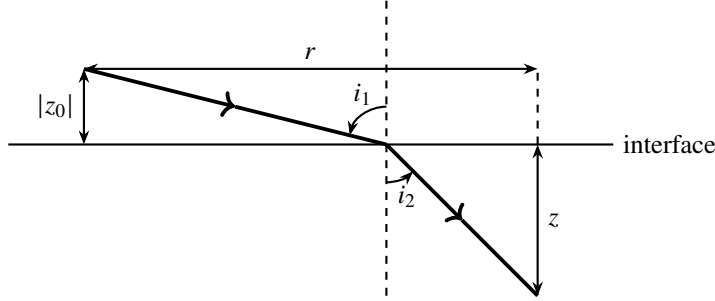


Fig. 6.1 Illustration of the transmitted ray, and the condition satisfied in Eq. (6.13).

6.4 Question 4

The Rayleigh function $R(p)$ is defined as

$$R(p) = 4p^2\xi\eta + (\beta^{-2} - 2p^2)^2, \quad \text{with } \xi = \sqrt{\alpha^{-2} - p^2}, \quad \eta = \sqrt{\beta^{-2} - p^2}. \quad (6.14)$$

In one of the nonphysical Riemann sheet $\{\text{Re } \xi < 0; \text{Re } \eta \geq 0\}$, for a real ray parameter p within the range $0 < p < \alpha^{-1}$, now we have

$$\tilde{\xi} = -\sqrt{\alpha^{-2} - p^2}, \quad \tilde{\eta} = \sqrt{\beta^{-2} - p^2}. \quad (6.15)$$

Based on Snell's law, the incidence angles for P- and S-waves satisfy

$$p = \frac{\sin i}{\alpha} = \frac{\sin j}{\beta} \implies \tilde{\xi} = -\frac{\cos i}{\alpha}, \quad \tilde{\eta} = \frac{\cos j}{\beta}. \quad (6.16)$$

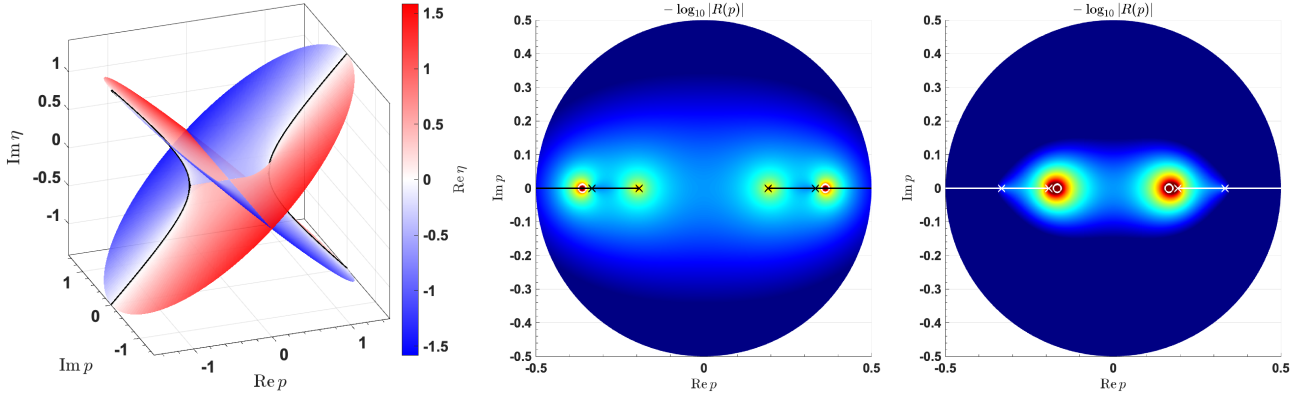


Fig. 6.2 (Left) Riemann sheets of $\eta = \sqrt{\beta^{-2} - p^2}$. Red surface corresponds to $\text{Re } \eta > 0$, which is discontinuous across the branch cuts. (Middle) Rayleigh poles on the physical Riemann sheet $\{\text{Re } \xi \geq 0; \text{Re } \eta \geq 0\}$. Branch points are denoted by \times , and poles by \circ at $p = \pm 1/c_R$. (Right) Rayleigh poles on the nonphysical Riemann sheet $\{\text{Re } \xi < 0; \text{Re } \eta \geq 0\}$. The poles are near $p = \pm 1/\alpha$ in this case with $\nu = 0.25$ (i.e., Poisson solid).

Therefore, on this nonphysical Riemann sheet (+), the Rayleigh function becomes

$$\tilde{R}(p) = \left(\beta^{-2} - 2p^2\right)^2 - 4p^2 \frac{\cos i}{\alpha} \frac{\cos j}{\beta}, \quad \text{with } 0 < p < \alpha^{-1}. \quad (6.17)$$

This is exactly the numerator of $\dot{P}\dot{P}$ and $\dot{S}\dot{S}$ (see eqs 5.28 & 5.32 in the book). Therefore, the zero crossings of $\dot{P}\dot{P}$ and $\dot{S}\dot{S}$ occur precisely at the zero of Rayleigh function on the nonphysical Riemann sheet $\{\text{Re } \xi < 0; \text{Re } \eta \geq 0\}$. For figure 5.6 in the book, the coefficients are plotted for $\alpha = 5 \text{ km/s}$ and $\beta = 3 \text{ km/s}$, corresponding to $\nu \approx 0.23 < 0.263$ and thus, the \bar{P} -pole is on the real p -axis for this case.

To visualize the Riemann sheets and the Rayleigh poles, Fig. 6.2 plots the complex function $\eta = \sqrt{\beta^{-2} - p^2}$ and the inverse Rayleigh function $1/R(p)$. The Poisson's ratio is chosen as $\nu = 0.25$. Now we see the branch cuts separating the $\{\text{Re } \eta \geq 0\}$ sheet from the $\{\text{Re } \eta < 0\}$ sheet. Furthermore, we see the Rayleigh poles in both the physical and nonphysical Riemann sheets and, more importantly, the leaking mode from the \bar{P} -pole into the physical Riemann sheet.

6.5 Question 5: 2D Lamb's Problem (First kind)

1. Solution to the homogeneous wave equations for potentials

Because the source is at the surface $z = 0$, we can treat it as the boundary condition and solve the homogeneous wave equations. The displacement \mathbf{u} is related to the scalar potentials ϕ and ψ as

$$\mathbf{u} = \nabla\phi + \nabla \times (0, \psi, 0) = \left(\frac{\partial\phi}{\partial x} - \frac{\partial\psi}{\partial z}, 0, \frac{\partial\phi}{\partial z} + \frac{\partial\psi}{\partial x} \right). \quad (6.18)$$

Since the problem is y -invariant, we consider $\phi(x, z, t)$ and $\psi(x, z, t)$. The potentials satisfy

$$\ddot{\phi} = \alpha^2 \nabla^2 \phi, \quad \ddot{\psi} = \beta^2 \nabla^2 \psi. \quad (6.19)$$

Taking the Fourier transform in x and the Laplace transform in t , we have

$$\frac{\partial^2}{\partial z^2} \phi(k_x, z, s) = \left(k_x^2 + \frac{s^2}{\alpha^2} \right) \phi(k_x, z, s), \quad \frac{\partial^2}{\partial z^2} \psi(k_x, z, s) = \left(k_x^2 + \frac{s^2}{\beta^2} \right) \psi(k_x, z, s). \quad (6.20)$$

In the halfspace $z > 0$, we require the solutions to be bounded as $z \rightarrow \infty$. The homogeneous solutions are given as

$$\phi(k_x, z, s) = Ae^{-s\xi z}, \quad \psi(k_x, z, s) = Be^{-s\eta z}, \quad (6.21)$$

in which the coefficients A and B are to be determined by the boundary conditions, and we define

$$k_x = isp, \quad \xi = \sqrt{\alpha^{-2} - p^2}, \quad \eta = \sqrt{\beta^{-2} - p^2}, \quad \text{with } \operatorname{Re} \xi > 0, \quad \operatorname{Re} \eta > 0. \quad (6.22)$$

Note When p is slightly above the branch cut (e.g., in the case $z = 0$), the above definition gives $\sqrt{z_0 - z} = -i\sqrt{z - z_0}$ for real variable $z > z_0$. This should be taken care of when coding up the expressions.

2. Boundary conditions at $z = 0$

The traction components are calculated as

$$\tau_{xz} = 2\mu \frac{\partial^2 \phi}{\partial x \partial z} + \mu \left(\frac{\partial^2 \psi}{\partial^2 x} - \frac{\partial^2 \psi}{\partial^2 z} \right), \quad \tau_{zz} = \lambda \nabla^2 \phi + 2\mu \frac{\partial^2 \phi}{\partial^2 z} + 2\mu \frac{\partial^2 \psi}{\partial x \partial z}. \quad (6.23)$$

At the surface, we have the boundary conditions

$$\tau_{xz}(x, t) = 0, \quad \tau_{zz}(x, t) = -I \delta(x) \delta(t), \quad \text{at } z = 0. \quad (6.24)$$

In the transformed domain, these become

$$\tau_{xz}(k_x, s) = 0, \quad \tau_{zz}(k_x, s) = -I, \quad \text{at } z = 0. \quad (6.25)$$

From Eqs (6.21) and (6.25), we obtain the linear system for the coefficients

$$\begin{bmatrix} -2p\xi & \eta^2 - p^2 \\ a^2\xi^2 + (\alpha^2 - 2\beta^2)p^2 & 2\beta^2\eta p \end{bmatrix} \begin{bmatrix} A \\ B \end{bmatrix} = \begin{bmatrix} 0 \\ -I/\rho s^2 \end{bmatrix}. \quad (6.26)$$

The determinants are obtained as

$$|D| = -\beta^2 R(p), \quad |D_A| = \begin{vmatrix} 0 & \eta^2 - p^2 \\ -I/\rho s^2 & 2\beta^2\eta p \end{vmatrix} = \frac{I(\eta^2 - p^2)}{\rho s^2}, \quad |D_B| = \frac{2Ip\xi}{\rho s^2}, \quad (6.27)$$

where we see the Rayleigh function $R(p)$ shows up. The coefficients are solved as

$$A = \frac{|D_A|}{|D|} = -\frac{I}{\rho\beta^2 s^2} \frac{\eta^2 - p^2}{R(p)}, \quad B = \frac{|D_B|}{|D|} = -\frac{I}{\rho\beta^2 s^2} \frac{2p\xi}{R(p)}. \quad (6.28)$$

3. Exact solution of displacement fields

In the transformed domain, the displacement components at arbitrary depth z become

$$u_x(k_x, z, s) = u_x^P + u_x^S = \frac{I}{\rho\beta^2 s} \frac{p(\eta^2 - p^2)}{R(p)} e^{-s\xi z} - \frac{I}{\rho\beta^2 s} \frac{2p\xi\eta}{R(p)} e^{-s\eta z}, \quad (6.29)$$

$$u_z(k_x, z, s) = u_z^P + u_z^S = \frac{I}{\rho\beta^2 s} \frac{\xi(\eta^2 - p^2)}{R(p)} e^{-s\xi z} + \frac{I}{\rho\beta^2 s} \frac{2p^2\xi}{R(p)} e^{-s\eta z}. \quad (6.30)$$

The inverse Fourier transform of u_x^P , as an example, is obtained as

$$u_x^P(x, z, s) = \frac{I}{2\pi\rho\beta^2} \int_{-\infty}^{+\infty} \frac{p(\eta^2 - p^2)}{s R(p)} e^{ik_x x - s\xi z} dk_x. \quad (6.31)$$

With $k_x = i\omega$, we have

$$\begin{aligned} u_x^P(x, z, s) &= \frac{I}{2\pi\rho\beta^2} \int_{-i\infty}^{+i\infty} \frac{-ip(\eta^2 - p^2)}{\mathsf{R}(p)} e^{-s(px + \xi z)} dp \\ &= \frac{I}{\pi\rho\beta^2} \operatorname{Im} \left\{ \int_0^{i\infty} \frac{p(\eta^2 - p^2)}{\mathsf{R}(p)} e^{-s(px + \xi z)} dp \right\}. \end{aligned} \quad (6.32)$$

The final step is similar to eq. (6.48) in the book. To demonstrate it, denote

$$\frac{p(\eta^2 - p^2)}{\mathsf{R}(p)} e^{-s(px + \xi z)} = E(\tilde{p}) + iO(\tilde{p}), \quad \text{with } p = i\tilde{p}, \quad \tilde{p} \in \mathbb{R}. \quad (6.33)$$

We can show that

$$E(\tilde{p}) = \frac{\tilde{p}(\beta^{-2} + 2\tilde{p}^2)}{-4\tilde{p}^2\xi\eta + (\beta^{-2} + 2\tilde{p}^2)^2} e^{-s\xi z} \sin(s\tilde{p}x), \quad O(\tilde{p}) = \frac{\tilde{p}(\beta^{-2} + 2\tilde{p}^2)}{-4\tilde{p}^2\xi\eta + (\beta^{-2} + 2\tilde{p}^2)^2} e^{-s\xi z} \cos(s\tilde{p}x), \quad (6.34)$$

and thus, $E(\tilde{p})$ is even and $O(\tilde{p})$ is odd for \tilde{p} , which leads to Eq. (6.32). Now define $t = px + \xi z$, and the path C , given by $p = p(t)$ where t is real and positive, is the Cagniard path. Solving for p as a function of t gives (for $x > 0$)

$$p = \begin{cases} \frac{xt - z\sqrt{\frac{R^2}{\alpha^2} - t^2}}{R^2} & \text{for } 0 \leq t \leq \frac{R}{\alpha}, \\ \frac{xt + iz\sqrt{t^2 - \frac{R^2}{\alpha^2}}}{R^2} & \text{for } t \geq \frac{R}{\alpha}, \end{cases} \quad (6.35)$$

where $R = \sqrt{x^2 + z^2}$ is the distance function. It can be shown that the integral (6.32) up the positive imaginary p -axis can instead be taken over the Cagniard path C on which t increases from zero to infinity, which leads to

$$u_x^P(x, z, s) = \frac{I}{\pi\rho\beta^2} \operatorname{Im} \left\{ \int_0^\infty \frac{p(\eta^2 - p^2)}{\mathsf{R}(p)} e^{-st} \frac{dp}{dt} dt \right\}. \quad (6.36)$$

The exact solution in the time domain becomes

$$u_x^P(x, z, t) = \frac{I}{\pi\rho\beta^2} \operatorname{Im} \left\{ \frac{p(\eta^2 - p^2)}{\mathsf{R}(p)} \frac{dp}{dt} \right\} \Big|_{p=p(t)}. \quad (6.37)$$

The derivative is given as

$$\frac{dp}{dt} = \begin{cases} \frac{\xi}{\sqrt{\frac{R^2}{\alpha^2} - t^2}} & \text{for } 0 < t < \frac{R}{\alpha}, \\ \frac{i\xi}{\sqrt{t^2 - \frac{R^2}{\alpha^2}}} & \text{for } t > \frac{R}{\alpha}, \end{cases} \quad (6.38)$$

in which an integrable singularity is present at the ray arrival time of direct P waves, $t = R/\alpha$. For other components u_z^P , u_x^S and u_z^S , the procedure is the same. The exact solution of displacement fields is summarized below.

• P-wave components

$$u_x^P(x, z, t) = \frac{I}{\pi\rho\beta^2} \operatorname{Im} \left\{ \frac{p(\eta^2 - p^2)}{\mathsf{R}(p)} \frac{dp}{dt} \right\} \Big|_{p=p(t)}, \quad u_z^P(x, z, t) = \frac{I}{\pi\rho\beta^2} \operatorname{Im} \left\{ \frac{\xi(\eta^2 - p^2)}{\mathsf{R}(p)} \frac{dp}{dt} \right\} \Big|_{p=p(t)}. \quad (6.39)$$

The complex ray parameter $p = p(t)$ is given as (we can set $p = 0$ for $t < z/\alpha$)

$$p = \begin{cases} \frac{xt - z\sqrt{\frac{R^2}{\alpha^2} - t^2}}{R^2} & \text{for } \frac{z}{\alpha} \leq t \leq \frac{R}{\alpha}, \\ \frac{xt + iz\sqrt{t^2 - \frac{R^2}{\alpha^2}}}{R^2} & \text{for } t \geq \frac{R}{\alpha}, \end{cases} \quad \frac{dp}{dt} = \begin{cases} \frac{\xi}{\sqrt{\frac{R^2}{\alpha^2} - t^2}} & \text{for } 0 < t < \frac{R}{\alpha}, \\ \frac{i\xi}{\sqrt{t^2 - \frac{R^2}{\alpha^2}}} & \text{for } t > \frac{R}{\alpha}. \end{cases} \quad (6.40)$$

• S-wave components

$$u_x^S(x, z, t) = -\frac{I}{\pi\rho\beta^2} \operatorname{Im} \left\{ \frac{2p\xi\eta}{R(p)} \frac{dp}{dt} \right\} \Big|_{p=p(t)}, \quad u_z^S(x, z, t) = \frac{I}{\pi\rho\beta^2} \operatorname{Im} \left\{ \frac{2p^2\xi}{R(p)} \frac{dp}{dt} \right\} \Big|_{p=p(t)}. \quad (6.41)$$

The complex ray parameter $p = p(t)$ is given as

$$p = \begin{cases} \frac{xt - z\sqrt{\frac{R^2}{\beta^2} - t^2}}{R^2} & \text{for } \frac{z}{\beta} \leq t \leq \frac{R}{\beta}, \\ \frac{xt + iz\sqrt{t^2 - \frac{R^2}{\beta^2}}}{R^2} & \text{for } t \geq \frac{R}{\beta}, \end{cases} \quad \frac{dp}{dt} = \begin{cases} \frac{\eta}{\sqrt{\frac{R^2}{\beta^2} - t^2}} & \text{for } 0 < t < \frac{R}{\beta}, \\ \frac{i\eta}{\sqrt{t^2 - \frac{R^2}{\beta^2}}} & \text{for } t > \frac{R}{\beta}. \end{cases} \quad (6.42)$$

4. Numerical illustration

Figs 6.3 and 6.4 show the displacement fields at $(x, z) = (5 \text{ km}, 0)$ and $(5 \text{ km}, 1 \text{ km})$, respectively, with shear wave speed $\beta = 1.73 \text{ km/s}$ and Poisson's ratio $\nu = 0.2$. We can identify the P and S arrivals, as well as the head wave for $z > 0$. The head wave corresponds to $p = \alpha^{-1}$, and the arrival time can be calculated as

$$t_h = \frac{x}{\alpha} + z\sqrt{\beta^{-2} - \alpha^{-2}}. \quad (6.43)$$

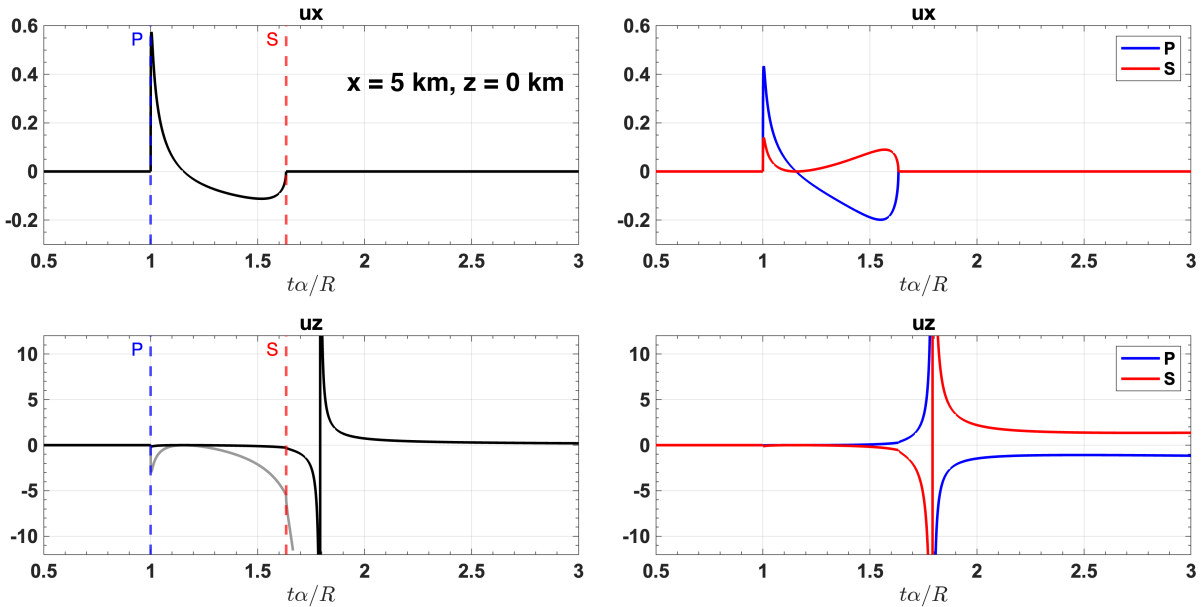


Fig. 6.3 Displacement fields at $(5 \text{ km}, 0)$. The time axis is normalized by P-arrival time $t_P = R/\alpha$. The displacement is normalized by $I/\pi\mu$. The thick gray line is $20 \times$ the original amplitude to visualize this part of the seismogram. The contributions from u_x^P , u_x^S , u_z^P and u_z^S are shown in the right panels.

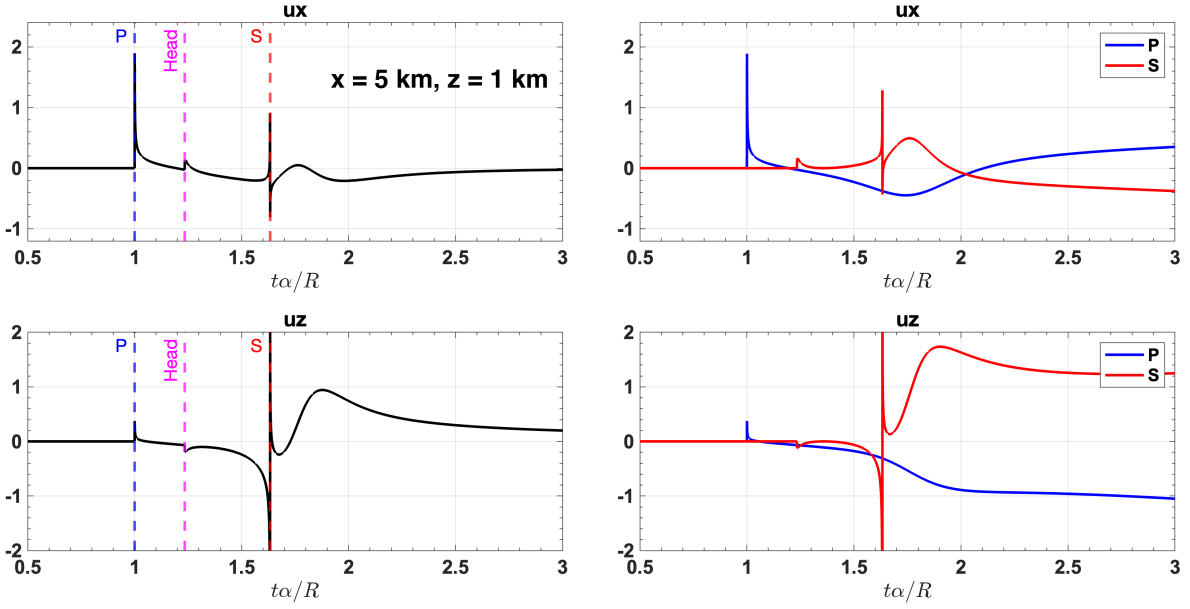


Fig. 6.4 Same as Fig. 6.3 but for displacement fields at (5 km, 1 km). The head wave becomes a separate pulse.

At the surface, we have $t_h = t_p$ and thus the S components u_x^S and u_z^S also contribute to the P arrival. After the S arrival, the Rayleigh pulse shows up and dominates the vertical component u_z . As $t \rightarrow \infty$, both P and S components are divergent, but they cancel out each other due to their similar behavior (as discussed later in Problem 6.8).

• Convolution with Gaussian pulse

Fig. 6.5 shows the synthetic seismograms by convolution of the previous results with a 1st derivative Gaussian pulse $\psi_0(t)$, which is defined as

$$\psi_0(t) = -C t e^{-t^2}. \quad (6.44)$$

The normalization factor C ensures the pulse amplitude to be 1. The period of $\psi_0(t)$ is denoted by two times the distance between the peak and the trough, which is $T_0 = 2\sqrt{2}$. For arbitrary central frequencies, the pulse is stretched or shrunk accordingly. The first motions can be better identified from the synthetic seismograms.

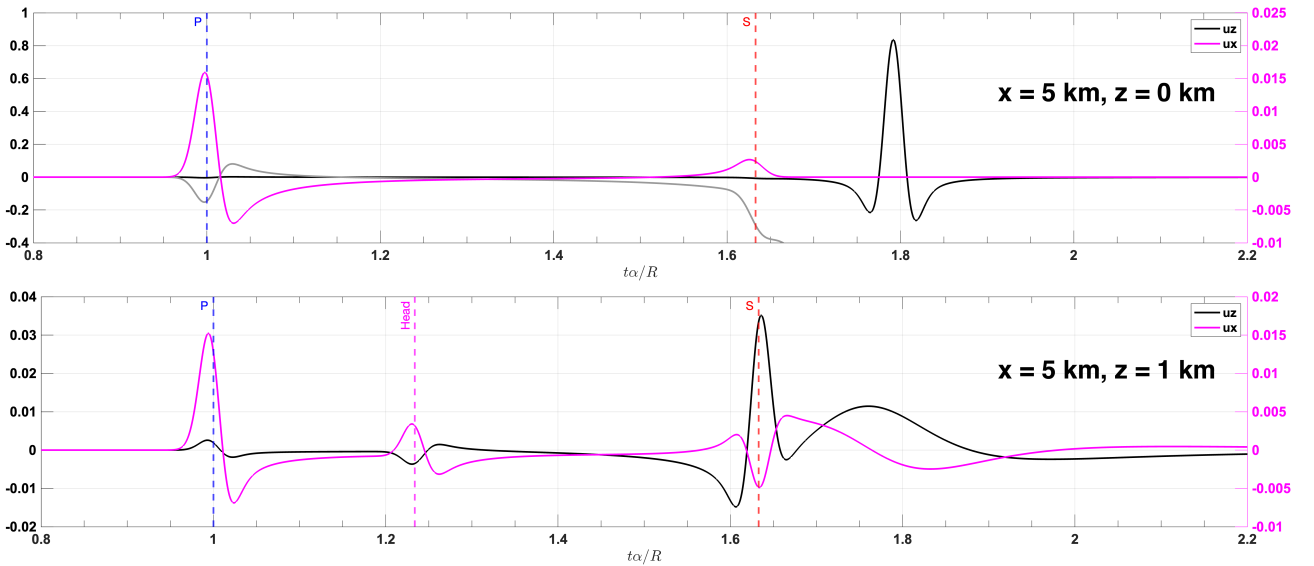


Fig. 6.5 Synthetic seismograms by convolution of signals in Figs. 6.3 and 6.4 with a 1st derivative Gaussian pulse. The central frequency of the wavelet is $f_c = 20/t_p$. Note the difference in the ranges of vertical axes. The thick gray line is $40 \times$ the original amplitude of u_z to visualize this part of the seismogram.

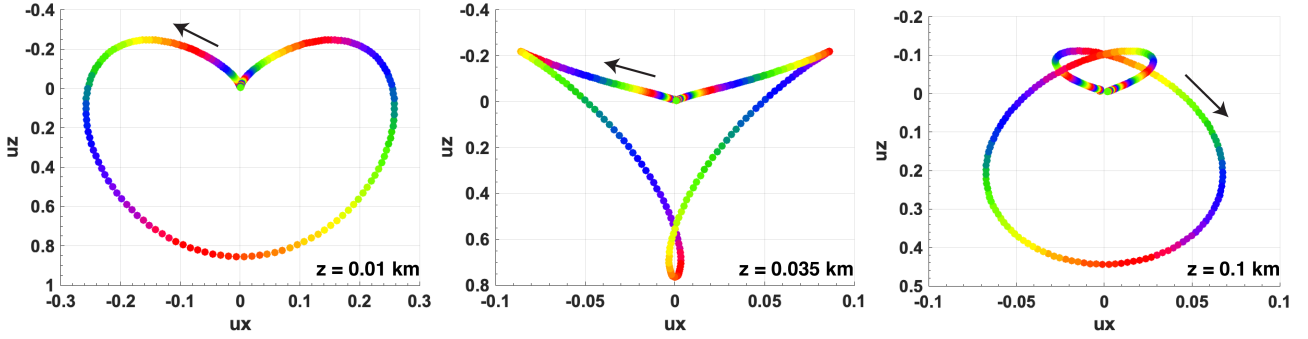


Fig. 6.6 Particle motion plots at different depths $z = 0.01 \text{ km}$, 0.035 km and 0.1 km . Increasing time is indicated by the rainbow color order. The particle motion transitions from retrograde elliptical to prograde elliptical as the depth increases.

• Rayleigh wave particle motion

Based on the synthetic seismograms, we can further analyze the Rayleigh wave particle motion. Fig. 6.6 shows the Rayleigh pulse particle motion at different receiver depths. The time window $t_S < t < 1.2 t_S$ is selected for visualization. The central frequency of the Gaussian pulse is $f_c = 20/t_P$, which corresponds to a Rayleigh wavelength of $\lambda_R = 0.14 \text{ km}$ with $c_R = 1.576 \text{ km/s}$. The transition from retrograde to prograde motion occurs around $z \sim 0.3 \lambda_R$.

• Rayleigh poles and leaking mode

Fig. 6.7 shows the influence of Poisson's ratio ν on the synthetic seismograms. When $\nu < 0.263$, the \bar{P} -pole on the nonphysical Riemann sheet $\{\operatorname{Re} \xi < 0; \operatorname{Re} \eta \geq 0\}$ is on the real p -axis and close to $p = 1/\alpha$ (Fig. 6.2), which contributes to the head wave arrival. On the other hand, when $\nu > 0.263$, the \bar{P} -pole is in the fourth quadrant of the nonphysical $(-+)$ sheet with $1/\alpha < \operatorname{Re} p < 1/\beta$. This leads to the \bar{P} -pulse after the head wave.

5. Exact solution of surface displacement fields

A special case occurs when the receiver is on the surface $z = 0$. The Cagniard path then becomes the real p -axis

$$p = \frac{t}{x}, \quad \frac{dp}{dt} = \frac{1}{x}, \quad \text{for } t > 0. \quad (6.45)$$

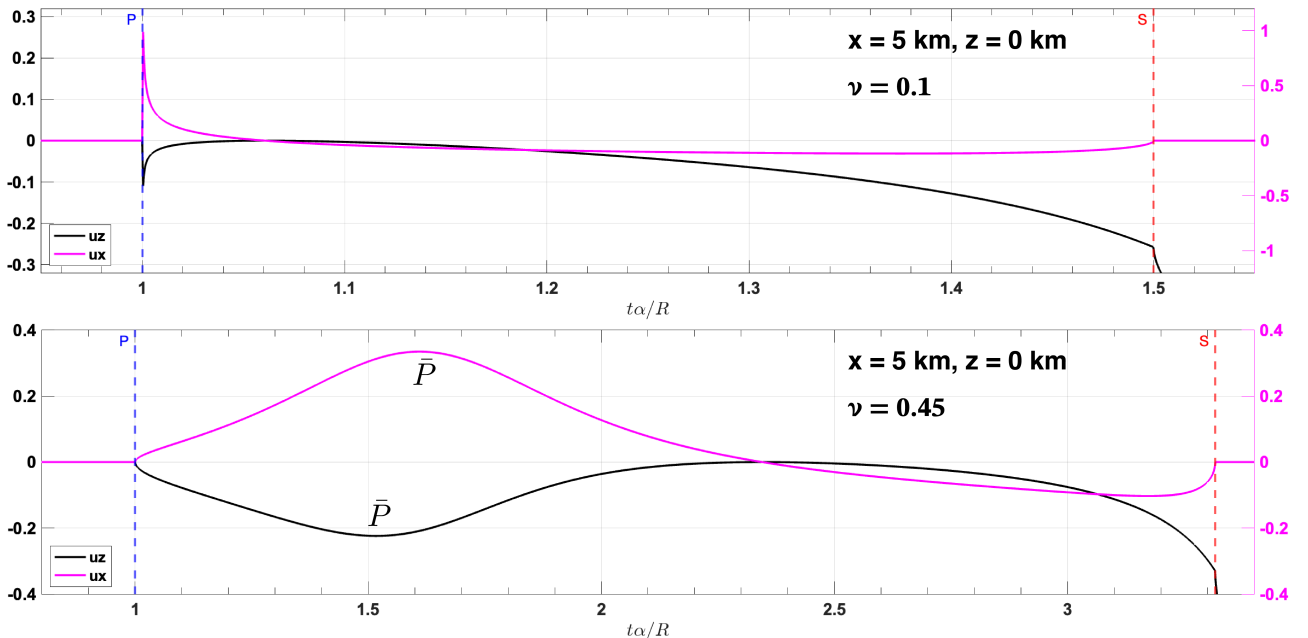


Fig. 6.7 Influence of Poisson's ratio ν on synthetic seismograms. The portion between P-wave and S-wave arrivals is zoomed in. The receiver is at $(5 \text{ km}, 0)$. Two example values of Poisson's ratio $\nu = 0.1$ and $\nu = 0.45$ are chosen. Note that \bar{P} -pulse appears when $\nu > 0.263$.

When $t < t_P$, everything is real and there is no displacement as expected. We thus need to discuss the following two cases.

- $t_P < t < t_S$

Within this time interval, we have

$$\xi = -\frac{i}{x} \sqrt{t^2 - t_P^2}, \quad \eta = \frac{1}{x} \sqrt{t_S^2 - t^2}, \quad R(p) = \frac{1}{x^4} \left[(t_S^2 - 2t^2)^2 - 4it^2 \sqrt{t^2 - t_P^2} \sqrt{t_S^2 - t^2} \right]. \quad (6.46)$$

Now denote the following quantities

$$A(t) = (t_S^2 - 2t^2)^2 \geq 0, \quad B(t) = 4t^2 \sqrt{t^2 - t_P^2} \sqrt{t_S^2 - t^2} \geq 0, \\ D(t) = \sqrt{A^2(t) + B^2(t)} > 0, \quad \theta(t) = \arctan \left[\frac{B(t)}{A(t)} \right] \in \left[0, \frac{\pi}{2} \right]. \quad (6.47)$$

The surface displacement fields can then be expressed as

$$u_x^P(x, 0, t) = \frac{I}{\pi\mu} t (t_S^2 - 2t^2) \frac{\sin \theta(t)}{D(t)}, \quad u_z^P(x, 0, t) = -\frac{I}{\pi\mu} \sqrt{t^2 - t_P^2} (t_S^2 - 2t^2) \frac{\cos \theta(t)}{D(t)}. \quad (6.48)$$

$$u_x^S(x, 0, t) = \frac{I}{\pi\mu} 2t \sqrt{t^2 - t_P^2} \sqrt{t_S^2 - t^2} \frac{\cos \theta(t)}{D(t)}, \quad u_z^S(x, 0, t) = -\frac{I}{\pi\mu} 2t^2 \sqrt{t^2 - t_P^2} \frac{\cos \theta(t)}{D(t)}. \quad (6.49)$$

- $t > t_S$

Within this time interval, we have

$$\xi = -\frac{i}{x} \sqrt{t^2 - t_P^2}, \quad \eta = -\frac{i}{x} \sqrt{t^2 - t_S^2}, \quad R(p) = \frac{1}{x^4} \left[(t_S^2 - 2t^2)^2 - 4t^2 \sqrt{t^2 - t_P^2} \sqrt{t^2 - t_S^2} \right]. \quad (6.50)$$

Now we can denote

$$R(t) = (t_S^2 - 2t^2)^2 - 4t^2 \sqrt{t^2 - t_P^2} \sqrt{t^2 - t_S^2}, \quad \text{with } R(t_R) = 0, \quad (6.51)$$

where $t_R = x/c_R$ is the Rayleigh arrival time. The surface displacement fields can then be expressed as

$$u_x^P(x, 0, t) = 0, \quad u_z^P(x, 0, t) = -\frac{I}{\pi\mu} \sqrt{t^2 - t_P^2} (t_S^2 - 2t^2) \frac{1}{R(t)}. \quad (6.52)$$

$$u_x^S(x, 0, t) = 0, \quad u_z^S(x, 0, t) = -\frac{I}{\pi\mu} 2t^2 \sqrt{t^2 - t_P^2} \frac{1}{R(t)}. \quad (6.53)$$

We can further obtain

$$u_x(x, 0, t) = 0, \quad u_z(x, 0, t) = -\frac{I}{\pi\mu} t_S^2 \sqrt{t^2 - t_P^2} \frac{1}{R(t)}, \quad \text{for } t > t_S. \quad (6.54)$$

Around $t = t_R$, the vertical displacement can be approximated as

$$u_z(x, 0, t) \approx -\frac{I}{\pi\mu} t_S^2 \sqrt{t^2 - t_P^2} \frac{1}{t - t_R} \frac{1}{R'(t_R)} \propto \frac{1}{t - t_R}. \quad (6.55)$$

Therefore, the shape of the Rayleigh wave is the Hilbert transform of the input pulse, which leads to a $\pi/2$ phase shift.

6.6 Question 6

In general, the SV-displacement is represented by $\mathbf{u}^{SV} = \nabla \times \nabla \times (0, 0, \psi)$. If the field is independent of the y -coordinate, we have $\psi = \psi(x, z, t)$ and then

$$\nabla \times \psi = \left(\frac{\partial \psi}{\partial y}, -\frac{\partial \psi}{\partial x}, 0 \right) = \left(0, -\frac{\partial \psi}{\partial x}, 0 \right). \quad (6.56)$$

Now we can define a new scalar function $\tilde{\psi} = -\partial \psi / \partial x$, and then the SV-displacement becomes $\mathbf{u}^{SV} = \nabla \times (0, \tilde{\psi}, 0)$.

6.7 Question 7

The new path gives the same result as Γ in Fig. 6.9 in the book. Note that F' and D are on the sheet $\{\text{Im } \xi_1 > 0; \text{Im } \xi_2 > 0\}$, while E is on the sheet $\{\text{Im } \xi_1 > 0; \text{Im } \xi_2 < 0\}$. For the closed path $F' \rightarrow D \rightarrow E \rightarrow F'$, the integrand is analytic within the path, and thus, the net contribution is zero. Fig. 6.8 visualizes the analytic nature of ξ on different Riemann sheets across the branch cut.

6.8 Question 8

Eq. (6.70) in the book gives

$$u_{SS}(x, z, t) = \frac{M_0}{2\pi\mu} \text{Im} \left\{ \frac{4p^2\xi\eta - (\beta^{-2} - 2p^2)^2}{4p^2\xi\eta + (\beta^{-2} - 2p^2)^2} \frac{dp}{dt} \right\}_{p=p(t)}. \quad (6.57)$$

When t is large, we have the following expressions

$$p(t) = \frac{1}{R_0} \left(t \sin \theta + i \sqrt{t^2 - \frac{R_0^2}{\beta^2}} \cos \theta \right), \quad \frac{dp}{dt} = \frac{i\eta}{\sqrt{t^2 - R_0^2/\beta^2}}, \quad t > \frac{R_0}{\beta}, \quad (6.58)$$

where θ denotes the incidence angle. As $t \rightarrow \infty$, we have

$$\sqrt{t^2 - \frac{R_0^2}{\beta^2}} \approx t \left(1 - \frac{R_0^2}{2\beta^2 t^2} \right) = t(1 - \varepsilon), \quad \text{with } \varepsilon = \frac{R_0^2}{2\beta^2 t^2}. \quad (6.59)$$

Therefore, from Eq. (6.58) we have

$$p \approx \frac{ite^{-i\theta}}{R_0} \left(1 - \varepsilon e^{i\theta} \cos \theta \right), \quad \frac{dp}{dt} \approx \frac{i\eta}{t} (1 + \varepsilon), \quad \text{as } t \rightarrow \infty. \quad (6.60)$$

On the Riemann sheet $\{\text{Re } \xi > 0; \text{Re } \eta > 0\}$, we have

$$\xi = \sqrt{\frac{1}{\alpha^2} - p^2} \approx -ip \left(1 - \frac{1}{2\alpha^2 p^2} \right) \approx \frac{te^{-i\theta}}{R_0} + \frac{R_0}{2t} \left(\frac{e^{i\theta}}{\alpha^2} - \frac{\cos \theta}{\beta^2} \right), \quad (6.61)$$

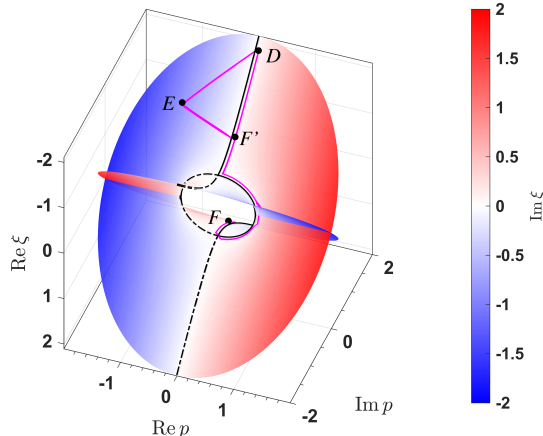


Fig. 6.8 Riemann sheets of $\xi = \sqrt{\alpha^{-2} - p^2}$. The z -axis indicates $\text{Re } \xi$ and the color for $\text{Im } \xi$. The z -axis is flipped to see $\text{Im } \xi > 0$ in the first quadrant where F' and D are located. The magenta line shows a portion of the integration path in Figure 6.9 in the book.

$$\eta = \sqrt{\frac{1}{\beta^2} - p^2} \approx -ip \left(1 - \frac{1}{2\beta^2 p^2}\right) \approx \frac{te^{-i\theta}}{R_0} + \frac{iR_0 \sin \theta}{2t\beta^2}, \quad \text{as } t \rightarrow \infty. \quad (6.62)$$

Therefore, the numerator and denominator in Eq. (6.57) can be approximated as

$$N(p) = -8p^4 + O(p^2), \quad R(p) = 2p^2 \left(\frac{1}{\alpha^2} - \frac{1}{\beta^2}\right) + O(1). \quad (6.63)$$

Note that the denominator is just the Rayleigh function $R(p)$. Finally, we obtain

$$u_{SS}(x, z, t) = \frac{2M_0}{\pi\mu\rho} \frac{\lambda+2\mu}{\lambda+\mu} \operatorname{Im} \left\{ \frac{-it^2 e^{-i3\theta}}{R_0^3} + O(1) \right\} \propto t^2, \quad (6.64)$$

which shows that u_{SS} diverges to infinity as $t \rightarrow \infty$.

Similarly, we can write down the motion u_{SP} in the transformed domain as (for a step function $M_0(t) = M_0 H(t)$)

$$u_{SP}(k_x, z, s) = -\frac{M_0}{2\rho\beta^2 s} \frac{\alpha p}{\beta\eta} \hat{S}\hat{P} \exp[-s(\xi z + \eta h)]. \quad (6.65)$$

Although $\hat{S}\hat{P}$ is odd in p , the factor $p \hat{S}\hat{P}$ is still even. The inverse k_x -transform can be written as (recall that $k_x = isp$)

$$u_{SP}(x, z, s) = -\frac{M_0}{2\pi\mu\beta} \frac{\alpha}{\beta} \operatorname{Im} \left\{ \int_0^{i\infty} \frac{p}{\eta} \hat{S}\hat{P}(p) \exp[-s(px + \xi z + \eta h)] \right\}. \quad (6.66)$$

Define a Cagniard path by $t = px + \xi z + \eta h$, and for large t we also have

$$p(t) = \frac{ite^{-i\theta}}{R_0} + O(t^{-1}), \quad \frac{dp}{dt} = \frac{ie^{-i\theta}}{R_0} + O(t^{-2}). \quad (6.67)$$

The exact solution of u_{SP} in the time domain is

$$u_{SP}(x, z, t) = \frac{M_0}{2\pi\mu} \operatorname{Im} \left\{ \frac{4p^2 (2p^2 - \beta^{-2})}{4p^2 \xi\eta + (\beta^{-2} - 2p^2)^2} \frac{dp}{dt} \right\}_{p=p(t)}. \quad (6.68)$$

Now the numerator is approximated as $N(p) = 8p^4 + O(p^2)$, which has the exact opposite dominant term compared with the SS-wave. Therefore, the divergent behavior of u_{SS} is canceled out by the similar behavior arising from u_{SP} .

7 Chapter 7: Surface Waves in a Vertically Heterogeneous Media

8 Chapter 8: Free Oscillations of the Earth

8.1 Question 1

From eq. (8.34) in the book, the torsional oscillations of a homogeneous elastic solid sphere satisfy

$$\frac{dW}{dr} = \frac{W}{r} + \frac{T}{\mu}, \quad (8.1)$$

$$\frac{dT}{dr} = \left[\frac{\mu(l-1)(l+2)}{r^2} - \rho\omega^2 \right] W - \frac{3T}{r}. \quad (8.2)$$

This 1st-order ODE system is equivalent to the following second-order ODE

$$\frac{d}{dr} \left(r^2 \frac{dW}{dr} \right) = r \frac{dW}{dr} + W + \frac{1}{\mu} \left(r^2 \frac{dT}{dr} + 2rT \right) \quad (8.3)$$

From Eq. (8.2) we can obtain

$$r^2 \frac{dT}{dr} + 2rT = \mu \left[(l-1)(l+2) - \frac{\omega^2 r^2}{\beta^2} \right] W - rT. \quad (8.4)$$

Eventually, we have

$$\frac{1}{r^2} \frac{d}{dr} \left(r^2 \frac{dW}{dr} \right) + \left[\frac{\omega^2}{\beta^2} - \frac{l(l+1)}{r^2} \right] W = 0. \quad (8.5)$$

Although Eq. (8.5) looks the same as the governing equation for free oscillations of a homogeneous liquid sphere, except for a different wave speed, the free surface condition should be applied to traction T . Furthermore, the angular degree starts from $l = 1$ for toroidal modes because $\mathbf{C}_{00} = \mathbf{0}$. The solution of $W(r)$ is the spherical Bessel function, and the traction $T(r)$ can be obtained as

$$W(r) \propto j_l \left(\frac{\omega r}{\beta} \right), \quad T(r) = \frac{\mu}{r} \frac{d(rW)}{dr} \propto \frac{\mu}{r} \left[(l-1)j_l \left(\frac{\omega r}{\beta} \right) - \frac{\omega r}{\beta} j_{l+1} \left(\frac{\omega r}{\beta} \right) \right]. \quad (8.6)$$

For $l = 1$, we have

$$T_1(r) \propto j_2 \left(\frac{\omega r}{\beta} \right) = \left(\frac{3}{x^3} - \frac{1}{x} \right) \sin x - \frac{3}{x^2} \cos x, \quad \text{with } x = \frac{\omega r}{\beta}. \quad (8.7)$$

To satisfy $T_1(r_0) = 0$ at the free surface, the eigenfrequencies should be

$$x_n = \frac{n\omega_1 r_0}{\beta}, \quad \tan x_n = \frac{3x_n}{3-x_n^2}, \quad n = 1, 2, 3, \dots. \quad (8.8)$$

The first root with $n = 0$ is $\omega_1 = 0$ which corresponds to the rigid-body rotation, as $W_1(r) = j_1(0) = 1$ is a non-trivial solution. With $r_0 = 6000$ km and $\beta = 5$ km/s, the periods can be evaluated as

$${}_1 T_1 = \frac{2\pi}{5.76(\beta/r_0)} \approx 21.8 \text{ min}, \quad {}_2 T_1 = \frac{2\pi}{9.10(\beta/r_0)} \approx 13.8 \text{ min}. \quad (8.9)$$

For $l = 2$, we have

$$T_2(r) \propto j_2(x) - x j_3(x) = \left(\frac{5}{x} - \frac{12}{x^3} \right) \sin x - \left(1 - \frac{12}{x^2} \right) \cos x. \quad (8.10)$$

The first root with $n = 0$ is still $x = 0$, but for $l \geq 2$, we have $j_l(0) = 0$ corresponding to a trivial solution of $W(r)$. Hence, we start with the non-zero roots and obtain

$${}_0 T_2 = \frac{2\pi}{2.50(\beta/r_0)} \approx 50.3 \text{ min}, \quad {}_1 T_2 = \frac{2\pi}{7.14(\beta/r_0)} \approx 17.6 \text{ min}. \quad (8.11)$$

Similarly, for $l = 3$ we obtain

$${}_0 T_3 = \frac{2\pi}{3.86(\beta/r_0)} \approx 32.5 \text{ min}, \quad {}_1 T_3 = \frac{2\pi}{8.44(\beta/r_0)} \approx 14.9 \text{ min}. \quad (8.12)$$

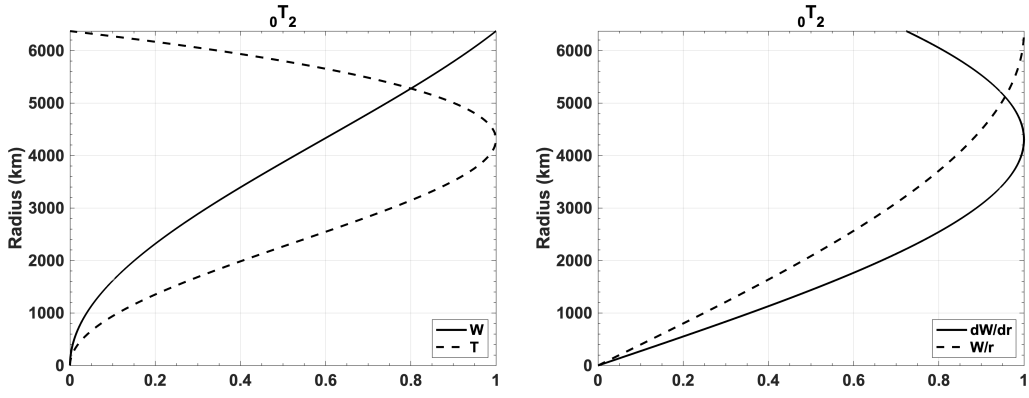


Fig. 8.1 Radial eigenfunction $W(r)$ and $T(r)$ for mode $_0T_2$, as well as the radial derivative dW/dr and the quantity W/r . All amplitudes are normalized by their maximum value.

In summary, the two longest periods are $_0T_2 \approx 50.3$ min and $_0T_3 \approx 32.5$ min. They are not so different from the periods of these two modes calculated in the PREM model, i.e., $_0T_2(\text{PREM}) \approx 44.0$ min and $_0T_3(\text{PREM}) \approx 28.5$ min.

For a single force, the excitation coefficient of the i -th normal mode is

$$E_i = {}_i\mathbf{u}^* \cdot \mathbf{f} = {}_nW_l(r) \mathbf{T}_l^m \cdot \mathbf{f}. \quad (8.13)$$

A horizontal force contributes to $\mathbf{T}_l^m \cdot \mathbf{f} \neq 0$. Therefore, we only need to study the radial eigenfunction $W(r)$. For a force couple with moment about a vertical axis, the forces are horizontal and the separation is also in the horizontal direction. The difference thus lies in an extra horizontal derivative of the eigenfunction, which results in $W(r)/r$ as the excitation coefficient and it also reaches the maximum at the surface. For $_0T_2$ mode in a homogeneous elastic solid sphere, the displacement eigenfunction $_0W_2(r) = j_2(_0\omega_2 r/\beta)$ is plotted in Fig. 8.1. The horizontal force at the Earth's surface is the most favorable for exciting Love mode.

If the horizontal force couple is separated in the vertical direction, then we need the radial derivative dW/dr to evaluate coefficient excitation, which is also plotted in Fig. 8.1.

8.2 Question 2

From eq. (7.91) in the book, we have

$$\left(\frac{\delta c}{c} \right)_l = \left(\frac{c}{c_e} - 1 \right) - \frac{i}{2Q}, \quad Q^{-1} = -2 \operatorname{Im} \left(\frac{\delta c}{c} \right)_l. \quad (8.14)$$

According the phase velocity $c = \omega/k$, for a fixed angular order l , which is equivalent to a fixed wavenumber k , we have

$$\delta c = \frac{\delta \omega}{k}, \quad \left(\frac{\delta c}{c} \right)_l = \left(\frac{\delta \omega}{\omega} \right)_l. \quad (8.15)$$

Eq. (8.65) in the book states that

$$\left(\frac{\delta \omega}{\omega} \right)_l = \int_0^{r_\oplus} \left[\frac{\rho}{\omega} \left(\frac{\partial \omega}{\partial \rho} \right)_{l,\beta} \frac{\delta \rho}{\rho} + \frac{\beta}{\omega} \left(\frac{\partial \omega}{\partial \beta} \right)_{l,\rho} \frac{\delta \beta}{\beta} \right] dr. \quad (8.16)$$

Similar to Eq. (8.14) the attenuation factor Q_β is defined as

$$\operatorname{Im} \left\{ \frac{\delta \beta}{\beta} \right\} = -\frac{1}{2Q_\beta}. \quad (8.17)$$

Eventually, the temporal Q of a toroidal mode is related to the $Q_\beta(r)$ of body waves at radius r by

$$Q^{-1} = -2 \operatorname{Im} \left(\frac{\delta\omega}{\omega} \right)_l = -2 \int_0^{r_\oplus} \frac{\beta}{\omega} \left(\frac{\partial\omega}{\partial\beta} \right)_{l,\rho} \operatorname{Im} \left\{ \frac{\delta\beta}{\beta} \right\} dr = \int_0^{r_\oplus} \frac{\beta}{\omega} \left(\frac{\partial\omega}{\partial\beta} \right)_{l,\rho} Q_\beta^{-1}(r) dr. \quad (8.18)$$

8.3 Question 3

The argument is wrong in several aspects:

1. The Earth's daily rotation is not a free oscillation because it is unrelated to the elastic wave equation under study.
2. The trivial toroidal mode ${}_0T_1$, although denoted as the rigid-body rotation, is different from Earth's daily rotation.
The toroidal mode ${}_0T_1$ has a frequency ${}_0\omega_1 = 0$, which means that we can add an arbitrary static rigid-body rotation to the final displacement field, and it still satisfies the elastic wave equation.
3. The Earth's daily rotation causes the splitting of normal modes, especially for modes with very long periods. This effect is similar to the Zeeman effect.

8.4 Question 4

Fig. 8.2 shows the spheroidal mode dispersion computed by MINOS with an isotropic PREM model. The identified spheroidal modes in seismic data are indicated by larger symbols and listed below.

${}_{30}S_{10}$ ${}_{29}S_{11}$ ${}_{30}S_{12}$ ${}_{31}S_{12}$ ${}_{28}S_{13}$ ${}_{27}S_{14}$ ${}_{28}S_{14}$ ${}_{25}S_{15}$
 ${}_{22}S_{18}$ ${}_{25}S_{18}$ ${}_{22}S_{19}$ ${}_{23}S_{19}$ ${}_{25}S_{19}$ ${}_{23}S_{20}$ ${}_{23}S_{21}$

The reference phase-velocity lines in Fig. 8.2 correspond to a ray parameter regime

$$\frac{c}{\alpha_{c-}} < p < \frac{b}{\alpha_{b+}}, \quad (8.19)$$

where $r = b$ and $r = c$ denote CMB and ICB, respectively. In fact, this range of ray parameter p includes Regime VII and Regime VIII. To analyze if a mode is associated with PKP but not with PKIKP, it is better to visualize the eigenfunctions, as shown in Fig. 8.3. A PKP mode eigenfunction is expected to have negligible values below ICB. Therefore, we can conclude that among the selected modes, those from the second row (i.e., with $l \geq 18$) are associated with PKP but not

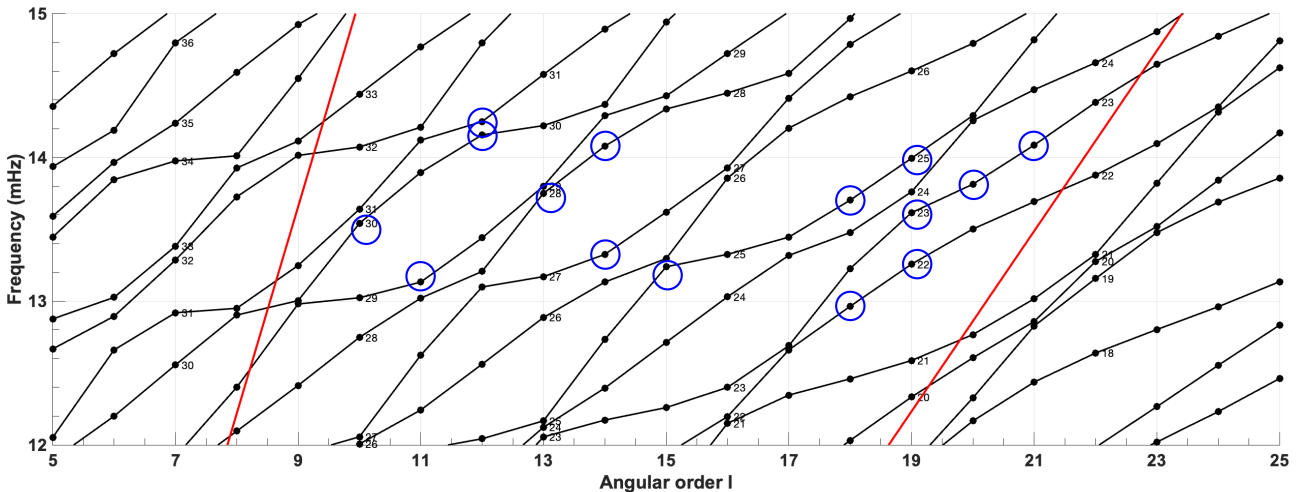


Fig. 8.2 Spheroidal mode dispersion diagram. Red lines are reference phase-velocity lines. The larger blue symbols indicate modes identified in seismic data, with frequencies around 13 and 14 mHz. The overtone number n is annotated on the plot.

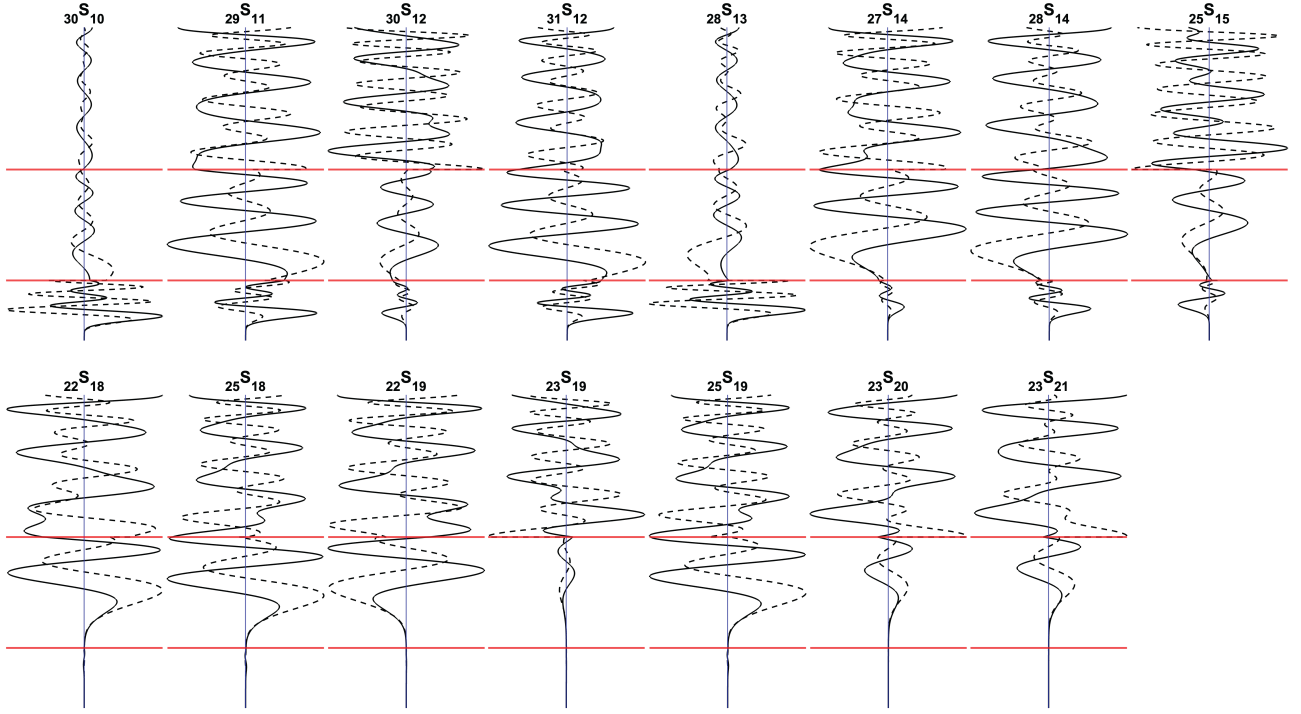


Fig. 8.3 Radial eigenfunctions of the selected spheroidal modes. Solid and dashed lines correspond to $U(r)$ and $V(r)$ respectively. Red horizontal lines indicate the depth of CMB and ICB. The second row shows the modes associated with PKP but not with PKIKP.

PKIKP, with one potential exception $_{23}S_{19}$ which is more likely to be contributed from CMB reflection phases. On the other hand, modes from the first row (i.e., with $l \leq 15$) mostly correspond to PKIKP, with two exceptions $_{30}S_{10}$ and $_{28}S_{13}$ which are dominated by J_{SV} .

8.5 Question 5

Denote the Earth's radius as R_E and the station epicentral distance as Δ . Assume the overtone number $n > m$ and their arrival time difference is $t_n - t_m$.

- When they differ by an even number, i.e., $n - m = 2N$, the polar phase shift results in an (extra) phase advance $N\pi$ of Gn compared to Gm . Therefore, the phase velocity satisfies

$$\omega(t_n - t_m) - k(x_n - x_m) = N\pi, \quad c(T) = \frac{N \cdot 2\pi R_E}{t_n - t_m - NT/2}, \quad (8.20)$$

where k denotes wavenumber and T is the period.

- When they differ by an odd number, i.e., $n - m = 2N - 1$, the polar phase shift results in an (extra) phase advance $(N - 1/2)\pi$ of Gn compared to Gm . However, in this case, we must also consider the initial phase difference $\phi_n - \phi_m$ originating from the source. Therefore, the phase velocity satisfies

$$\omega(t_n - t_m) - k(x_n - x_m) + (\phi_n - \phi_m) = \left(N - \frac{1}{2}\right)\pi. \quad (8.21)$$

This results in

$$c(T) = (x_n - x_m) \left[t_n - t_m + \frac{\phi_n - \phi_m}{2\pi} T - \left(\frac{N}{2} - \frac{1}{4}\right) T \right]^{-1}, \quad (8.22)$$

while the difference in distance depends on if Gm is related to the minor arc $R_E\Delta$ or the major arc $R_E(2\pi - \Delta)$.

The arrival time difference $t_n - t_m$ “can be uncertain by a multiple of the period T , and the computation of $c(T)$ leads to a discrete set of possible phase velocity curves, one of which must be correct” (Nafe & Brune, 1960).

Based on eq. (7.149) in the book, the azimuthal dependence of Love wave radiation occurs in the following factor

$$A^{\text{Love}} = a^{\text{Love}} + i b^{\text{Love}}, \quad (8.23)$$

with the real and imaginary parts given as (with source depth denoted by h)

$$\begin{aligned} a^{\text{Love}} &= -\left. \frac{dl_1}{dz} \right|_h (M_{xz} \sin \phi - M_{yz} \cos \phi), \\ b^{\text{Love}} &= kl_1(h) \left(M_{xx} \sin \phi \cos \phi - M_{yx} \cos^2 \phi + M_{xy} \sin^2 \phi - M_{yy} \sin \phi \cos \phi \right). \end{aligned} \quad (8.24)$$

For Love waves, we can see that if the moment tensor does not contain M_{xz} and M_{yz} component in general, then with $\phi \rightarrow \phi + \pi$ the initial phase does not change. Similarly, for Rayleigh waves, we can obtain

$$\begin{aligned} a^{\text{Rayleigh}} &= kr_1(h) [M_{xx} \cos^2 \phi + (M_{xy} + M_{yx}) \sin \phi \cos \phi + M_{yy} \sin^2 \phi] + \left. \frac{dr_2}{dz} \right|_h M_{zz}, \\ b^{\text{Rayleigh}} &= \left. \frac{dr_1}{dz} \right|_h (M_{xz} \cos \phi + M_{yz} \sin \phi) - kr_2(h) (M_{zx} \cos \phi + M_{zy} \sin \phi). \end{aligned} \quad (8.25)$$

We can see that the conclusion remains the same, and the initial phase at opposite azimuths will be influenced by M_{xz} and M_{yz} components of the moment tensor.

8.6 Question 6

a) As shown in Problem 4.13, at the traction-free surface of the Earth, we have $e_{zx} = e_{zy} = 0$. Therefore, we have

$${}_i e_{zx}^*(\mathbf{x}_S) M_{zx} + {}_i e_{xz}^*(\mathbf{x}_S) M_{xz} + {}_i e_{zy}^*(\mathbf{x}_S) M_{zy} + {}_i e_{yz}^*(\mathbf{x}_S) M_{yz} \approx 0 \quad (8.26)$$

if the source position \mathbf{x}_S is taken very close to the surface.

b) A dip-slip earthquake (vertical fault, vertical slip) has a moment tensor consisting of M_{xz} and M_{yz} . From **part a)**, we know that if the hypocenter is very shallow, a dip-slip earthquake is very inefficient in exciting normal modes.

c) From Table 8.1 and Table 8.2 in the book, the shear strain components e_{zx} and e_{zy} are related to the radial eigenfunctions as

$$e_{zx}^S \propto \sqrt{l(l+1)} \frac{U}{r} + \frac{dV}{dr} - \frac{V}{r}, \quad e_{zx}^T \propto \frac{dW}{dr} - \frac{W}{r} \quad (8.27)$$

for spheroidal and toroidal modes, respectively. Fig. 8.4 shows the shear strain component for several surface wave modes with periods on the order of 100 s. Note that the traction-free surface condition is satisfied. For a fixed depth h , if the

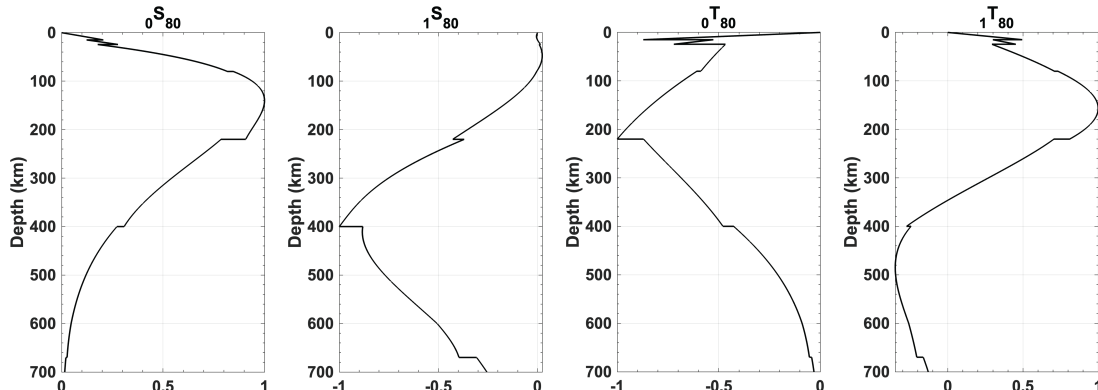


Fig. 8.4 Shear strain component evaluated from radial eigenfunctions. The amplitudes are normalized.

period (equivalently the wavelength) is long enough with $\lambda \gg h$, the radial eigenfunctions are approximately constant when $z < h$. This is true not only for the shear strain component shown in Fig. 8.4, but also for other strain components.

- d) The excitation coefficient for a particular mode i is

$$_i e_{pq}^*(\mathbf{x}_S) M_{pq}. \quad (8.28)$$

For a dip-slip earthquake, as we have shown that e_{zx} and e_{zy} are essentially zero when $h \ll \lambda$, the sum of amplitudes in the P-wave group and the S-wave group should also be close to zero, given that the period is sufficiently long.

- e) In general, there are six independent moment tensor components: $M_{rr}, M_{r\theta}, M_{r\phi}, M_{\theta\theta}, M_{\theta\phi}, M_{\phi\phi}$. For a large **shallow** earthquake, the dip-slip components $M_{r\theta}, M_{r\phi}$ are very inefficient in generating normal modes, and thus, the seismic data are not sensitive to them (in other words, null space of the inverse problem).

The traction-free surface condition also states $e_{rr} = 0$, which indicates that an earthquake is inefficient in generating normal modes as well if the moment tensor satisfies

$$M_{rr} = \frac{\kappa + \frac{4}{3}\mu}{\kappa - \frac{2}{3}\mu} M_{\theta\theta} = \frac{\kappa + \frac{4}{3}\mu}{\kappa - \frac{2}{3}\mu} M_{\phi\phi}. \quad (8.29)$$

This is from eq. (10.68) in Dahlen & Tromp (1998). This non-uniqueness in the isotropic components can be eliminated by considering a pure deviatoric moment tensor with $\text{tr}(\mathbf{M}) = 0$.

- f) The previous answers are based on the Earth's free oscillations in an SNREI model, which is Spherically symmetric, Non-Rotating, Elastic and Isotropic. If the Earth is laterally heterogeneous, then the radial and surface eigenfunctions are coupled together, making the analysis much more complicated.

9 Chapter 9: Body Waves in Media with Depth-Dependent Properties

10 Chapter 10: The Seismic Source: Kinematics

11 Chapter 11: The Seismic Source: Dynamics

12 Chapter 12: Principles of Seismometry

12.1 Question 1

The response $\zeta(t)$ of the seismometer to an arbitrary ground acceleration $\ddot{u}(t)$ can be obtained by a convolution with the acceleration impulse response $f(t)$, as given by eq. (12.13) in the book:

$$\zeta(t) = \int_0^{+\infty} \ddot{u}(t - \tau) f(\tau) d\tau. \quad (12.1)$$

For an inertial seismometer, the response $f(t)$ satisfies

$$f(t) = 0, \quad \text{for } t < 0. \quad (12.2)$$

Therefore, the integral can be evaluated from $-\infty$ to $+\infty$, and in the frequency domain we have

$$\hat{\zeta}(\omega) = (-i\omega)^2 \hat{u}(\omega) \cdot \hat{f}(\omega) = \hat{u}(\omega) \cdot (-i\omega)^2 \hat{f}(\omega). \quad (12.3)$$

The derivative operator can be applied to either $u(t)$ or $f(t)$. From Eq. (12.2), the initial rest condition also holds for $\ddot{f}(t)$. Hence, we obtain

$$\zeta(t) = \int_{-\infty}^{+\infty} u(t - \tau) \ddot{f}(\tau) d\tau = \int_0^{+\infty} u(t - \tau) \ddot{f}(\tau) d\tau. \quad (12.4)$$

12.2 Question 2

At equilibrium, the mass-spring system satisfies

$$mg = k(l - l_0), \quad (12.5)$$

where k is the spring stiffness. The period of small oscillation is

$$T = 2\pi \sqrt{\frac{m}{k}} = 2\pi \sqrt{\frac{l - l_0}{g}}. \quad (12.6)$$

12.3 Question 3

a) At the surface $z = 0$, the boundary conditions $\tau_{zx} = 0$ and $\tau_{zz} = -P \exp[i\omega(x/c - t)]$ give

$$\mathbf{F}\mathbf{w} = \mathbf{f} = [\tilde{u}_x, \tilde{u}_z, 0, -P]^T, \quad \text{with } p = \frac{1}{c}. \quad (12.7)$$

The ray parameter p is determined by matching the horizontal slowness of the moving pressure. The procedure to solve this problem is first to consider $\mathbf{w} = [w_1, w_2, 0, 0]^T$ including only downgoing P and SV waves, and then match $(\mathbf{F}\mathbf{w})_3 = 0$ and $(\mathbf{F}\mathbf{w})_4 = -P$ with $z = 0$ substituted into the matrix \mathbf{F} . The above two equations finally give the solution of w_1 and w_2 . However, since \mathbf{w} is provided for this question, we can directly check if it satisfies the boundary conditions. Choosing $z_{\text{ref}} = 0$, from eq. (5.69) in the book, at the surface we have

$$\mathbf{F}(z = 0) = \mathbf{E} = \begin{bmatrix} \alpha p & \beta \eta & \alpha p & \beta \eta \\ \alpha \xi & -\beta p & -\alpha \xi & \beta p \\ 2i\omega\rho\alpha\beta^2 p\xi & i\omega\rho\beta(1 - 2\beta^2 p^2) & -2i\omega\rho\alpha\beta^2 p\xi & -i\omega\rho\beta(1 - 2\beta^2 p^2) \\ i\omega\rho\alpha(1 - 2\beta^2 p^2) & -2i\omega\rho\beta^3 p\eta & i\omega\rho\alpha(1 - 2\beta^2 p^2) & -2i\omega\rho\beta^3 p\eta \end{bmatrix}. \quad (12.8)$$

The solution vector \mathbf{w} is given as

$$\mathbf{w} = \frac{iP}{\omega\rho\beta^2\mathsf{R}(p)} \begin{bmatrix} \left(\frac{1}{\beta^2} - 2p^2\right) \frac{1}{\alpha} & \frac{-2p\xi}{\beta} & 0 & 0 \end{bmatrix}^\top. \quad (12.9)$$

The Rayleigh function $\mathsf{R}(p)$ and the parameters ξ and η are given as

$$\mathsf{R}(p) = \left(\frac{1}{\beta^2} - 2p^2\right)^2 - 4p^2 \sqrt{p^2 - \frac{1}{\alpha^2}} \sqrt{p^2 - \frac{1}{\beta^2}}, \quad \xi = \sqrt{\frac{1}{\alpha^2} - p^2}, \quad \eta = \sqrt{\frac{1}{\beta^2} - p^2}. \quad (12.10)$$

We can evaluate the product $\mathbf{F}\mathbf{w}$ as

$$(\mathbf{F}\mathbf{w})_3 = -\frac{P}{\beta\mathsf{R}(p)} \cdot \frac{2p\xi}{\beta} \left[(1 - 2\beta^2 p^2) - (1 - 2\beta^2 p^2) \right] = 0, \quad (12.11)$$

$$(\mathbf{F}\mathbf{w})_4 = -\frac{P}{\mathsf{R}(p)} \left[\left(\frac{1}{\beta^2} - 2p^2\right)^2 + 4p^2\xi\eta \right] = -P. \quad (12.12)$$

The boundary conditions are satisfied as expected.

b) The displacement at arbitrary depth $z > 0$ can be obtained as

$$\tilde{u}_x(z) = (\mathbf{F}\mathbf{w})_1 = \frac{iP}{\omega\rho\beta^2} \frac{p}{\mathsf{R}(p)} \left[\left(\frac{1}{\beta^2} - 2p^2\right) e^{i\omega\xi z} - 2\xi\eta e^{i\omega\eta z} \right], \quad u_x = \tilde{u}_x e^{i\omega(px-t)}, \quad (12.13)$$

$$\tilde{u}_z(z) = (\mathbf{F}\mathbf{w})_2 = \frac{iP}{\omega\rho\beta^2} \frac{\xi}{\mathsf{R}(p)} \left[\left(\frac{1}{\beta^2} - 2p^2\right) e^{i\omega\xi z} + 2p^2 e^{i\omega\eta z} \right], \quad u_z = \tilde{u}_z e^{i\omega(px-t)}. \quad (12.14)$$

With $p = c^{-1}$ and the assumption $c \ll \beta < \alpha$, we can expand all terms into powers of c/α and c/β , and only retain the low-order terms. The following approximations can be made

$$\xi \approx \frac{i}{c} \left(1 - \frac{1}{2} \frac{c^2}{\alpha^2}\right), \quad \eta \approx \frac{i}{c} \left(1 - \frac{1}{2} \frac{c^2}{\beta^2}\right), \quad \mathsf{R}(p) \approx \frac{2}{c^2} \left(\frac{1}{\alpha^2} - \frac{1}{\beta^2}\right). \quad (12.15)$$

With another assumption $\omega z c / 2\beta^2 \ll 1$ ($\omega > 0$), the exponential term can be approximated as

$$e^{i\omega\xi z} \approx e^{-\omega z/c} \left(1 + \frac{\omega z c}{2\alpha^2}\right), \quad e^{i\omega\eta z} \approx e^{-\omega z/c} \left(1 + \frac{\omega z c}{2\beta^2}\right). \quad (12.16)$$

After some algebra, we can obtain

$$u_x(x, z, t) = \frac{icP}{2\omega\rho\beta^2} \left(\frac{\beta^2}{\alpha^2 - \beta^2} - \frac{\omega z}{c} \right) e^{-\omega z/c} e^{i\omega(x/c-t)}, \quad (12.17)$$

$$u_z(x, z, t) = \frac{cP}{2\omega\rho\beta^2} \left(\frac{\alpha^2}{\alpha^2 - \beta^2} + \frac{\omega z}{c} \right) e^{-\omega z/c} e^{i\omega(x/c-t)}. \quad (12.18)$$

Eqs (12.17) and (12.18) are the same as eqs (21) and (22) in Sorrells (1971), except for a difference in the sign convention for the vertical displacement. The expressions given in the book are not correct. Both u_x and u_z exponentially decay with depth and propagate in x -direction with the pressure wave speed c .

c) Consider $P \sim 100$ Pa, $T \sim 300$ s and $c \sim 5$ m/s for the pressure wave. Using the PREM upper crust properties, we have $\rho = 2600$ kg/m³, $\alpha = 5.8$ km/s and $\beta = 3.2$ km/s. To ensure that the seismic noise due to atmospheric disturbances is at most a few nanometers, long-period seismometers should be buried 2 km deep. The depth profiles of the displacement amplitudes are shown in Fig. 12.1.

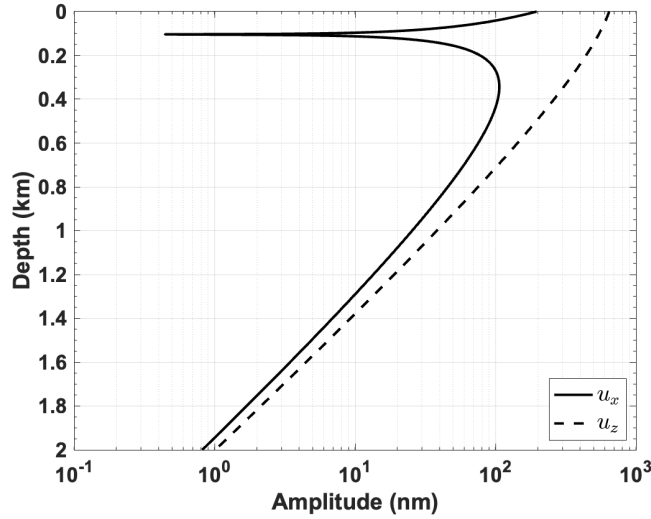


Fig. 12.1 Depth profiles of horizontal and vertical displacement amplitudes under surface pressure wave loading.

12.4 Question 4

The coil response is proportional to ω , which can be expressed as

$$X_c(\omega) = A\omega, \quad 20 \log_{10} \left(\frac{X_c(2\omega)}{X_c(\omega)} \right) = 20 \log_{10} 2 \text{ dB} = 6 \text{ dB}. \quad (12.19)$$

The coil response rises at 6 dB per octave. The low frequency total response ($\omega < \omega_g$) is proportional to ω^3 , which can be expressed as

$$X(\omega) = B\omega^3, \quad 20 \log_{10} \left(\frac{X(2\omega)}{X(\omega)} \right) = 20 \log_{10} 8 \text{ dB} = 18 \text{ dB}. \quad (12.20)$$

The total response rises at 18 dB per octave at low frequency $\omega < \omega_g$.

12.5 Question 5

For a monochromatic surface wave at frequency ω , the ratio between strain and displacement amplitudes is the wavenumber $k(\omega)$. The phase velocity $c(\omega)$ can thus be measured from the narrow-band filtered strain and displacement recordings.

12.6 Question 6

For a velocity feedback seismometer, the coil output goes to an amplifier with output voltage $V(s) = KAs\xi(s)$. The feedback system then delivers an acceleration βV , which is applied as a negative acceleration to the inertial sensor. The

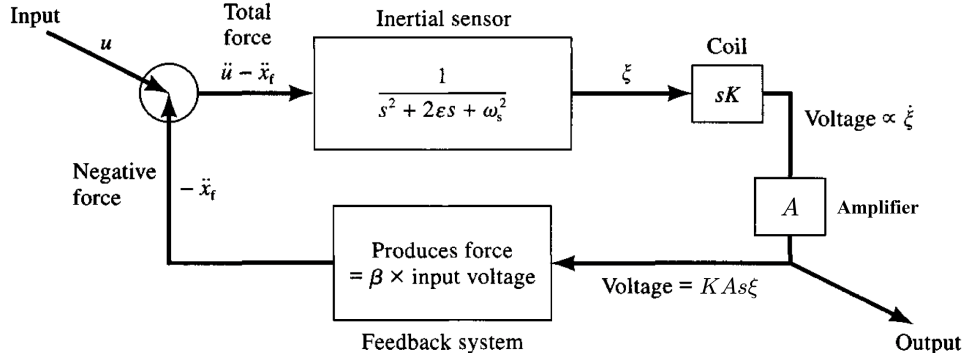


Fig. 12.2 Schematic for a velocity feedback seismometer. The seismometer damping is made to appear very high.

governing equations for this system are

$$\ddot{x}_{\text{total}} = \ddot{u} - \ddot{x}_{\text{f}}, \quad V = \frac{KAs}{s^2 + 2\varepsilon s + \omega_s^2} \ddot{x}_{\text{total}}, \quad \ddot{x}_{\text{f}} = \beta V. \quad (12.21)$$

The overall response can be solved as

$$\frac{V}{\ddot{u}} = \frac{KAs}{s^2 + (2\varepsilon + KA\beta)s + \omega_s^2}. \quad (12.22)$$

The original damping 2ε has been increased to $2\varepsilon + KA\beta$.

12.7 Question 7

The building is subjected to ground acceleration $\ddot{u}(t) = A \sin(\Omega t) H(t)$. The resulting building displacement $\xi(t)$ satisfies

$$\ddot{\xi} + 2\varepsilon\dot{\xi} + \omega^2\xi = -\ddot{u}. \quad (12.23)$$

When $\varepsilon = 0$ (no damping), the solution is given as

$$\begin{aligned} \xi(t) &= -\ddot{u}(t) * \left[\frac{\sin(\omega t)}{\omega} H(t) \right] = -\frac{A}{\omega} \int_0^t \sin(\Omega\tau) \sin[\omega(t-\tau)] d\tau \\ &= \frac{A}{2\omega} \int_0^t [\cos(\Omega\tau - \omega\tau + \omega t) - \cos(\Omega\tau + \omega\tau - \omega t)] d\tau \\ &= \frac{A}{2\omega} \left[\frac{\sin(\Omega t) - \sin(\omega t)}{\Omega - \omega} - \frac{\sin(\Omega t) + \sin(\omega t)}{\Omega + \omega} \right] \\ &= \frac{A}{2\omega} \left[\frac{\sin(\Delta\omega t)}{\Delta\omega} \cos[(\omega + \Delta\omega)t] - \frac{\sin[(\omega + \Delta\omega)t]}{\omega + \Delta\omega} \cos(\Delta\omega t) \right]. \end{aligned} \quad (12.24)$$

The difference between the forcing frequency and resonant frequency is denoted as $\Delta\omega = (\Omega - \omega)/2$. According to Eq. (12.24), in the limit as $\Omega \rightarrow \omega$, we have

$$\xi(t) = \frac{A}{2\omega} \left[t \cos(\omega t) - \frac{\sin(\omega t)}{\omega} \right] = \frac{A}{2\omega^2} [\omega t \cos(\omega t) - \sin(\omega t)]. \quad (12.25)$$

In summary, displacements can grow with time to large and thus hazardous values if a building is subjected to ground motion close to its resonant frequency. The growth continues indefinitely because the input shaking has no end.

Now consider that the ground motion has a finite duration at a fixed frequency, i.e., $\ddot{u}(t) = A \sin(\Omega t) H(t) H(T-t)$. When $t < T$, the convolution result is the same as Eq. (12.24). On the other hand, when $t > T$ we have

$$\xi(t) = \frac{A}{2\omega} \left[\frac{\sin(\Omega T - \omega T + \omega t) - \sin(\omega t)}{\Omega - \omega} - \frac{\sin(\Omega T + \omega T - \omega t) + \sin(\omega t)}{\Omega + \omega} \right], \quad \text{for } t > T. \quad (12.26)$$

The engineering displacement response spectrum $SD(\omega, \varepsilon)$ is defined to be the maximum value of $|\xi(t)|$ given a specific frequency ω and damping parameter ε . Consider $|(\Omega - \omega)T| \ll 1$ and $\omega T \gg 1$. For small $t < T$, we have $|\Delta\omega t| \ll 1$ and thus can directly apply Eq. (12.25), which gives

$$|\xi(t)| \approx \frac{A}{2\omega^2} |\omega t \cos(\omega t) - \sin(\omega t)| \leq \frac{A\sqrt{\omega^2 t^2 + 1}}{2\omega^2} \lesssim \frac{AT}{2\omega}. \quad (12.27)$$

For large $t > T$, Eq. (12.26) leads to

$$|\xi(t)| \approx \frac{A}{2\omega^2} |0 - \sin[(\omega + \Delta\omega)T] \cos[(\omega + \Delta\omega)T - \omega t]| \approx \frac{A}{2\omega} \frac{|\sin(\omega T)|}{\omega} \ll \frac{AT}{2\omega}. \quad (12.28)$$

Therefore, we conclude that $SD(\omega, \varepsilon = 0) \approx AT/(2\omega)$. The duration of shaking is important because, close to the resonant frequency, the undamped response spectrum has an amplitude proportional to T .

List of Figures

2.1	A small disc within a stressed medium (Figure 2.4)	5
4.1	Three component seismograms generated by a vertical point-force at receiver $\mathbf{x} = (2, 1, 3)$ km. The time axis is normalized by the P-wave travel time $t_P = r/\alpha$, and the displacement is multiplied by factor $8\pi\mu r$, which also helps visualize the dependence on $1/r$. The source time function is a Gaussian with $\sigma = 0.01$ s.	12
4.2	Three component seismograms generated by a vertical point-force at receiver $\mathbf{x} = (2, 1, 3)$ km. The source time function is a Gaussian with $\sigma = 0.1$ s.	12
4.3	Illustration of the side length in the take-off angle direction.	13
4.4	Illustration of the surface-reflected phase in a homogeneous sphere. The true ray path is $A-P_0-B$ with P_0 being the midpoint of the arc, while P denotes the perturbed surface reflection point.	19
5.1	Stress-strain hysteresis loop. The attenuation is exaggerated for visualization.	31
6.1	Illustration of the transmitted ray, and the condition satisfied in Eq. (6.13).	33
6.2	(Left) Riemann sheets of $\eta = \sqrt{\beta^2 - p^2}$. Red surface corresponds to $\text{Re } \eta > 0$, which is discontinuous across the branch cuts. (Middle) Rayleigh poles on the physical Riemann sheet $\{\text{Re } \xi \geq 0; \text{Re } \eta \geq 0\}$. Branch points are denoted by \times , and poles by \circ at $p = \pm 1/c_R$. (Right) Rayleigh poles on the nonphysical Riemann sheet $\{\text{Re } \xi < 0; \text{Re } \eta \geq 0\}$. The poles are near $p = \pm 1/\alpha$ in this case with $v = 0.25$ (i.e., Poisson solid).	34
6.3	Displacement fields at (5 km, 0). The time axis is normalized by P-arrival time $t_P = R/\alpha$. The displacement is normalized by $I/\pi\mu$. The thick gray line is $20 \times$ the original amplitude to visualize this part of the seismogram. The contributions from u_x^P, u_x^S, u_z^P and u_z^S are shown in the right panels.	37
6.4	Same as Fig. 6.3 but for displacement fields at (5 km, 1 km). The head wave becomes a separate pulse.	38
6.5	Synthetic seismograms by convolution of signals in Figs. 6.3 and 6.4 with a 1st derivative Gaussian pulse. The central frequency of the wavelet is $f_c = 20/t_P$. Note the difference in the ranges of vertical axes. The thick gray line is $40 \times$ the original amplitude of u_z to visualize this part of the seismogram.	38
6.6	Particle motion plots at different depths $z = 0.01$ km, 0.035 km and 0.1 km. Increasing time is indicated by the rainbow color order. The particle motion transitions from retrograde elliptical to prograde elliptical as the depth increases.	39
6.7	Influence of Poisson's ratio v on synthetic seismograms. The portion between P-wave and S-wave arrivals is zoomed in. The receiver is at (5 km, 0). Two example values of Poisson's ratio $v = 0.1$ and $v = 0.4$ are chosen. Note that \bar{P} -pulse appears when $v > 0.263$	39
6.8	Riemann sheets of $\xi = \sqrt{\alpha^2 - p^2}$. The z -axis indicates $\text{Re } \xi$ and the color for $\text{Im } \xi$. The z -axis is flipped to see $\text{Im } \xi > 0$ in the first quadrant where F' and D are located. The magenta line shows a portion of the integration path in Figure 6.9 in the book.	41
8.1	Radial eigenfunction $W(r)$ and $T(r)$ for mode ${}_0T_2$, as well as the radial derivative dW/dr and the quantity W/r . All amplitudes are normalized by their maximum value.	45
8.2	Spheroidal mode dispersion diagram. Red lines are reference phase-velocity lines. The larger blue symbols indicate modes identified in seismic data, with frequencies around 13 and 14 mHz. The overtone number n is annotated on the plot.	46
8.3	Radial eigenfunctions of the selected spheroidal modes. Solid and dashed lines correspond to $U(r)$ and $V(r)$ respectively. Red horizontal lines indicate the depth of CMB and ICB. The second row shows the modes associated with PKP but not with PKIKP.	47
8.4	Shear strain component evaluated from radial eigenfunctions. The amplitudes are normalized.	48
12.1	Depth profiles of horizontal and vertical displacement amplitudes under surface pressure wave loading.	53
12.2	Schematic for a velocity feedback seismometer. The seismometer damping is made to appear very high.	53

List of Tables

2.1	Constitutive laws for isotropic and deviatoric components. Modified from Dahlen & Tromp (1998).	6
-----	---	---